HYDRAULIC FRACTURE PROPAGATION THROUGH

GEOLOGICAL DISCONTINUITIES

By

Ella María Llanos Rodríguez

The Australian School of Petroleum

This thesis is submitted in fulfilment of the requirements for the degree of

Doctor of Philosophy

in the Faculty of Engineering, Computer and Mathematical Sciences

The University of Adelaide

June 2015

ABSTRACT

Hydraulic fracturing is a stimulation technique widely used to enhance hydrocarbon production and geothermal energy extraction. Other applications include waste disposal and cave inducement and preconditioning of ore for mining. Rocks are naturally fractured and therefore the little-understood problem of hydraulic fracture growth through these pre-existing discontinuities is a key area of research.

Mathematical criteria for predicting whether an induced fracture will cross a discontinuity have been published by several authors. Some used parameters that are difficult to quantify, neglected the stress induced by the hydraulic fracture itself and ignored fluid viscosity effects on crossing behaviour. Others ignored the presence of fluid in the hydraulic fracture, the possibility of fracture re-initiation after slippage and the effect of surface features on crossing. Numerical studies have shown that viscosity-dominated hydraulic fractures would induce slip on the discontinuity more easily than toughness-dominated hydraulic fractures. This implies that crossing should be more difficult for viscosity-dominated hydraulic fractures. To investigate the interaction between hydraulic and natural fractures, laboratory experiments are combined with numerical and analytical work in this thesis to extend two previously published criteria.

This thesis shows the effect of viscosity on the crossing interaction is complex and cannot be predicted based only on whether slip occurs on the discontinuity before the hydraulic fracture intersects it. The laboratory work can also be applied to improved understanding of the effect of the stress field on crossing as it relates to hydraulic fracture height growth. Prediction of the effect of weak bedding planes on height growth has recently gained importance as the risk of vertical growth of fractures into aquifers has emerged as a concern in shale gas and coal seam gas operations. The findings herein can be applied to this problem if the frictional interfaces are considered to represent weak bedding planes. Complete treatment of the height growth problem requires considering fracture growth through elastic layers with contrasts in physical properties.

The experiments show hydraulic fractures may grow to become elliptical because they extend more quickly and further in the direction of maximum stress or in the direction with fewer discontinuities. The preparation of the samples underlined the effect of local imperfections on discontinuities. Small areas of higher or lower contact stress can aid or inhibit fracture initiation. Rock plates must be smooth and flat in order to control this parameter and obtain valid experimental comparisons for contact stress and the other parameters controlling crossing.

Numerical and analytical results are presented as a mathematical expression with universal curves for the locations of slip starting points, providing an important aid for designing industrial hydraulic fractures. One difference between the approach used here and that used by others is their use of the fracture-tip singular stress solution, meaning they do not consider the effect of the non-singular stresses existing around a pressurised fracture. This thesis therefore improves their work.

Experimental and theoretical outcomes herein suggest that hydraulic fracture growth through an orthogonal discontinuity does not depend primarily on the interface friction coefficient. This finding contradicts several models.

ACKNOWLEDGEMENTS

The Hydraulic Fracturing Laboratory at CSIRO Energy is a university in itself. Here I grew not only technically, but also as a person, thanks to the times shared with the experienced technicians who helped me in so many ways. Leo Connelly tops the list, as he was my right-hand man and an unforgettable friend. He, together with his exceptional wife Jennifer, taught me lessons that have improved my nature and spirit. Lessons on precision and elegance, even in dealing with rocks and tools, were passed on to me by Nigel Smith and Anthony Coleman. I extend to them my admiration and respect for their professionalism. Thanks as well to Kevin Quinlan, Michael Camilleri and Greg Lupton for sharing with me their experiences of working at a laboratory. Finally, my gratitude to them all for welcoming me into their families and for teaching me about the Australian culture.

The laboratory work would not have been possible without the financial support of Schlumberger Moscow and CSIRO Energy. My gratitude to them. Special thanks to Dr. Marc Thiercelin (dec.), from Schlumberger, for his understanding. The Endeavour International Postgraduate Research and The University of Adelaide Scholarships represent a grand gesture of generosity and altruism from Australia, which I admire and am grateful for. These two scholarships are administered by a kind and efficient team at the University of Adelaide Graduate Centre. Thanks to all of them as well as to the Petroleum Exploration Society of Australia for awarding me the 2009 Federal Scholarship.

Sincere recognition to the Stress Group at the Australian School of Petroleum especially to Rosalind King and Marie Neubauer for their friendship. Thanks to: Stephen Begg for his support; Noune Melkoumian a thoughtful friend; Richard Daniel for his encouragement; Maureen Sutton for her genuine care; Andy Mitchell, Ian West, Delise Hollands, Eileen Flannery, Themis Carageorgos and the administrative staff for their kind support.

Deep gratitude goes to the staff at Parklands Medical Centre at the University of Adelaide for their support. I will especially keep in my 'box' of treasured memories the natural kindness of Dr. Maree White, the interesting challenges suggested by Dr. Jane Vernon-Roberts and the friendly patience of Dr. Brenton Martin. Thanks as well to the Security Escorts of the University of Adelaide for walking with me on so many nights from the Santos Building to their office. The university shuttle was always there, always on time to take the students home. I remember the friendly faces of the drivers of the university shuttle, Andre and Bob. All these great people made my student life much easier.

I was born and raised in **Colombia**, a country of positivity, passion and dreams. My trips have introduced me to beautiful people who have made a special impact on my life, like: Marco and Rose Cassetta, Gerd Van den Daele, Miroslav Brajanowski, Diana Arbeláez, Gabriela Marinoni, Ximena Crescini, Marcela Moreno, Feisar Joya, Miguel Quintero, Craig Mortimer, Mercedes and Damien Hunt, Mónica Polanco, Erika and Jan Bon, Antonina Mikocka-Walus, Bart Walus, Catherine Leahy, Peter Beilby and Graham Thamm. My gratitude as well to: Lynda Catlow, Greg Rogers, Roz Dunk, Sally Edwards, Kaia Little, Angela Moloney, Hugo Salcedo, Mónica Cleves, Betina Bendall, Jude Marlow, Andrés Vidal, Judith Miller, Andrew Rohde, Yumiko Bonnardeaux, and James Kear. The following families also contributed to the fantastic memories I have: Bon, Bravo, Bunger, Castro, Livore, Marinoni, Oloworaran, Pitaluga, Sandström and Toro. My respect to Angel Bravo (dec.) for the gift of freedom through the practice of valuing the truth.

Immense thanks to 'my little friends', all the children that have accompanied me through this journey to remind me that life is to be enjoyed in the simplest way possible. My gratitude to María Alejandra Peña for trusting me and becoming an inspiration in my life. Thanks to the advocates for children's rights like my friend Yoana Walschap and those who I met through the "*Amigos de María Alejandra*'" group, especially Sandra Sarmiento.

I feel very fortunate for the family moments shared, and the bond of love created, with whom I consider my Australian Family. I thank them for the many lessons: my 'Australian grandmother' Mrs. Jean Hayman (dec.), on honesty and simplicity; my 'Viejito' Mr. Bruce Thamm, on trust and humanity; the Haymans on gratitude and reliability; the Lows on generosity and perseverance; the Aristeguietas on transparency and comradeship; the Connellys on loving life and discipline; the Burkes on listening and acceptance; Marianne Sandström on listening and patience and Drew Breen on true friendship and compassion.

Thanks to my group of soul mates: Onil Ballestas, Isis Dávila, Rania Dughman, Luz Lozano, Janny May, Myrsa Maya, Nohra Muñoz, Saray Torres, Verónica Uribe and Guillermo Obando for their unconditional friendship despite the distance; Mercedes Palacios and Angel Marinoni for sharing their wisdom with me; my incomparable Brice Lecampion for his gentleness; my German sister Carmen Krapf and Mario Werner for their joyfulness; my one and only rowing partner Treena Bron for her support; Amelia and Sean Burke who were there to hug me with the power only children can offer and to their father, Nicholas for his genuine interest in getting to know me which was nurtured by trust.

I had the privilege of growing up with my paternal grandmother **Mamá Rosa**, who passed away during my PhD studies. This thesis honours her lessons on courage and perseverance and acknowledges the sacrifices she endured in achieving her dream to have an educated family. The influence of my maternal grandmother **Ana** is evident in the fact that we always do our best, even in chores and in situations that we take for granted.

My siblings and I are constant teachers and students to each other, so to **Flavio, Lyra, David, Rocío** and **Jaime**: this achievement of mine is for us all. I cannot forget to send my love to my nieces and nephews, **Silvia, Isabella, Alejandra, Paula, Laia, Sebastián and Flavio**. Loving acknowledgements to my brother in law **John Hincapié** for his contagious encouragement and to my sister in law **Ophélie Pain** for her kindness and understanding.

Finally, but the most important, the unconditional love I have constantly received from my parents **Sebastián** and **Mariela**. Despite numerous differences, they always supported myself and my siblings in achieving our dreams. More importantly through their own life experience, they set a constant example of loving what one chooses to do. I always admired my dad´s capacity for redeeming himself after difficult times and my mum´s genuine ability to forgive. These two lessons have been very helpful while doing my PhD. I thank them with a big smile of satisfaction and fulfilment with my life, their lovely gift to me.

I dedicate this thesis to my beloved father, who passed away about one year ago. Dad, I miss you but I am proud of you for having achieved all your dreams. The image of your eyes with its endless love and the energy of your hugs accompany me in the rest of my journey. Infinite thanks for everything you did for me. I love you.

These four pages were the only ones I wrote with my heart, as the thesis had to be written with my brain. However, the underlying basis of it is my passion and love for life, especially **my own**, so I will dedicate this last paragraph to the thesis itself. I must thank it for being the medium that helped me achieve skills that have made me both a better person and a better professional. I take this opportunity to ask it for forgiveness, as sometimes I denied its beauty and value. For all those days, nights, months and years that witnessed its birth, I humbly toast it with joy and respect. Despite all the life tests I encountered, I finished it and it will always be a nice reminder that it is essential to treasure every single minute lived.

With heartfelt gratitude,   Ella María.

Declaration

I certify that this work contains no material which has been accepted for the award of any other degree or diploma in my name, Ella María Llanos Rodríguez, in any university or other tertiary institution and, to the best of my knowledge and belief, contains no material previously published or written by another person, except where due reference has been made in the text.

I give consent to this copy of my thesis, when deposited in the Adelaide University Library, being made available for loan and photocopying, subject to the provisions of the Copyright Act 1968.

I also give permission for the digital version of my thesis to be made available on the web, via the Adelaide University's digital research repository, the Library catalogue, and also through web search engines, unless permission has been granted by the Adelaide University to restrict access for a period of time.

Ella María Llanos Rodríguez

4 June 2015

TABLE OF CONTENTS

LIST OF FIGURES

LIST OF TABLES

SELECTED NOMENCLATURE

m: coefficient of friction of the discontinuity

T_o: tensile strength [MPa]

E: Young's Modulus [GPa]

K: Permeability of the rock [mD]

K_{Ic}: Fracture toughness [MPa $\sqrt{m}$]

Q: Injection rate [ml/s]

T: Fluid temperature [˚C]

k: permeability of the natural fracture

K: dimensionless fracture toughness

t: time (s)

t_{mk}: characteristic time (s)

H: distance between closest tip of the hydraulic fracture and the discontinuity

L: distance between furthest tip of the hydraulic fracture and the discontinuity

P_f: internal pressure

Y_s: slip front location

L_*: characteristic length

h: evolving non-dimensional parameter

σ_x: horizontal compressive stress acting perpendicular to the interface [MPa]

σ_z: horizontal compressive stress acting parallel to the interface [MPa]

σ_y: vertical compressive stress [MPa]

τ: shear stress

σ_n: normal stress

ϕ: Porosity

ν: Poisson's ratio

ρ: Density [gm/cm^3]

μ: Viscosity [Pa·s]

ϖ: residual opening of a closed natural fracture

Σ_*: characteristic stress

Chapter 1

INTRODUCTION

1.1.   Preamble

Hydraulic or fluid-driven fractures are a type of fracture that may be man-made, which are created by injecting pressurized fluid into a rock mass. Dykes and other magma-driven fractures are a class of natural hydraulic fractures, and the theory developed for hydraulic fracture propagation can be applied to describe this type of transport mechanism of magma through the lithosphere (Spence and Turcotte, 1985). The idea of hydraulically fracturing an oil-producing zone to enhance production by creating highly permeable channels was developed by R. F. Farris in the 1920s (Brady et al., 1992). The first experimental hydraulic fracturing petroleum stimulation treatment was performed in 1947 and the first commercial application was carried out in 1949 (Brady et al., 1992). Since then, hydraulic fracturing has been widely used as a stimulation technique to enhance oil and gas recovery in low permeability reservoirs (McCoy et al., 1990; Clark, 1949). Highly permeable reservoirs have also been hydraulically stimulated with treatment designs modified accordingly (Boyer et al., 2005; Cleary, 1994; Smith et al., 1987). Hydraulic fracturing treatments have also been shown to improve wellbore stability, especially for sand production, during production (Chase et al., 1997; Bale et al., 1993).

Enhancing oil and gas production has not been the only use found for hydraulic fracturing, as it has been used as a stress measurement tool (Engelder, 1993). Other industrial applications of hydraulic fracturing include waste disposal into underground rock formations (Moschovidis et al., 1994), excavation of hard rocks (Young, 1999) and remediation projects in contaminated soils (Reed et al., 2001). Hydraulic fracturing has also been used to stimulate geothermal wells since the early 1970s (Entingh, 2000) and for cave inducement and preconditioning of rock masses in the mining industry (van As and Jeffrey, 2002; Jeffrey et al., 2013).

1.2.   Motivation

It is often assumed that hydraulic fractures grow as single, planar and symmetrical fractures (Hopkins et al., 1998; Mahrer and Aud, 1996). However the interaction between hydraulic fractures and pre-existing geological discontinuities such as cracks, joints, veins, faults and bedding planes, can result in a complex hydraulic fracture geometry (Nelson et al., 2007; Potluri et al., 2005). The term 'pre-existing' refers to the discontinuities that are present prior to a

fracturing treatment. Natural fractures, perhaps the most common type of pre-existing geological discontinuities, have been studied since the late nineteenth century (Pollard and Aydin, 1988). They are important as almost every reservoir can be considered to be fractured to some degree (Lamont and Jessen, 1963). Natural fractures may slow or arrest the vertical or lateral growth of the induced fracture, reducing total fracture length by fluid loss, or leakoff, into the formation, and enhancing the creation of secondary fractures (Warpinski and Teufel, 1987). The loss of fluid into natural fractures can be as much as 50 times greater than matrix leakoff (Warpinski, 1990). In naturally fractured reservoirs, leakoff is dominated by the natural fractures and depends on effective stress. Consequently leakoff becomes pressure dependent and more difficult to predict, and a stimulation treatment in a naturally fractured reservoir frequently ends sooner than planned (Britt et al., 1994).

The cost of fracturing a well depends on well location, treatment type and volumes pumped. In the United States alone, at least US$3.8 billion dollars were spent on hydraulic fracturing in 2005 (Bennett et al., 2006). In 2008, more than 50,000 fracturing jobs were completed worldwide at a cost of US$10,000 to US$6 million each (Montgomery and Smith, 2010). Worldwide, as of 2012, 2.5 million hydraulic fracturing jobs were estimated and over 1 million in the United States (King, 2012). According to Grand View Research (Market Research and Consulting) in their October – 2014 report, the hydraulic fracturing market worldwide was valued at US$41.62 billion in 2013 and it is expected to reach US$90.55 billion by 2020. This figure implies a compound annual growth rate (CAGR) of 11.8% from 2014 to 2020.

Unconventional resources include gas from tight sand, coalbed or coal seam methane, and shale gas. In contrast to conventional reservoirs, very few shale wells, for example, can achieve commercial production without hydraulic fracture stimulation. The analysis carried out by Grand View Research (2014) refers to the fracturing of shale gas as the leading application segment accounting for 28.3% of total market revenue in 2013. Shale gas is also being rapidly developed in China with expectations on the demand for hydraulic fracturing growing accordingly (Grand View Research, 2014).

Studies by the United States Energy Information Administration (EIA) suggest shale gas accounts for 49% of the country's total natural gas production in 2035, more than double its 23% share in 2010 (EIA, 2012). Estimated proved and unproved shale gas resources amount to a combined 542 Tcf out of a total resource of 2,203 Tcf Tight gas and coalbed methane production are

projected as the second and third largest source of domestic supply for the United States, averaging 6.1 Tcf and 1.8 Tcf per year from 2010 to 2035, respectively. The EIA and the Advanced Resources International (ARI) carried out an assessment of 137 Shale formations in 41 countries outside of the United States (EIA/ARI, 2013). The EIA/ARI study identified approximately 6,634 Tcf and 286.9 billion barrels technically recoverable of shale gas and oil resources respectively. According to the EIA/ARI (2013) report, Australia is within the 10 top countries with 437 Tcf technically recoverable from shale gas resources.

Gas exploration and production in the organic-rich Barnett Shale, of the Forth Worth Basin (Texas, the United States) has been ongoing for almost 35 years. This play may hold as much as 39 Tcf and its rapid growth began in the late 1990s with the combined application of slickwater-fracture stimulation and improved technology in horizontal drilling (Bruner and Smosna, 2011). In the Barnett Shale, natural fractures strongly influence hydraulic fracture behaviour because the horizontal principal stresses are about equal and the effective stress is low, which means the injected fluid is able to more easily open the pre-existing fracture network (Maxwell et al., 2003). The effectiveness of stimulating the Barnett Shale formation, in which commercial production is only achieved through fracture stimulation, by hydraulic fracturing is proven through experience but the fracturing process is not completely understood (Daniels et al., 2007).

About half of the United States sits atop gas or oil-bearing shale plays and seven areas located in the Lower 48 states are described as the most prolific ones. These regions are known as Eagle Ford, Bakken, Niobrara, Marcellus, Haynesville, Utica and Permian. According to the EIA these regions accounted for nearly 95% of domestic oil and 100% natural gas production growth during 2011 and 2013 (EIA, 2014). The use of hydraulic fracturing has extended considerably among these areas as commercial success of the Barnett Shale became apparent. Estimations for the Marcellus Shale, where activity spans just over nine years, suggest it may hold 50 Tcf (Bruner and Smosna, 2011).

Despite hydraulic fracturing enabling the hydrocarbon industry to significantly increase production, concerns have been raised about hydraulic fracture growth in unconventional reservoirs and the risk of fractures propagating from shale formations to reach overlying aquifers specifically concerns that this may impact on drinking water supplies. The popular concern is that fracturing might allow chemicals, gases, and other pollutants to leak into aquifers (Tiemann and

Vann, 2013). Fisher and Warpinski (2011) presented real fracture growth data collected during thousands of fracturing treatments in the Barnett, Woodford, Marcellus and Eagle Ford Shales. A number of containment mechanisms have been proposed to justify the mismatch observed between directly measured height growth and height growth predicted by conventional hydraulic fracture propagation models. The containment mechanisms include the presence of pre-existing discontinuities such as faults and natural fractures. Highly permeable layers, complex geologic layering and the formation of hydraulic fracture networks are part of the list as well as other factors like high fluid leakoff and rock mechanical properties. The complexity of the geology in the Woodford Shale includes significant faulting, highly dipping bedding planes, and overturned beds. Like in the Barnett and Eagle Ford Shales, the hydraulic fracture heights at Woodford are fairly contained. All the created fractures were reported to remain separated from the local drinking-water aquifers by large distances.

Osborn et al., (2011) report evidences for methane contamination of drinking water in aquifers overlying the Utica and Marcellus shale formations. However, Siegel et al. (2015) refuted this apparent association between domestic water contamination with the proximity to hydrocarbon wells located in north-eastern Pennsylvania where several operators are actively developing the Marcellus Shale. The extensive dataset used by Siegel et al. (2015) consisted of 11309 dissolved methane analyses from domestic water wells located near 639-gas and 22-oil wells. Siegel et al. (2015) included both the 92% unconventional wells, which were drilled with horizontal legs and hydraulically stimulated, as well as the remaining 8% conventional wells. This approach differs from the study by Osborn et al., (2011) which only included unconventional natural gas wells and was based on a smaller dataset.

The sampling method used by Siegel et al. (2015) involved the use of the inverted bottle method. Each water sample was paired with the closest geographic hydrocarbon well and in some cases multiple water samples were sometimes associated with the same well. The analysis involved plotting dissolved methane concentrations versus distance and assessing different concentration ranges using boxplots. Next, four different statistical testing combinations were applied. Consistent with the recommendation of Osborne et al., (2011), the data studied by Siegel et al. (2015) corresponds to pre-drill samples of downhole water collected between 2009 and 2011. Nevertheless, at the time of collection, other active gas wells were already present in the vicinity. Therefore, groundwater samples also reflect post-drill analysis. The results from the study by

Siegel et al. (2015) show no significant correlation between dissolved methane concentrations in groundwater and the presence of nearby wells.

Australia has a number of sedimentary basins which are prospective for shale gas and which would also require hydraulic stimulation (Cook et al., 2013). On the other hand, coal seam gas (CSG) reservoirs are shallower and have a higher concentration of gas than shale reservoirs but perhaps only half of CSG reservoirs require fracture stimulation. In Australia, the first commercial production of CSG began in 1996 and billions of dollars will be spent within the next few years to exploit coal seam gas wells to supply gas for liquefied natural gas (LNG) plants. Between 2013 and 2015 an estimate of $500 million are budgeted for the exploration of unconventional gas, mostly shale gas, in the Cooper Basin. Additionally, some basins such as the Cooper Basin contain tight gas in deep low permeability sandstones, which can be extracted by hydraulic fracturing.

Fracture stimulation has also been used to enhance the fluid conductivity in geothermal reservoirs, especially in hot dry rock (HDR) projects. The key element in successful heat extraction is the development of an Enhanced or Engineered Geothermal System (EGS) in a hot and impermeable rock mass. EGS are artificially made by using hydraulic fracturing or hydraulic stimulation to create a network of interconnected fractures in the hot rock, which allow transfer of the heat in the rock to water circulating through the artificially created system. Hydraulic stimulation involves injection of water at pressures below the level of the in situ minimum principal stress so that no opening mode fractures are propagated. The increased pressure in the naturally fractured rock mass reduces the effective normal stress acting across natural fractures, which promotes shearing. Shear induced dilation then results in an enhancement of their permeability (Pine and Batchelor, 1984). The overall size of the reservoir is a direct function of the total volume of water injected. However, the shape, orientation, and internal structure of the reservoir, are entirely functions of the local geological pre-existing discontinuities and conditions.

The first attempt to enhance the permeability in impermeable geothermal reservoirs was initiated at Fenton Hill (New Mexico, United States) in the early 1970s. The resulting stimulated fracture pattern at Fenton Hill did not match that predicted, as the pre-existing geological discontinuities and stress conditions controlled the fracture propagation (Duchane and Brown, 2002). A similar result was obtained from stimulation work in a hot dry rock project at Rosemanowes Quarry, Cornwall, United Kingdom (Tester et al., 2007).

Fracture stimulation works in the Paralana geothermal field in Australia were carried in 2011 (Reid et al., 2011). The fracture treatment was carried out at a pressure above the minimum principal stress level and the hydraulic fracture had proppant placed into it. The fracture network comprised at least four main structures, with the principal area of growth an en-echelon style tensile opening fracture apparently bounded by other structures. It appears that the stimulated volume is over-pressured, connected into a naturally over-pressured zone. This may assist in the recovery of hot fluids from the reservoir. The subsequent flow test confirmed the existence of a natural geothermal system at Paralana, which may aid future energy recovery from the hot rocks at depth (Reid et al., 2012).

The Australian EGS Habanero reservoir is interpreted to be a critically stressed low angle fault zone, which is prone to slip, triggered by injection. Active shearing of the Habanero fault during hydraulic stimulation creates both porosity and structural permeability. This permeability is anisotropic as reflected by the ellipsoidal shape of the seismic cloud (Holl and Barton, 2015). Real-time monitoring during the stimulation indicated seismicity commenced around the Habanero 4 well and was constrained by an apparent eastern boundary (McMahon and Baisch, 2013). At Habanero, induced seismicity begins at pressures considerably less than the overburden stress proving that shear failure happens along pre-existing weaknesses rather than through tensile opening of fractures (Holl and Barton, 2015). On the other hand the stimulation of the Jolokia 1 well, located 10 km from Habanero, is considered to be the only stimulation within this project that included some fracture growth at pressures above the minimum principal stress level. Image logs show a fracture network at the wellbore within the granite however the stimulation was not sufficient for production (Holl and Barton, 2015).

The effectiveness of a hydraulic fracturing treatment in a naturally fractured environment is governed by the treating pressure, in situ stresses, pore pressure, permeability, intact rock and natural fracture strength, as well as the natural fractures' spacing, distribution and orientation (Lecampion and Zhang, 2005; Warpinski and Teufel, 1987). However, it is clear from the above hydrocarbon and geothermal examples that an enhanced understanding of the interaction between hydraulic fractures and natural fractures is still needed to improve fracture stimulation procedures.

1.3.   Background

Rock formations are confined under stress which can be described by the magnitude and orientation of three principal stresses: σ_1 (maximum principal stress), σ_2 (intermediate principal stress) and σ_3 (minimum principal stress). Hubbert and Willis (1957) established the principle that hydraulic fracture propagation occurs in a plane normal to the least principal stress (i.e. the fracture lies in the σ_1/σ_2 plane) because such an orientation minimizes the energy necessary to propagate the fracture. Hydraulic fractures thus propagate in a vertical plane when σ_3 is the minimum horizontal stress and in a horizontal plane when σ_3 is the vertical stress or overburden stress (Figure 1). Hubbert and Willis (1957) considered the case for fractures propagating in a homogeneous, isotropic rock mass. However, rocks are frequently jointed and fractured as a result of deformations or tectonic movements.
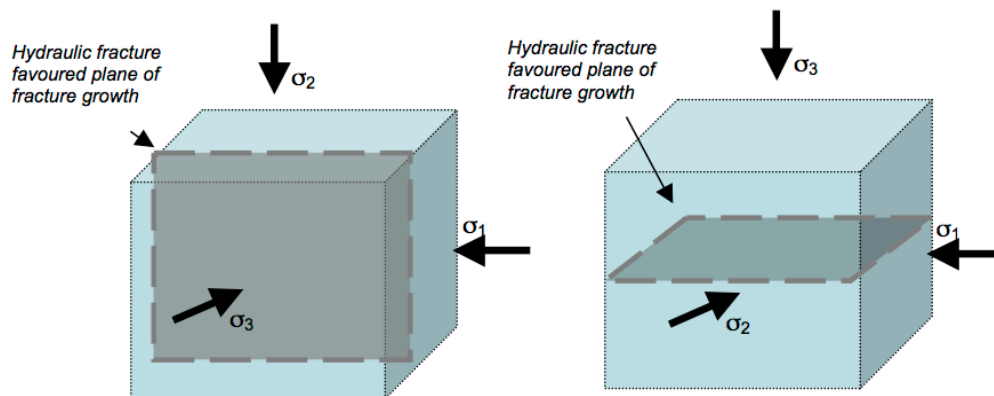
Figure 1. In situ stresses for vertical (left) and horizontal (right) grow of hydraulic fractures

The possible interactions between a hydraulic and a natural fracture can be classified as crossing, opening or arresting (Blanton, 1982), as shown in Figure 2. A hydraulic fracture propagating straight through a pre-existing discontinuity is described as crossing. An opening case occurs when the hydraulically induced fracture intersects the natural fracture, with the natural fracture then dilated. The opening case can also lead to crossing if the hydraulic fracture reinitiates on the far side of the natural fracture at a different point along the natural fracture. This leads to the development of an offset in the hydraulic fracture path also called a step-over (Cooke and Underwood, 2001). Crossing and opening have also been referred to as penetration and diversion respectively (Thiercelin et al., 1987). Based on ultrasound growth data and visual inspection, Bunger et al., (2015) defined "partial crossing" as another possible interaction. Partial

crossing refers to crossing cases but most of the fluid permeates along the interface and the velocity of propagation after crossing goes to zero.

Finally, arresting behaviour occurs when the hydraulic fracture terminates prior to, or upon reaching the natural fracture. Arresting is also known as blunting (Zhang et al., 2007), stopping (Lam and Cleary, 1982; Keer and Chen, 1981; Weertman, 1980) and terminating or abutment (Cooke and Underwood, 2001).
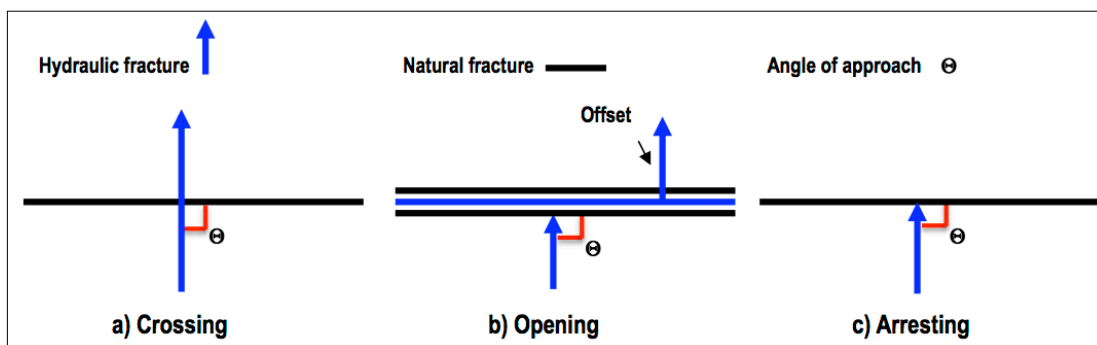
Figure 2. Possible interactions between a hydraulic and a natural fracture: a) Crossing, b) Opening and c) Arresting

The key aim of this thesis is to investigate the interaction between hydraulically induced and natural fractures. Consideration is limited to orthogonal crossing, i.e. cases where the angle of approach (Θ) between the hydraulic and the natural fracture is 90°, as depicted in Figure 2**. In this thesis Blanton's (1982) nomenclature for fracture interaction will be used.**

There are several methods for detecting and characterizing fractures in the subsurface which range from extrapolation of surface observations to sophisticated seismic and electromagnetic soundings (Long et al., 1996). Real-time microseismic data has also been used to monitor the propagation of hydraulic fractures in petroleum and geothermal wells (Maxwell et al., 2003; Hasting et al., 2011; McMahon and Baisch, 2013), and is an important tool to characterize the hydraulic fracture shape that develops. Llanos et al., (2015) used the areal extent of the seismic cloud to define the area of stimulated porosity and permeability and the permeability anisotropy ratio as input in the simulation model of the Habanero geothermal field in Australia. The results of this type of modelling feed into the financial models when making decisions on the future large-scale commercial development. Extremely sensitive tiltmeters can also be placed on the surface of the ground to monitor the dip, dip direction and volume of hydraulic fractures (Lecampion et al., 2005).

Not only is the cost of fracturing a well significant, as previously mentioned, but these monitoring methods add to the time and cost of the treatment. Therefore, in the design of a hydraulic fracturing treatment, it is important to know the conditions at which the abovementioned fracture interaction behaviours could occur so that precautions can be taken or the treatment design altered. For this purpose, the effect of natural fractures on the propagation of hydraulic fractures has been studied by numerous laboratory and field experiments as reviewed in the following section. However, the difference in scale and the different processes acting in the field mean that laboratory experiments can only consider a part of the overall process. Accurate design models must be used to establish the fracture parameters to be used in a full size treatment. The design models applied to commercial treatments must include a simple yet accurate criterion to determine if the fracture will cross, divert or blunt as it encounters natural fractures in the reservoir. Therefore this thesis includes some analysis for crossing interactions of fractures of various lengths that can be applied to large scale hydraulic fracture propagation.

This thesis considers the conditions under which hydraulic fractures cross, open or arrest at natural fractures, initially motivated by some observations from a field experiment carried at Northparkes E26 mine, located in New South Wales, Australia (van As and Jeffrey, 2002). Therefore laboratory experiments were conducted at the Hydraulic Fracturing Laboratory at CSIRO[1] Energy. Finally, numerical modelling to investigate these processes was done by using a theoretical approach and a 2D hydraulic fracturing modelling code called MineHF2D, both developed at CSIRO Energy.

1.4.   Literature Review

The most common hydraulic fracturing laboratory experiment setup to investigate the interaction of a hydraulic fracture with a frictional discontinuity consists of a nearly cubical rock sample set that contains one or more frictional discontinuities that can be then subjected to compressive and shear stress according to the objectives of the test, followed by the injection of fluids through a previously drilled wellbore. The parameters usually evaluated in the laboratory are those that can be manipulated and controlled by the experimentalist. These parameters involve the material properties (including the frictional properties of the interfaces), in situ stresses, the angle between

---

[1] Commonwealth Scientific and Industrial Research Organization, Clayton, Victoria, Australia.

hydraulic and natural fractures, the injected fluid rate and viscosity as well as the setup of the experiments.

Natural fractures have been simulated at a laboratory scale in many different ways. Zhou et al., (2008) for instance, reproduced pre-existing fractures by casting paper into a mixture of cement and sand. Teufel and Clark (1981) simulated discontinuities by pressing together two saw cut blocks made of materials of different stiffness. Sarmadivaleh and Rasouli (2014) created interfaces by placing two thin sheets of steel into a cast mortar sample before it set. Next, the interfaces were glued with four different adhesives to study the effect of the filling material.

The reproduction of the stress states of rocks in nature is done in the laboratory by axial compression tests, which can vary depending on the number of applied stress directions. Different authors have named these tests and loading types differently. Therefore, the following definitions as per Jaeger et al., (2007) will be used in this thesis. If only one pair of opposing sides of a sample is under compression the test is referred to as uniaxial. When lateral stresses of equal value are also applied, the load case is known as traditional triaxial tests. However, the more common state of stress occurs when three applied stresses differ from each other, which can be achieved with true-triaxial or polyaxial tests (Figure 3). For the case where the vertical stress is zero, the tests are referred to as biaxial.

In this thesis uniaxial and biaxial experiments have been carried out. The natural fractures were simulated by producing a frictional boundary between the rock slabs, similar to the approach used by Blanton (1982). The effect of the in situ stress and injected fluid viscosity were evaluated. Finally, the angle between hydraulic and natural fractures was always orthogonal.
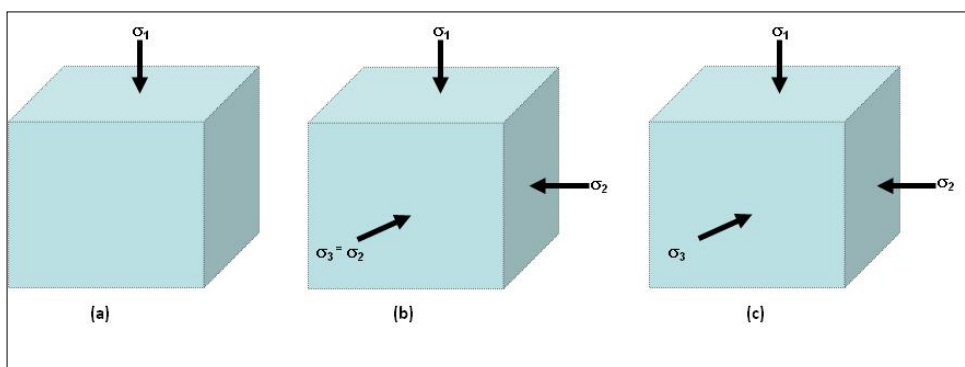
Figure 3. Cubic specimen under: a) uniaxial stress, b) triaxial stress, c) true-triaxial stress. After Jaeger et al., (2007)

The early reported efforts in understanding the mechanics of hydraulic fracturing in a naturally fractured environment at a laboratory scale include the triaxial tests by Lamont and Jessen (1962). Their results suggested the natural fractures have little effect on hydraulic fractures. The fabricated natural fractures by Lamont and Jessen (1962) were not prepared by grinding flat and uniform surfaces. From the observations obtained in the experiments carried out for this thesis (section 2.1.2), any unevenness or slight curvature of the sample surfaces used by Lamont and Jessen (1962) would have produced high local contact stresses that then promote crossing interactions. Daneshy (1971, 1974) ran similar tests to those by Lamont and Jessen (1962) and observed the hydraulic fractures appeared to cross the closed discontinuities and to arrest before crossing open discontinuities. Daneshy (1976) found that the nature of the discontinuity itself was sufficient to arrest a hydraulic fracture.

Laboratory studies by Haimson and Fairhurst (1969) and Daneshy (1974) showed the importance of the stress intensity factor, the mechanical properties of the material on either side of the interface and the shear strength of the interface itself in determining whether or not a fracture will cross the interface**.** Teufel and Clark (1981) suggested that a contrast in stiffness does not stop the fracture from crossing. The same conclusion was reached by Blanton (1982), Warpinski and Teufel (1987) and Beugelsdjk (2000). Teufel and Clark (1981) also concluded that a weak interfacial shear strength and increment in the minimum horizontal in situ stress in the bounding layers are the most significant factors in the containment of the hydraulic fracture. Shear slippage will occur if the shear strength of the discontinuity is not enough to resist the shear stress acting on the fracture plane, and this slip could eventually prevent the hydraulic fracture from crossing.

In general terms, in the laboratory hydraulic fractures have been found to cross discontinuities only under high differential stress conditions and angles of approach of 60° or greater (Blanton, 1982; Warpinski and Teufel, 1987). The orthogonal cases have proved to more often result in crossing outcomes. As for the setup of the experiments, Lamont and Jessen (1962) for instance, limited a hydraulic fracture to approach a discontinuity from one side and the fracture was allowed to propagate freely in the opposite direction. However, Blanton and Yost (1986) conducted experiments where the wellbore, from which the fracture was initiated, was located between two discontinuities.

Casas et al., (2006) designed two experiments based on similitude laws that are related to experimental parameters of the physical process of hydraulic fracturing, such as those reported

by de Pater et al. (1994), Bunger et al. (2005) and Lhomme (2005). Casas et al. (2006) and Sarmadivaleh and Rasouli (2014) confirmed the importance of scaling principles in the design of experiments in order to obtain similar results to field conditions.

Although these laboratory experiments offer an insight into the hydraulic and natural fracture interaction problem, the results are difficult to apply directly because they represent a significant simplification of the problem compared to the full-scale reservoir environment. Conversely, in situ experiments or field tests provide a more complete documentation of complex hydraulic fracture geometries in naturally fractured reservoirs, but the parameters acting in the field case are never completely defined.

Procedures like excavating and exposing an induced fracture directly, also called mineback, have been commonly used to obtain a detailed description, through photography and mapping, of the fracture path. However, these types of experiments are very expensive and as a result few have been conducted. Successful in situ experiments have been carried out at The United States Department of Energy (DOE) Nevada Test Site since the 1970s (Tyler and Vollendorf, 1975) but are no longer being conducted because of the associated costs. As an alternative, experimental wells that rely on sophisticated remote monitoring measurements have been used as a method of improving understanding of fracture behaviour (OTA-Report, 1985).

The mineback experiments conducted at the DOE site showed that differences in the material properties are not enough to arrest fracture growth. Instead, the results showed the importance of contrasts in the minimum in situ stresses in controlling the hydraulic fractures' height and in limiting fracture growth. Joints, faults and bedding planes affected the induced fracture geometry by increasing leakoff and preventing fracture growth as well as affecting the treatment pressure. Crossing, opening, offsetting and arresting behaviours were observed (Warpinski et al., 1982; Warpinski and Teufel, 1987).

The Bureau of Mines of the United States Department of the Interior developed the technique of stimulating vertical wells to remove gas from coalbed in advance of mining. Diamond and Oyler (1987) reported on twenty-two hydraulically stimulated boreholes in coalbeds mostly located in the eastern side of the United States. The report focuses on the effects of these stimulations on the coalbed and surrounding layers with this data obtained by mineback mapping of the fractures in the seams. Vertical fractures were evident for most cases and usually grew short distances in

lateral extent and were widely propped near the borehole. Horizontal fractures were observed in nearly half of the treatments and found to be within bedding planes at the top of the coalbed. Fluorescent paint added to the fracturing fluid helped in tracing the extent of the fractures. Penetration into pre-existing discontinuities in layers overlying coalbeds was observed. Several factors influenced the propagation of the induced fractures, e.g. type and volume of fracturing fluid, and depth and physical characteristics of the coalbed. The stimulations did not seem to affect the mining of the coal but the report suggested that injection rates and pressure should be controlled to minimize any chance of affecting later mining activities.

Vertical wells of the German Creek Mine Central Colliery, located in Queensland (Australia), were hydraulically fractured as a way of stimulating drainage of methane from the seam in advance mining (Jeffrey et al., 1992). The possibility of damages caused by the hydraulic fracturing operations to the rock layers overlying the coal seam was a concern. The fractures were mapped during and after mining. The results revealed that such stimulation treatment have no effect on mining operations. The coal mining research project also aimed to measure the size and geometry of the fractures formed (Jeffrey et al., 1992). One T-shaped horizontal and three vertical fractures were created in the coal seam. Investigations of fracturing treatments at the German Creek Mine, have shown that proppant in the fractures was distributed asymmetrically with respect to the injection well (Jeffrey et al., 1993). The authors suggested that one of the reasons for this asymmetry could be related to convection current transport of the proppant, i.e. sized particles mixed with fracturing fluid to hold the fractures open after a hydraulic fracturing treatment.

As a result of the asymmetry mapped in the German Creek field experiments, a laboratory model representing a shut-in hydraulic fracture was constructed to study gravity currents moving in a dipping fracture (Jeffrey, 1996). Gravity currents are convection currents driven by a density difference between fluids of different density or from density contrasts arising from sand slurry and the clear fracturing fluid. The results obtained in the laboratory support the hypothesis that gravity current transport of proppant can explain the shape of the fractures obtained at German Creek.

Some other hydraulic fracturing mining applications have also allowed a direct observation of fracture offsets in a naturally fractured rock mass. van As and Jeffrey (2002) in a study in the Northparkes E26 mine, located in New South Wales (Australia) observed significant offsets in the

hydraulic fracture at several locations, with minor offsets occurring frequently as the hydraulic fracture grew through pre-existing discontinuities (Figure 4). In the Northparkes E26 mine, fracture offsetting was the dominant interaction behavior when there was an acute angle between the induced and natural fractures. On the other hand, crossing seemed to be easier for hydraulic fractures oriented orthogonally to natural fractures. In addition it was observed that sometimes several hydraulic fractures branches can be formed as a result of the interaction (Figure 5).

A field experiment at the Northparkes E48 mine allowed measuring hydraulic fracture growth within pre-existing shear zones (Jeffrey et al., 2009). Many microseismic events were recorded during monitoring but, because of noise and events not being recorded by a sufficient number of accelerometers, only 5% of the events could be satisfactorily located and no clusters of these events coincided with the hydraulic fracture locations. Conversely, the outcome from the surface tiltmeter array data analysis resulted in a good fit when compared to the physical mapping and accurately predicting horizontal hydraulic fracture orientation. Any misfit was attributed to pressurization of a larger set of fracture segments with different orientation or strong shear displacement on a fault structure. Two piezometers were also used for monitoring but were not intersected by any of the hydraulic fractures. Some of the six successful hydraulic fractures crossed veins, natural fractures and shear zones. However, arresting was observed at a shear structure and at a sheared vein. Having two different types of rocks may have delineated a stress-change boundary promoting fracture arrest. Offsets also occurred in veined or shear zones. The larger offsets developed when a 45° dipping inclined shear zone cut across the induced fracture path.

Figure 4. Hydraulic fracture offsetting along a natural fracture. This photo was taken after mining of an access decline at Northparkes E26 mine. The hydraulic fracture growth was defined by using a red plastic proppant. The injected water contained fluorescein to serve as a fracture fluid marker. After van As and Jeffrey (2002)

Figure 5. Hydraulic fracture that consists of two parallel branches. This photo was taken after mining of an access decline at Northparkes E26 mine. The hydraulic fracture growth was defined by using a red plastic proppant. The injected water contained fluorescein to serve as a fracture fluid marker. After van As and Jeffrey (2002)

The experiments employed in the laboratory for the study of hydraulic fracture growth in naturally fractured reservoirs have allowed measuring parameters that cannot be made in the field. The field experiments complement the laboratory data by allowing mapping various geometries obtained after fracturing. However both approaches have their limitations and as a consequence the laboratory and field results provide a motivation for numerical and theoretical models to explore the fundamental physics of the hydraulic fracturing process.

Nevertheless there are also studies where no experimental information was available to support the findings. The research by Simonson et al. (1976) is an example when developing a theoretical two-dimensional analysis restricted to orthogonal discontinuities using elastic fracture mechanics. Simonson et al. (1976) concluded that when hydraulic fractures propagate from a low to a high modulus material, fractures are predicted to arrest at the discontinuity because the stress intensity at the fracture tip goes to zero as the fracture approaches the discontinuity. However, other studies have shown that it is more difficult, but entirely possible, for the hydraulic fracture to grow out of the soft rocks and propagate into stiff rocks. (Helgeson and Aydin, 1991; Erdogan and Biricikoglu, 1973).

Lam and Cleary (1984) developed a computer simulator to study slippage and friction effects. The point of intersection of an induced fracture with a discontinuity experienced the highest tensile stress only after discontinuity slippage had occurred, inducing fracture propagation into the discontinuity. Theoretical extensions of this work, begun by Keer and Chen (1981), were continued by Lee and Keer (1984), who investigated pressurized fractures using an incompressible fluid, propagating through an imperfectly bonded and rough discontinuity between two different materials. Their efforts were concentrated on study of offsetting and how to calculate fracture opening displacements and stress intensity factors for such cases.

Shaffer et al. (1984) developed a code that modelled fluid-driven discrete fracture propagation in jointed media. Linear elastic fracture mechanics was assumed, although the program can be combined with non-linear fracture mechanics theories. The accuracy of the code was verified through comparisons with results of experiments similar to those done by Blanton (1982). This model characterized the discontinuity frictional properties in more detail than the work of Blanton (1982), (Daneshy, 1974) and (Lamont and Jessen, 1962). Shaffer's (1984) analysis reported crossing or arresting, but no slipping or offsetting was considered. Shaffer et al. (1987) also developed a model that allowed tracking of the fluid front and flow pressures during the quasi-

static or dynamic fracturing of jointed rocks. The objective of the study was the calculation of displacements and stress intensity factors for the hydraulic fracture.

Jeffrey et al. (1987) considered the offset and branching effects when an interaction occurs. In their study they calculated the slip zone size near the tip of a hydraulic fracture growing in a pervasively fractured rock. The slip zone was shown to increase in size in proportion to fracture length. The energy available to extend the fracture was reduced by the energy consumed by non-elastic deformation in slip zones. A two-dimensional displacement discontinuity fracture model was also used and results of the model were compared with those of Blanton (1986). Single planar fracture propagation was found to require lower treating pressures than multiple sub-parallel fracture propagation. A post crossing mechanism for generating offsets was described. The inflation of a hydraulic fracture that had crossed a non-orthogonal frictional discontinuity without an initial offset caused frictional slip on the discontinuity and upon depressurising the hydraulic fracture, some of this slip displacement remains as an offset. For these simulations, fluid was not allowed to enter a joint and a re-initiation mechanism was not included.

Crossing, arresting and offsetting were the three main factors considered by He and Hutchinson (1989), who showed that when the fracture reaches the discontinuity, discontinuity dilation may occur before fracture re-initiation into the next layer if the ratio (energy release rate of the deflected fracture)/(maximum energy release rate needed by a penetrating fracture) is larger than a critical value. Dilation or deflection was also analyzed for single or double wing cases. Hydraulic fractures were not considered in the analysis.

Bobet and Einstein (1998a, b, 1996) used experimental results on gypsum samples that contained pre-existing fractures to look at parameters such as fracture initiation, propagation and coalescence of inclined fractures under uniaxial, triaxial and tensile loading. Their numerical model satisfactorily predicted the laboratory results based on their own modified version of a boundary element method developed by Chan et al. (1990). They concluded that a tensile fracture initiation occurs in the direction perpendicular to the maximum tensile tangential stress when the tangential stress reaches a critical value. In contrast, a shear fracture will occur in the direction of maximum shear stress. This study, however, did not consider fluid pressurisation or flow in the fractures.

Bahorich et al. (2012) focused their attention on the impact of cemented natural fractures, as opposed to frictional interfaces, on the propagation of hydraulic fractures. The discontinuities were modelled by embedding thin slides of glass, Berea sandstone into blocks of cured gypsum plaster. Hydraulic fractures were then grown through the blocks and their interaction with the embedded discontinuities was studied by dissecting the block. The authors reported no clear effect of the permeability of the discontinuity on the interaction. A linear guar-based gel was injected into the blocks under true-triaxial stress conditions. The effects of contained and uncontained height growth were also evaluated. The experiments had much lower confining stress and dimensionless time than average field treatments due to the limited size of the blocks and the low stress load frame used. Three propagation scenarios were obtained starting with a hydraulic fracture opening the block-discontinuity bond and sometimes propagating through the thin slide onto the host rock. Bahorich et al. (2012) referred to this as diversion, which was more common in tests where the natural fracture was non-orthogonal to the maximum horizontal stress. The second case describes a hydraulic fracture that does not cross the natural fracture but bypasses or propagates around it. Additionally opening of a weakly bonded interface without diverting along the tips was observed with orthogonal intersections. The third case corresponds to a hydraulic fracture bypassing a natural fracture by diverting along it to eventually form separate fractures from the ends of the natural fracture. Crossing of the natural fracture was not found and Bahorich et al. (2012) suggest it would only be possible if the hydraulic fracture breaks the discontinuity.

Additionally, Bahorich et al. (2012) tested two sizes of natural fractures, tall and short but with the same length and thickness. The effect of the tall natural fracture was observed as promoting diversion in addition to, or instead of, bypass. On the other hand, in experiments with shorter natural fracture, the hydraulic fracture sometimes exhibited only bypass and interface opening and at other times a combination of diversion and bypass but never pure diversion. This implies the ratio hydraulic/natural fracture heights influences the final geometry. The lower the ratio the more likely the hydraulic fracture will divert into a new propagation path.

Dahi Taleghani and Olson (2014) numerically analysed the interaction problem for the case of cemented natural fractures by use of an extended-finite-element-method. The rock/cement fracture energy ratio required for crossing of the natural fracture was higher for oblique cases than it was for orthogonal approach angles. When this ratio was less than the threshold, the discontinuity diverted the hydraulic fracture along the natural fractures to eventually extend from

the natural fracture tip. Hydraulic fractures that were double-deflected at a discontinuity were also modelled. The results demonstrate the sensitivity of the final fracture geometry to the differential stress and the orientation of discontinuites with respect to the maximum compressive stress.

Hydraulic fracture arresting behaviour due to frictional slip and discontinuity opening has been modelled by Cooke and Underwood (2001) for a uniformly pressurized hydraulic fracture. Their results imply that the strength or weakness of bedding contacts is the main reason leading to arrest of the fracture. Arrest happens with weak discontinuities, while propagation occurs through strong discontinuities. Similarly, Gudmundsson and Brenner (2001) studied the effect of stiffness contrasts and the distance between the hydraulic fracture tip and the discontinuity. Gudmundsson and Brenner (2001) concluded that fracture propagation stops at stiff layers under compression, which have become stress barriers due to a concentration of compressive stresses. On the contrary under tension the stiff layers would concentrate tensile stresses favouring the hydraulic fracture propagation.

Numerical and analytical studies on hydraulic fracturing have been extensively carried out at CSIRO using MineHF2D, an in-house 2D boundary element model. These studies have provided important information and developments, such as a model for shear fracture growth (Zhang et al., 2005a; Zhang et al., 2004), which can be applied to studying the stimulation of hot dry rock reservoirs, although these papers do not consider interaction with natural fractures. In contrast, Zhang et al. (2005b) focused on the growth of hydraulic fractures orthogonal to natural fractures. The results indicated the hydraulic fracture could be potentially arrested by natural fractures with weak shear strength. In addition, that fracture re-initiation from secondary flaws with a small coefficient of friction is very difficult. Therefore, the role of friction and secondary flaws on the growth of hydraulic fractures perpendicular to natural fractures was studied further by Zhang and Jeffrey (2006). Additionally, the effects of modulus contrast, in situ stresses and fluid viscosities on the fracture interaction were explored by Zhang et al. (2006). It was found that for intermediate values of confining stress, use of low viscosity hydraulic fracturing fluids allows the fracture to grow into a discontinuity with moderate frictional strength. Fractures growing from a stiff into a soft layer seemed more likely to arrest at the discontinuity. Other results by Zhang and Jeffrey (2007) suggested the lower the tensile strength of the intact rock on the far side of the discontinuity the longer the offset resulting from fracture.

Some studies have led to mathematical expressions to provide a practical basis for predicting whether an induced fracture will cross and be diverted into natural fractures. These expressions have been developed empirically and theoretically and are referred to as crossing or fracture interaction criteria. Blanton (1982) for instance, based on his laboratory experiments, developed a formulation for predicting crossing or opening; however some of the parameters he used are difficult to measure in the laboratory or field. Warpinski and Teufel (1987) derived another criterion to predict whether the hydraulic fracture causes shear slippage or dilation of the natural fracture. However, neither Blanton (1982) nor Warpinski and Teufel (1987) considered the mechanical interaction between natural and hydraulic fractures; i.e., it was assumed the hydraulic fracture did not affect the in-situ stresses along the natural fracture.

Although previous authors have investigated hydraulic fracture growth through naturally fractured rock; few have compared field results with crossing criteria. Van As and Jeffrey (2002) compared their results from the study in Northparkes E26 mine (Australia) to the Renshaw and Pollard's (1995) crossing criterion, which is based on superposition of fracture tip stresses with far field stresses. Likewise, Blanton (1986) used his criterion to delineate areas where crossing and opening interactions could occur in Devonian shales of the Appalachian Basin (The United States). Blanton's criterion (1986) predicts the type of interaction between a hydraulic and a natural fracture under various angles of approach and states of stress. However, these criteria do not include interactions between the discontinuity and the main extending hydraulic fracture. **Renshaw and Pollard's (1995) together with Blanton's (1986) criteria are reviewed next as the starting point of the problem discussed in this thesis.**

1.5. Statement of the Problem Investigated in this Thesis

Renshaw and Pollard (1995) referred to pre-existing geological discontinuities as interfaces, and considered compressional crossing as the mechanism for a fracture to propagate through a discontinuity. This mechanism involves the propagation of a fracture tip across a material interface, which is more likely to occur as depth, and compressional stress increases. Unless the interface is strongly bonded, interface slip and opening may occur, reducing the stress concentration in the rock on the far side of the discontinuity from the approaching fracture. The stress intensity factor may increase with slip, but the potential for the fracture to cross the interface may be reduced because the tip stress cannot be transmitted across the interface. As a

result, the fracture may arrest. However, crossing is likely to occur if the stresses normal to the interface prevent slip and opening.

Compressional crossing is assumed to occur by means of re-initiation rather than via continuous propagation. Re-initiation implies the growth of a new fracture on the other side of the interface, initiated by the stresses ahead of the approaching fracture tip. Renshaw and Pollard (1995) assume that re-initiation requires less compression than continuous propagation. Hence, the minimum amount of compression required for compressional crossing to occur is determined by the compression required for re-initiation.

Renshaw and Pollard (1995) used mechanical loading to propagate the fractures, i.e. they did not inject any fluids to induce the fractures. Instead, three slabs of brittle material were compressed and a fracture was initiated by driving a wedge device into a hole or slot previously made in the central slab (Figure 6). The fracture propagated towards the interfaces and arresting or crossing behaviours were recorded as a function of the compression applied across the interface and the interface frictional properties.
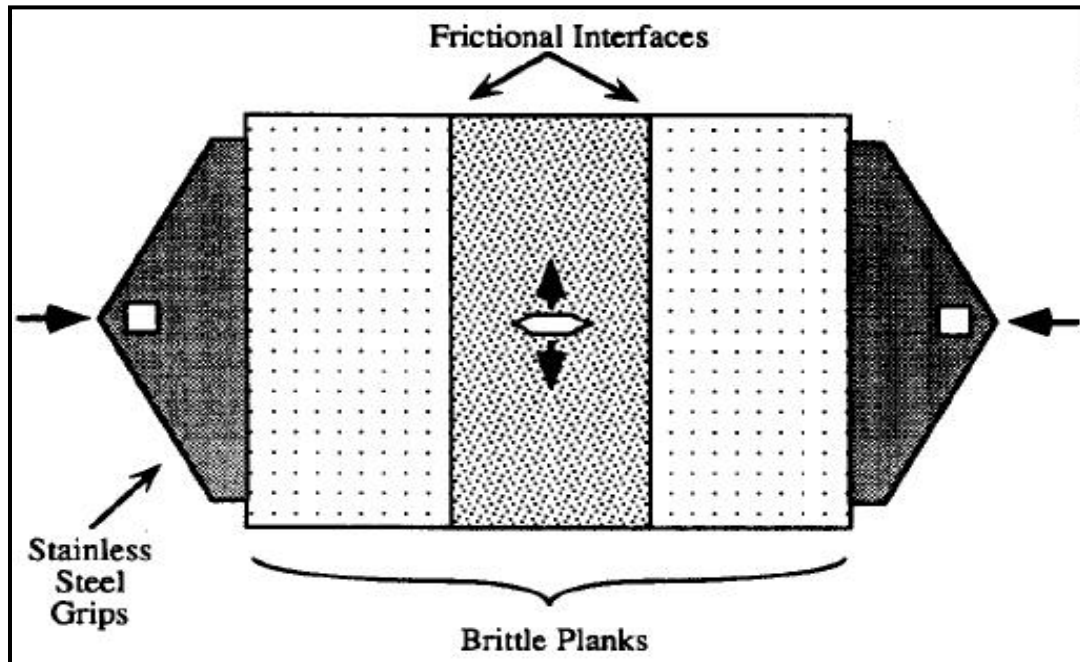
Figure 6. Schematic diagram of Renshaw and Pollard's (1995) compressional crossing experiment. After Renshaw and Pollard (1995)

The Renshaw and Pollard criterion (1995, herein referred to as R & P) is applicable to frictional interfaces orthogonal to the induced fracture path, and states that "*compressional crossing will*

occur if the magnitude of the compression acting perpendicular to the frictional interface is sufficient to prevent slip along the interface at the moment when stress ahead of the fracture tip is sufficient to initiate a fracture on the opposite side of the interface", (Renshaw and Pollard, 1995). When applied to hydraulic fracturing, this criterion suggests that hydraulic fractures, which grow in the plane of the maximum and intermediate principal stresses, will grow more readily through pre-existing geological discontinuities in the direction of the maximum principal stress (σ_1).

In the R & P (1995) crossing criterion (equation 1), σ_x and σ_y are the far-field effective stresses acting parallel and perpendicular to the hydraulic fracture plane respectively; m is the coefficient of friction of the discontinuity and To is the rock's tensile strength. The left hand side of the equation is defined as the "Crossing Stress Ratio" (CSR).

$$\frac{\sigma_x}{\left(T_o + \sigma_y\right)} > \frac{m+1}{3m}$$

Eq. 1

Blanton's (1986) laboratory work was one of several studies that have demonstrated compressional crossing. Contrary to Renshaw and Pollard (1995), Blanton (1986) considered the role of fluid within the fracture and developed his criterion from results of laboratory scale hydraulic fracturing tests. Blanton's criterion (1986) states that "*crossing will occur when the pressure required for re-initiation is less than the opening pressure of the natural fracture*". The configuration of the tests was intended to model a wellbore located between two vertical fractures (Figure 7) and only opening and crossing were observed.
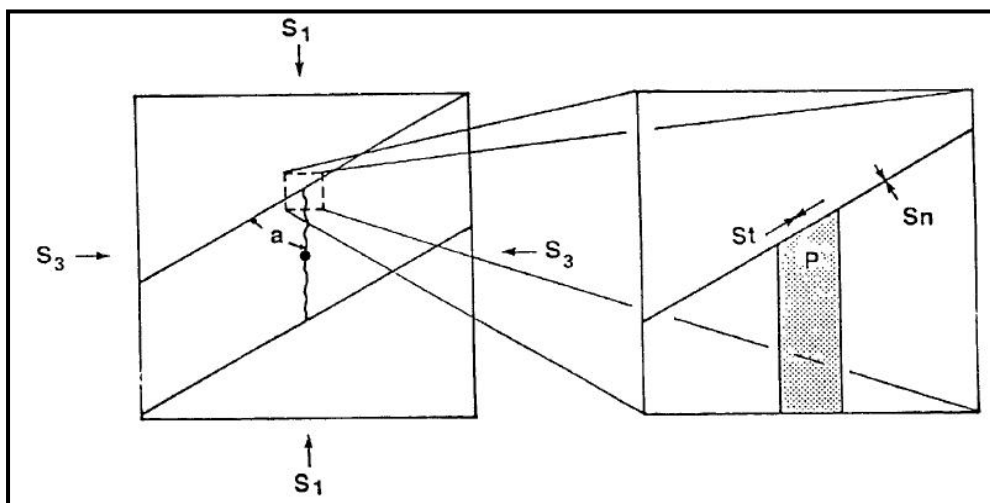
Figure 7. Schematic diagram of Blanton's (1986) test configuration. After Blanton (1986)

Blanton's (1986) published crossing criterion (equation 2) states.

$$(S_1 - S_3)/T > -1/(\cos 2a - b\sin 2a)$$

Where S_1 and S_3 are the maximum and minimum principal stresses respectively and T is the magnitude of the tensile stress required to fracture the rock. The angle between maximum principal stress direction and the natural fracture is labelled as 'a'. The parameter 'b' depends on the coefficient of friction and the length over which slippage has occurred on the natural fracture divided by the half-length of the section of the natural fracture that is open. When there is no slippage b goes to infinity. Blanton's results (1986) indicate that crossing is more likely to occur under high differential stress (S_1-S_3) and high angles of approach (a) which were the only parameters changed during the experiments. Opening seems to be favoured by low stresses and low angles of approach.

Gu and Weng (2010) and Sarmadivaleh and Rasouli (2013) extended the R & P (1995) criterion to include hydraulic fracture crossing of frictional interfaces with cohesion at non-orthogonal intersection angles. Hereafter the criteria by Gu and Weng (2010) and Sarmadivaleh and Rasouli (2013) will be referred to as e - R & P (2010) and m – R & P (2013) respectively. The e - R & P (2010) could not be expressed as an explicit equation but crossing and non-crossing can be determined by using a simple code routine to solve a quadratic equation. For smaller intersection angles Gu and Weng (2010) found slip is more likely to occur and hence minimizing the possibilities for crossing. Fracture re-initiation was considered to be perpendicular to the maximum principal tensile stress direction. Contrary to Gu and Weng (2010) the m – R & P (2013) was expressed in the form of a single analytical formula. Sarmadivaleh and Rasouli (2013) modified the interface shear condition by adding an apparent coefficient of friction to account for cohesion to the physical friction coefficient used by Renshaw and Pollard (1995). Using similar approaches to Renshaw and Pollard (1995), Sarmadivaleh and Rasouli (2013) derived a crossing stress ratio (shear strength over maximum horizontal stress). If the apparent coefficient of friction is zero the case corresponds to the R & P (1995) criterion and as it increases so does the ratio and higher the chances for crossing. The crossing ratio becomes less dependent on the coefficient of friction and crossing is more likely for angles higher than 60°.

The core of R & P (1995) criterion is to simultaneously require no slippage on the interface and that for the fracture initiation condition, that the maximum tensile stress acting parallel to the

interface, hence producing a new fracture perpendicular to the interface, matches the tensile strength of the rock. Gu and Weng (2010) and Sarmadivaleh and Rasouli (2013) also assumed that if slip occurs then crossing is not possible. However, Gu and Weng (2010) required that the maximum principal stress must equal the rock tensile strength for a new fracture to initiate on the opposite side of the interface. This tensile stress may not be perpendicular to the interface. This difference in the fracture initiation condition is reflected in the results, which suggest that for orthogonal cases a lower stress ratio is required for crossing to occur according to the Gu and Weng (2010) criterion when compared to the R & P (1995) criterion.

Gu et al. (2011) validated the e – R & P (2010) criterion using laboratory experiments, which included fluid injection into sandstone blocks under true–triaxial stress conditions. A discontinuity was cut at 45°, 75° and 90° and both of the faces were ground smooth and flat. The e - R & P (2010) criterion proved to be in good agreement with experiments by Blanton (1982). Additionally, Gu and Weng (2011) and Sarmadivaleh and Rasouli (2013) indicated consistency between the predictions by using their criteria and the results published by Zhou et al. (2008).

In developing his criteria, Blanton (1986) uses parameters that are difficult to quantify, and his analysis does not include the stress change caused by the interaction between the hydraulic and natural fractures. Blanton (1986) also assumed that a simplified shear stress distribution exists on the pre-existing geological discontinuity. In addition, neither Renshaw and Pollard (1995) nor Blanton (1986) considered fluid viscosity effects on crossing behaviour. Finally, Renshaw and Pollard (1995), Gu and Weng (2010) and Sarmadivaleh and Rasouli (2013) do not allow fracture re-initiation after slippage. Renshaw and Pollard (1995) also assumed unbounded discontinuities and did not consider surface curvature and roughness, or any features that could result in a stress concentration and promote or retard crossing.

In this thesis the effects of stress, fluid viscosity and slippage are considered with regards to the interaction between hydraulic and natural fractures oriented orthogonally to each other. Additionally, this thesis considers the effect of inhomogeneities (e.g. flaws, curvature mismatches or roughness) that result in a local change in stress or strength and may influence fracture crossing.

As was previously mentioned; van As and Jeffrey, (2002) compared their results from the study in Northparkes E26 mine (Australia) to the Renshaw and Pollard's crossing criterion. The hydraulic

fractures formed at the mine through site grew with sub-horizontal orientations. These fractures grew through a rock mass with multiple sets of nearly vertical natural fractures which, depending on their location, were subject to normal stresses that range in magnitude from the maximum horizontal stress to the minimum horizontal stress (the intermediate principal stress at this site). Stress and rock strength conditions at Northparkes were such that the R & P (1995) criterion predicts the hydraulic fracture would cross the natural fractures oriented perpendicular to the maximum principal stress (σ_1) and would be arrested by the natural fractures oriented perpendicular to the intermediate principal stress (σ_2). At the Northparkes E26 site, crossing occurred in both directions (van As and Jeffrey, 2002).

Observations of the geometry of the induced fracture were limited and the mapped fracture may have been circular in shape (equidimensional in σ_1 and σ_2 directions) or it may have been elliptical in plan view (elongated in σ_1 direction), as seen in Figure 8. Having a clear understanding of the effect of the stress field on the obtained hydraulic fracture shape is important for the design of borehole layout for preconditioning treatments (van As and Jeffrey, 2002).
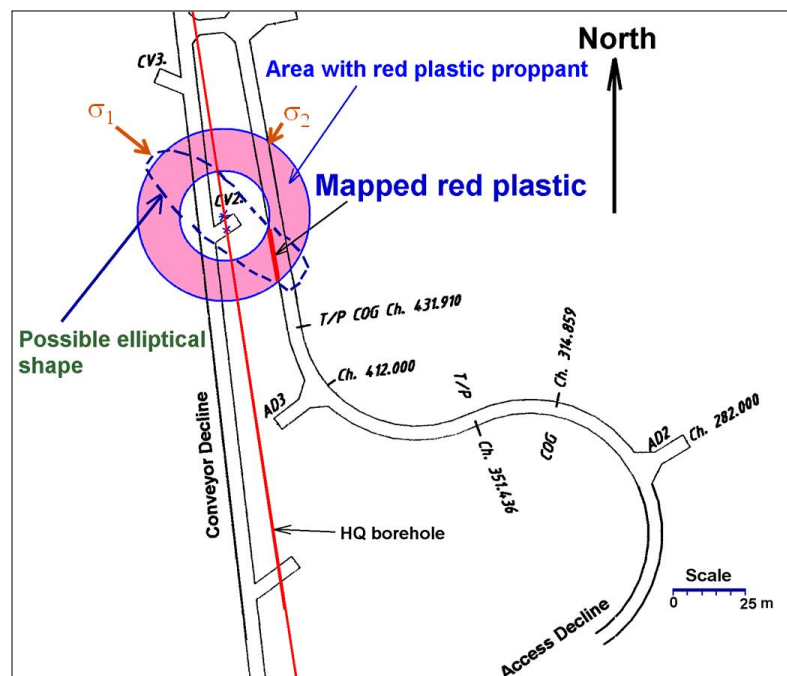
Figure 8. Plan of site after tunnels were extended through the area of hydraulic fractures. After van As and Jeffrey (2002)

The experiments carried out for this thesis also allow investigating whether hydraulic fractures in a naturally fractured rock tend to be more elongated in the maximum principal

stress (σ_1) direction. The findings of this thesis can be applied to the hydraulic fracture height growth problem if the frictional interfaces are considered to represent weak bedding planes.

Encompassing solid and fluid mechanics and their interaction, mathematical concepts and tools to quantify the physical processes taking place at each scale, have been developed. The discovery of the scaling laws is attributed to G.I. Taylor in 1940 (Barenblatt, 2003). The ultimate goal of scaling is to reduce the number of parameters on which the solution of a problem depends. The scaling presented herein is based on the work of Detournay (2004) which was carried out to better define the problem parameters controlling the propagation of a hydraulic fracture. Depending on the main energy dissipative mechanism two scalings can be derived: viscosity-dominated and toughness-dominated (Detournay, 2004). In the former regime, most of the energy required for a hydraulic fracture to grow in a rock medium is used by viscous fluid dissipation. In the toughness-dominated regime, the viscous dissipation is small compared to the energy consumed in fracturing the rock at the hydraulic fracture tip.

The effect of the fracturing fluid viscosity on the stress field around a hydraulic fracture has been shown to be significant by Lecampion and Zhang (2005) who analysed the onset of slip on a frictional natural fracture interacting with an approaching hydraulic fracture, that was either propagating in the viscous- or toughness-dominated regime. The analysis of Lecampion and Zhang (2005) indicated that the fracture propagating in the viscosity-dominated regime would induce slip on the natural fracture more easily than for a hydraulic fracture propagating in the toughness-dominated regime. This observation suggests that crossing according to Renshaw and Pollard (1995) and Gu and Weng (2010) should be more difficult for viscous-dominated hydraulic fractures. This finding contradicts the behaviour of the experiments undertaken in this thesis (Llanos et al., 2006). Thus it appears that the effect of viscosity on the crossing interaction is complex, and cannot be predicted based only on whether slip is predicted to occur on the natural fracture before the hydraulic fracture intersects it.

Since 2010, Schlumberger and CSIRO Energy have worked together in building a parametric model for understanding the problem of fracture interaction that combines the effects of stresses, geometry and fracture properties (Chuprakov et al., 2010). For this work, Chuprakov et al. (2010) considered a uniformly pressurized hydraulic fracture, which represents a toughness-dominated case. The interaction problem was broken into three stages of propagation of the hydraulic

fracture: approaching, contacting and infiltrating a discontinuity, which in this case it was a fault.

These initial efforts lead to the development of an analytical model called OpenT (Chuprakov et al., 2013a, 2013b). OpenT is a comprehensive model, which is sensitive to fracture parameters such as width, length, height and opening. Additionally, OpenT takes account of how the conditions of fluid injection such as pump rate and viscosity influence the interaction. The results by Chuprakov et al. (2013a, 2013b) agree with results of accurate numerical solutions by MineHF2D, microseismic field data and various laboratory experiments by Blanton (1986), Warpinski and Teufel (1987) and Gu et al. (2011). OpenT has been integrated into Schlumberger's unconventional fracturing design model (UFM), which is capable of simulating complex fracture network propagation in a naturally fractured environment (Kresse et al. 2013).

Figure 9 shows the geometry used by Chuprakov et al. (2013a, 2013b), which includes a pressurized hydraulic fracture in contact with a discontinuity, which was initially unpressurized. As the contact progresses, the intact formation pore pressure of the discontinuity is changed to equal the fluid pressure inside the hydraulic fracture. The name OpenT was given from the slanted T-shape obtained upon contact. Two principal stresses are acting parallel and perpendicular to the hydraulic fracture, Σ_{11} and Σ_{33}. From Chuprakov et al. (2010), OpenT considers offset to occur at the end of the open zone. Although Renshaw and Pollard (1995) did not consider slip or opening to occur along the interface, they assumed fracture re-initiation occurs prior to the fracture reaching the discontinuity. On the other hand, Blanton (1986) did consider offset as a possibility but contrary to Chuprakov et al. (2010) assumed it would always occur in the sliding zone.
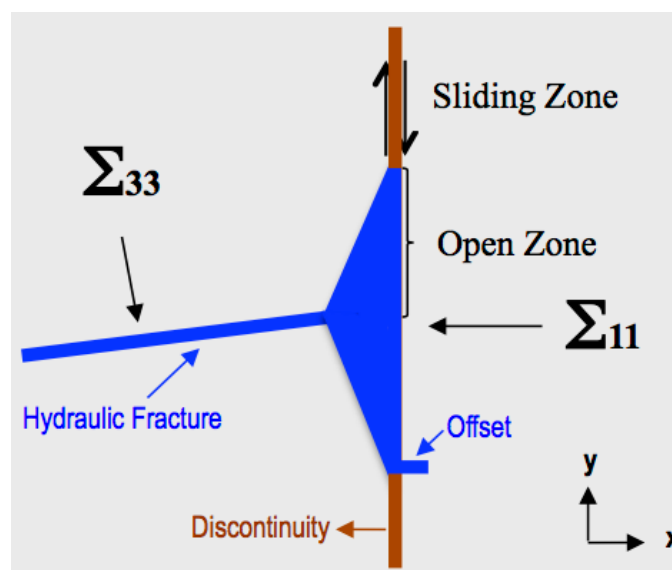
Figure 9. Geometry of OpenT by Chuprakov et al. (2013a, 2013b).

Recently, Chuprakov and Prioul (2015) developed the FracT and LamiFrac models. The former is an improved version of OpenT as it considers non-uniform opening of the hydraulic fracture. Like the OpenT model, FracT considered a pressurized fracture that has grown into a natural fracture to form an approximate T-shape geometry. In addition, they consider a second case where the hydraulic fracture simultaneously reaches two weak cohesive discontinuities that are parallel to each other, i.e. a two-sided fracture contact. To study the fracture arresting at and interface activation, the analytical solution of the problem narrows to the length of the slip zone, fracture width at the contact with the interface and the post-contact fracture volume. The result is given as explicit expressions for these characteristics, which were evaluated as a function of the relative hydraulic fracture net pressure and dimensionless interface toughness.

Chuprakov and Prioul (2015) by means of FracT found that the sizes of both the slip zone and fracture width increase with the net pressure. The volume of the hydraulic fracture at the contact point with the two natural fractures increases as a result of the fracture widening and the width change is reflected in a sudden drop of the net pressure there. If the relative net pressure is small then the pressure drop is also small. The activation of the contacted interfaces causes a decrease of the elastic energy of the hydraulic fracture and subsequently it stops propagating. Leakoff was considered to reduce the crossing function and cause full arrest at the interface. The one-sided contact T-fracture may exhibit arrest at contact but continuous propagation at the other tip. The OpenT and FracT models predict the outcome of a viscosity dominated hydraulic fracture interaction with a natural fracture, accounting for interface opening and sliding to predict blunting or re-initiation based on a combined stress and fracture energy approach.

LamiFrac allows numerical simulations of the 3D fracture propagation through several weak bonded discontinuities. The results indicate a retarded and intermittent vertical growth of the hydraulic fracture in the direction of the discontinuities but continuous in the horizontal direction. This height containment issue was more prominent for toughness-dominated conditions.

In this thesis the effect of the viscosity of the injected fluids on the crossing mechanics was studied by carrying out experiments for conditions where the energy to propagate the hydraulic fracture was dominated either by fracture toughness or by viscous dissipation. In addition, in order to understand the mechanics surrounding frictional crossing interactions, the effect of slip prior to intersection is studied using numerical and analytical methods. The numerical modelling was undertaken using MineHF2D, a hydraulic

fracturing modelling code, developed at CSIRO Energy. MineHF2D allows investigation of various interaction cases, including the fracture mechanisms of re-initiation of a hydraulic fracture from the far side of a natural fracture. Additionally, the zone of slippage on the natural fracture can be modelled as a hydraulic fracture grows toward it. Finally, this thesis studies the stress in the rock and on a natural fracture prior to the occurrence of frictional slip, using analytical solutions.

1.6.   Summary

Since its first commercial application, 65 years ago, hydraulic fracturing has become a widely used stimulation technique with multi-stage jobs costing up to US$6 million dollars per well. Although natural fractures have been studied since late 19th century, the understanding of the impact of discontinuities on hydraulic fractures growth remains a scientific challenge and has been addressed in the past by means of field, laboratory, and numerical and analytical studies.

Three possible interactions between a hydraulic and a natural fracture have been defined and classified as crossing, opening or arresting (Blanton, 1982). Several criteria to predict whether a hydraulic fracture will cross a pre-existing discontinuity have been developed (e.g. Renshaw and Pollard, 1995; Blanton, 1986; Gu and Weng, 2010; Sarmadivaleh and Rasouli, 2013). However, these criteria do not include interactions between the discontinuity and the main extending hydraulic fracture.

This thesis consists of experimental and numerical work to extend Renshaw and Pollard's (1995) work by studying hydraulic fracture interaction and crossing, as their experiments were done with no fluids. An analysis of and comparison to Blanton's (1986) and Gu and Weng's (2010) criteria has also been done. Additionally, the experimental data and modelling calculations are compared in detailed to the works by Chuprakov et al. (2010) and the comprehensive OpenT model (Chuprakov et al., 2013a, 2013b).

The purpose of the experimental and numerical approach undertaken in this thesis is to contribute to the development of a more accurate crossing criterion. This is required for determining borehole layout and injected volume for preconditioning applications in mining, and for designing hydraulic fracturing treatments for stimulation of naturally fractured hydrocarbon (e.g. shale gas) or of geothermal reservoirs.

A crossing criterion can be implemented into a hydraulic fracture design model to allow predictions as to whether the hydraulic fracture will or will not cross natural fractures. This approach avoids requiring the computational effort of a model like MineHF2D for each design. Natural fractures in the reservoir can be defined by using suitable statistical methods prior to the application of the fracture design model.

The methodology and the results of the experimental work are presented in Chapters 2 and 3 respectively. Chapter 4 provides the proposed mathematical model and scaling, followed by the modelling results presented in Chapter 5. This thesis ends with a comparison of the experimental data to the modelling results as presented in Chapter 6, followed by a list of conclusions and recommendations for further research in Chapter 7.

The following are specifically addressed in this thesis:

1. **The conditions leading to slip along the natural fracture prior to the intersection by the hydraulic fracture.**

2. **Analysis of stress and rock strength conditions that lead to hydraulic fracture crossing, opening, or arresting at a natural fracture.**

3. **Evaluation of above conditions for cases where the energy to propagate the hydraulic fracture through a natural fracture is either dominated by fracture toughness or by viscous dissipation.**

4. **An experimental investigation into whether hydraulic fractures propagating through naturally fractured reservoirs, grow further in the direction of the maximum compared to the intermediate stress direction acting on the discontinuities, to become elliptical in shape.**

5. **An evaluation of the effect of inhomogeneities of the natural fracture, which could influence the interaction between a hydraulic fracture and a pre-existing geological discontinuity.**

Chapter 2

LABORATORY METHOD

Renshaw and Pollard (1995) and Blanton (1986) developed criteria for use in predicting if a propagating fracture would cross a frictional interface in its path. The work in this thesis extends the existing body of work by studying the problem of understanding the interaction between a hydraulic and natural fracture via laboratory experiments and a theoretical approach. This chapter describes the experimental method undertaken in the laboratory, while the results and discussion are presented in chapter 3. The theoretical study accompanying these experiments is documented in the second half of this thesis.

As reviewed in section 1.4, the most common hydraulic fracturing laboratory experiment setup consists of one or more cubical rock samples. These are usually constructed from a set of rock plates stacked together and compressed according to the objectives of the test, followed by the injection of fluids through a previously drilled wellbore. This type of setup, after modifications and improvements described below, was also used for the experiments carried out for this thesis. In addition, the setup and test procedure allowed for determining the final shape and surface features of the hydraulic fracture as affected by stress and discontinuity strength. The experiments also permitted studying the effect of inhomogeneities of the natural fracture, which could influence the interaction between a hydraulic fracture and a pre-existing geological discontinuity.

Test conditions were selected to investigate the fracture growth in sandstone blocks for a range of different fluid viscosities and applied stresses. Furthermore, the experiments undertaken for this thesis were designed to evaluate the crossing behaviour for two regimes of fracture propagation, namely where the energy to propagate the hydraulic fracture was dominated (1) by fracture toughness or (2) by fluid viscous dissipation.

The parameters that were controlled independently of the applied stresses involved the injected fluid rate and viscosity, and the frictional properties of the interfaces. The angle between hydraulic fracture plane and the plane of the natural fractures was kept orthogonal for all the experiments.

The reproduction of the stress states acting in rocks in nature is done in the laboratory by applying axial compression in one or more directions to the rock samples. For this thesis, uniaxial

and biaxial experiments were carried out and the work was done at the Hydraulic Fracturing Laboratory of CSIRO Energy, located in Melbourne, Victoria (Australia). The natural fractures or discontinuities were simulated by the flat frictional boundary between the rock slabs.

The procedure followed in the laboratory consisted of injecting honey-based fluid containing blue food dye at a rate sufficient to initiate and propagate a hydraulic fracture through the sandstone blocks. The reason for choosing honey for the injection fluid was that it provides an environmentally benign fluid with a Newtonian viscosity, and its viscosity can be relatively easily modified by adding or reducing its water content or by changing its temperature. The dye was added to help in observing the propagation path of the fracture at the end of each test. The total injection volume was held constant throughout the series of tests. The applied load, fluid temperature and injection pressure were recorded. In addition, by using rock material from one supplier, the rock strength, elastic properties, and permeability were also controlled, within the variability inherent in the quarry stone used.

2.1 Sample Preparation

2.1.1 Rock and Fluid Properties

Donnybrook sandstone, which is a quarry stone available in the immediate vicinity of Donnybrook in the south of Western Australia, was used for both the uniaxial and biaxial experiments. As each set of samples was subjected to stress during the tests, it is necessary to understand the behavioural and strength properties of the rock material under compression. The rock elastic moduli and fracture toughness also enter into how a hydraulic fracture propagates. The effect of Young's modulus contrast on fracture height containment has been studied theoretically and experimentally (Simonson et al., 1976; Teufel and Clark, 1981). The study by Gu and Siebrits (2008) shows that low-to-high and high-to-low moduli contrast can hinder fracture height growth. The laboratory experiments carried out for this thesis do not include layers with modulus contrast.

Likewise, since one of the aims of this thesis is to study the effect of the viscosity of the injected fluids on the crossing mechanics, a detailed knowledge of the physical properties of the fluids is required. The rock and fluid properties are summarized in Table 1. The details of the procedures followed to obtain the rock and fluid properties are available in Appendix A and Appendix B respectively.

DONYBROOK SANDSTONE	
Porosity ϕ [%]	15
Poisson's ratio ν	0.28
Young's Modulus E [GPa]	7.0
Permeability K [mD]	5 - 50
Discontinuity friction coefficient (m)* From triaxial tests	0.4 – 0.6
Tensile strength (T_O) * From Brazilian tests [MPa]	4.40
Fracture toughness (K_{IC})* From Lim's method [MPa $\sqrt{m}$]	0.58
FRACTURING FLUID	
Density ρ [gm/cm^3]	1.42
Viscosity μ [Pa·s] * At 20°C	1; 100
Injection rate Q [ml/s]	0.0158
Fluid temperature T [°C]	20.0
Injection volume /uniaxial test [ml]	12.5
Injection volume /biaxial test [ml]	25.0, 40.0
Fluid Behaviour	Newtonian

Table 1. Physical properties of the Donnybrook Sandstone and of the fracturing fluid

2.1.2 Surface Curvature

Initial testing was carried out on sawn sandstone plates that were not ground flat. The slightly curved nature of the sawn plates affected the results, which for example, produced high contact stresses when two convex curved plates with different curvature were pressed together. These high contact stresses then resulted in a crossing interaction even for nominally applied normal stress levels considerably lower than those expected for crossing to occur.

Upon determining that surface curvature was the source of this problem, the procedure was changed so that, before testing, slabs were ground flat to less than 0.02 of a millimetre across each face. For this purpose a 60 grit Kinik silicon carbide (GC 60 K V) grinding wheel was used on a large surface grinder. The plate edges, for the biaxial tests were also ground flat and parallel to minimize differential stress induced by loading applied to the face of the block consisting of these edges. Figure 10 depicts the surface profile obtained on one face of a block before and after grinding.
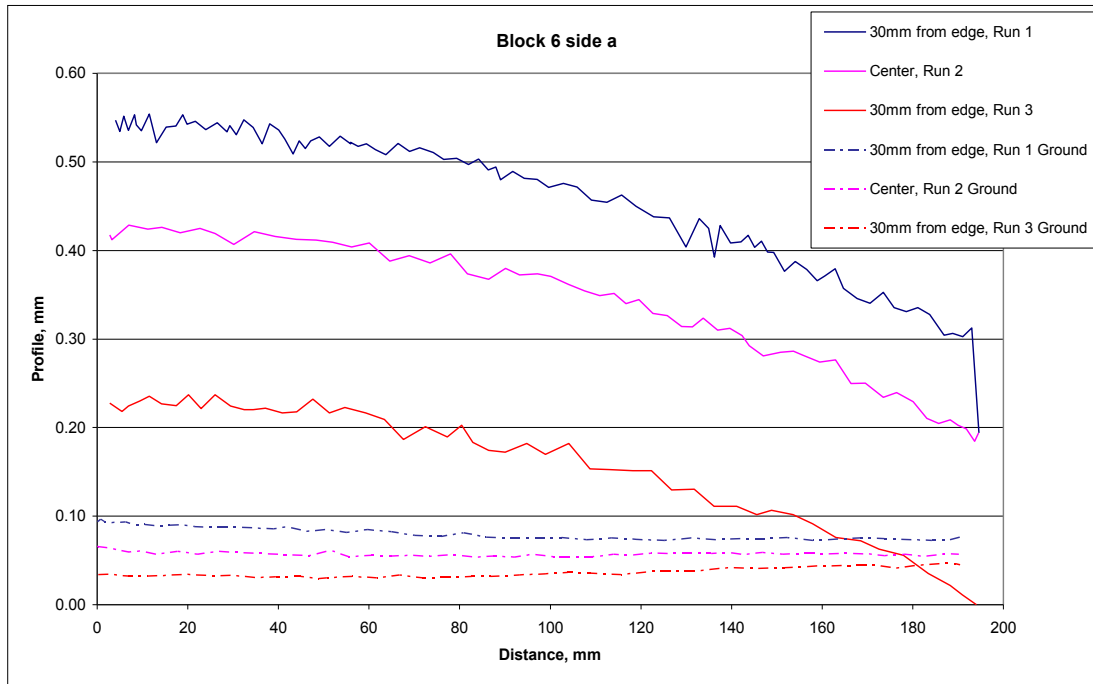
Figure 10. Surface curvature profile obtained for block 6 side a – Before and After Grinding (solid and dashed lines respectively)

2.1.3 Sample Dimensions

Initially five 12 x 12 x 4 cm plates were used for the uniaxial tests. However, stress concentrations at the borehole seem to have affected the stress on the nearest discontinuities. Therefore, in the polyaxial frame an initial biaxial test was carried out using a set of nine 36 x 40 x 4 cm thick plates. The central and two plates nearest to the borehole were cemented together prior to testing in order to simulate a monolithic thicker central layer. However fluid loss into the cement was observed after testing (Figure 11).

In order to avoid any stress disturbance from the hole affecting the stress on the first interface, the second set of uniaxial tests were run using a set of six slabs of size 20 x 20 x 4 cm with a thicker 10cm thick central slab that contained the borehole (Figure 12). For the same reason, the final test block configuration for the biaxial tests consisted of six 36 x 40 x 4 cm plates and a 12cm thick central slab (Figure 19). These thick central layers moved the first set of discontinuities away from the borehole so that stress concentration effects arising from the borehole did not affect the stresses on the discontinuities.
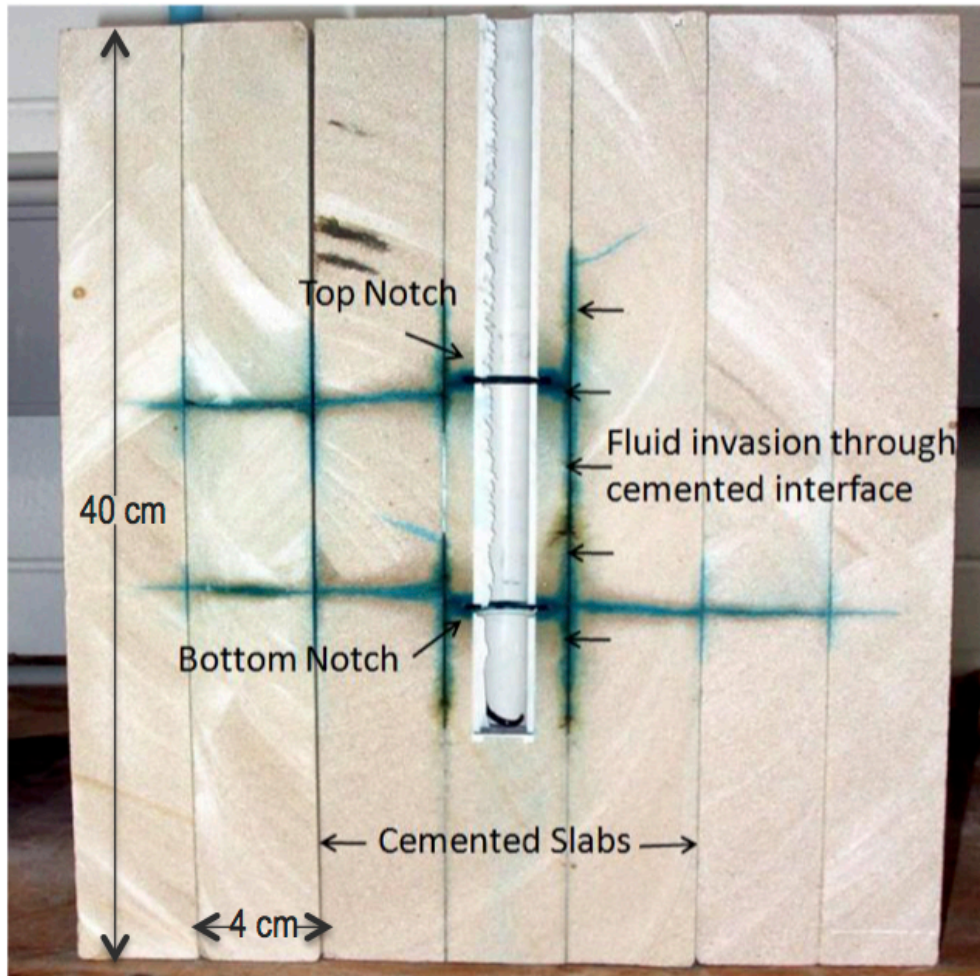
Figure 11. Borehole for biaxial setup

2.1.4 Borehole Details

A 22mm core drill was used to make a hole in each central slab. As the drilling mechanism requires water for cooling the bit and for removing the cuttings, the block was afterwards dried in the oven at 30°C temperature for approximately ten hours. The injection zone was cased or isolated from the rest of the wellbore by a 20mm polyvinyl chloride (PVC) tube sealed into the hole with epoxy (Figure 11 and Figure 12).
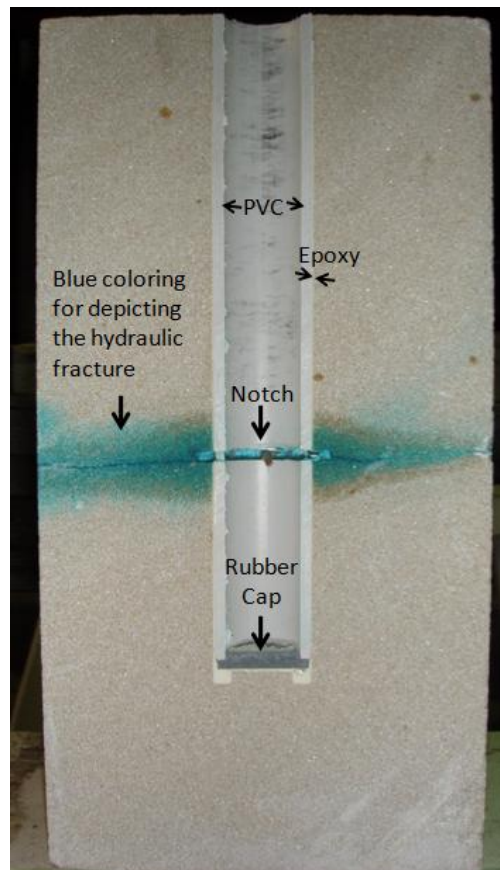
Figure 12. Borehole for uniaxial setup

The cylindrical piece of PVC tube to be used as casing was cut slightly longer than the hole and sealed at one end with a glued PVC or rubber cap. This tube was pushed into the hole, which contained a previously calculated volume of epoxy. The outer surface of the PVC cylinder was roughened with sand paper to provide an improved bonding surface and to prevent the epoxy from being unevenly displaced and potentially leading to borehole damage or collapse. It was observed that pushing the PVC into the hole too quickly could cause air bubbles to be trapped between the casing and rock that could potentially result in a poor seal and eventually a failed test.

Some of the epoxy collected at the hole collar was used to reinforce the upper end of the hole. The exposed bit of PVC was covered with tape to keep the inside of the hole clean. Both top and bottom of the sample were covered with a block of wood and then the PVC was clamped in the hole for twenty-four hours while curing the epoxy. The remaining excess length of PVC was trimmed as level as possible with the sample. A notch required for hydraulic fracture initiation was afterwards created using a pedestal drill fitted with a special notching bit. The final depth of the

notch into the cased borehole wall varied between 3mm and 5mm. Finally, the cased hole was reamed to ensure a good fit for the injection tool.

For the biaxial tests, two notches were machined at 15 cm and 25 cm below the top of the borehole, which allowed two fracture tests to be carried out in each block (Figure 11). The reasons for having two notches in the biaxial setup were to conserve test material and setup time and, more importantly, to allow two tests to be carried out under different stress conditions while keeping the rock properties and layering unchanged. For the uniaxial tests, each wellbore contained one machined circumferential notch located half way through the block, i.e. at 6 cm below the top of the borehole (Figure 12).

2.2 Test Preparation

2.2.1 Laboratory Setup

The laboratory setup used to conduct the laboratory experiments for this thesis is depicted in Figure 13. The setup consisted of a positive displacement pump (PDP) connected to a stainless steel 40 ml cylindrical vessel containing the fracturing fluid, which was attached to a stainless steel injection tool. The tool was placed in the borehole, and then the sample was axially compressed in a computer-controlled load frame. Stainless steel 1/4-inch tubes were used as connectors between the pump, the vessel and the injection tool.
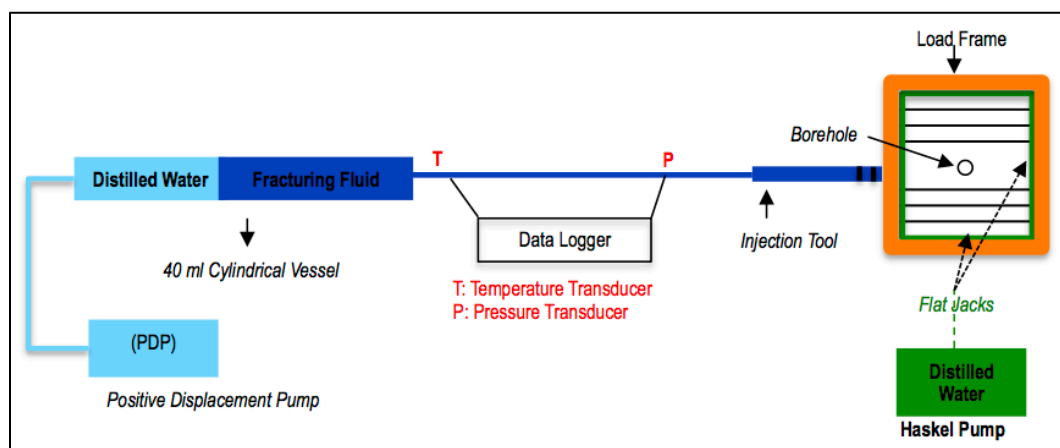
Figure 13. Laboratory setup

The cylindrical vessel, which was dried in the oven overnight, and the tube used to connect it to the injection tool were filled separately with fracturing fluid. The distilled water pumped by the PDP exerted pressure that pushed an internal piston in the cylindrical vessel. The piston acts as a barrier between the distilled water in the pump and the fracturing fluid. Thus the injection rate was controlled by the speed of the stepping motor attached to the PDP.

2.2.2 Injection Tool

To initiate a hydraulic fracture in the sample (stacked slabs), pressurised fluid must be supplied specifically at the location of the borehole notch. This is achieved by means of an o-ring straddle injection tool that isolates the outlets of the fluid injection system via two o-rings (Figure 14). A bypass hole that runs through the steel tool from top to bottom allows air to bypass the 2mm thickness o-rings, equalising the pressure above and below the tool when it is inserted into or removed from the borehole. Before positioning the injection tool in the borehole, the injection system was bled in order to remove any air present. A small amount of load was applied to the rock system to keep the samples still while pushing the injection tool into the borehole. The injection tool was then inserted into the PVC-lined hole and positioned so that a sealing o-ring was on either side of the notch. The location of the notches for the uniaxial and biaxial setup caused the fractures to initiate in the x-z plane (Figure 15 and Figure 16).
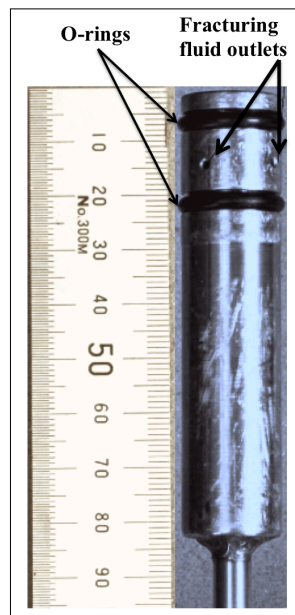
Figure 14. Fracturing fluid injection tool

2.2.3 Uniaxial Load Frame

The uniaxial experiments were conducted using a 150 KN servo–controlled compression frame (Figure 15). The CSIRO uniaxial frame consists of a movable bottom plate pushed by a hydraulic actuator towards a fixed top plate. Both plates are perfectly flat and smooth and of exact dimensions. Two Teflon sheets were used at the top and bottom rock slabs to minimise induced shear stress between the steel platens and the rock.
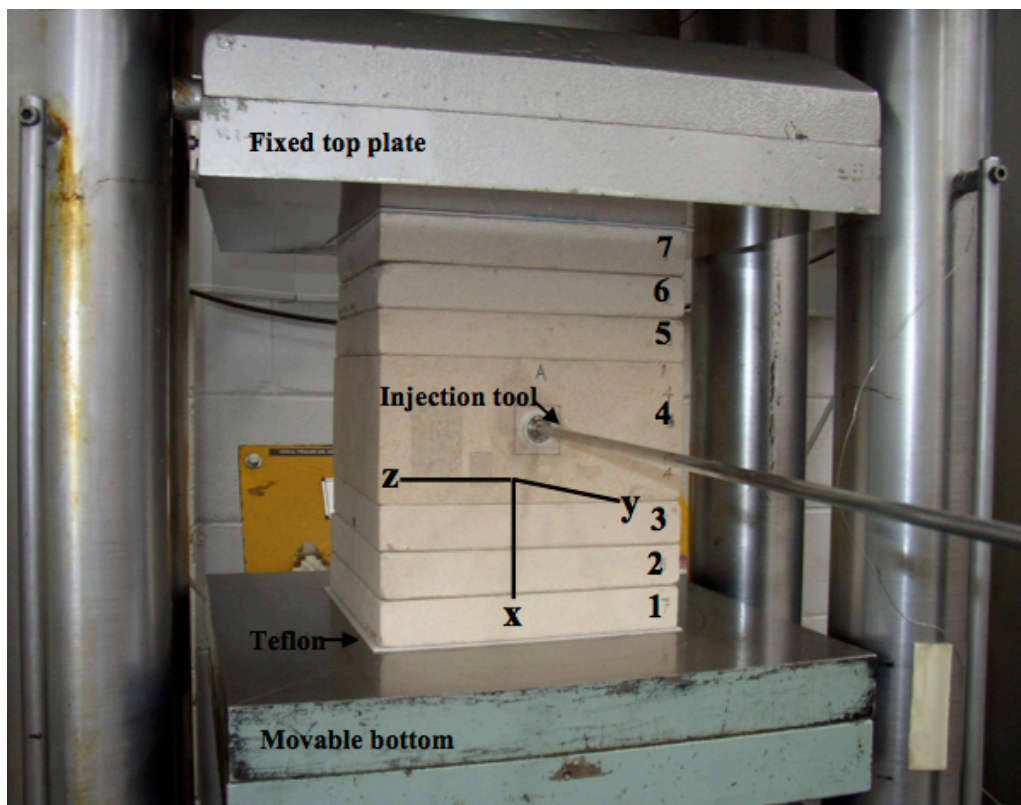
Figure 15. Uniaxial experimental setup

2.2.4 Polyaxial Load Frame

The experiments involving subjecting test samples to biaxial stress conditions were carried out in the CSIRO polyaxial frame. The safe working load of CSIRO's polyaxial frame is 4000 KN in each direction: lateral and vertical (Figure 16). The samples were located in the frame's rectangular sample loading area formed by fixed, flat and smooth metal plates. The small gap between the rock sample and the metal plates was filled with flat jacks, i.e. two stainless steel sheets welded together.
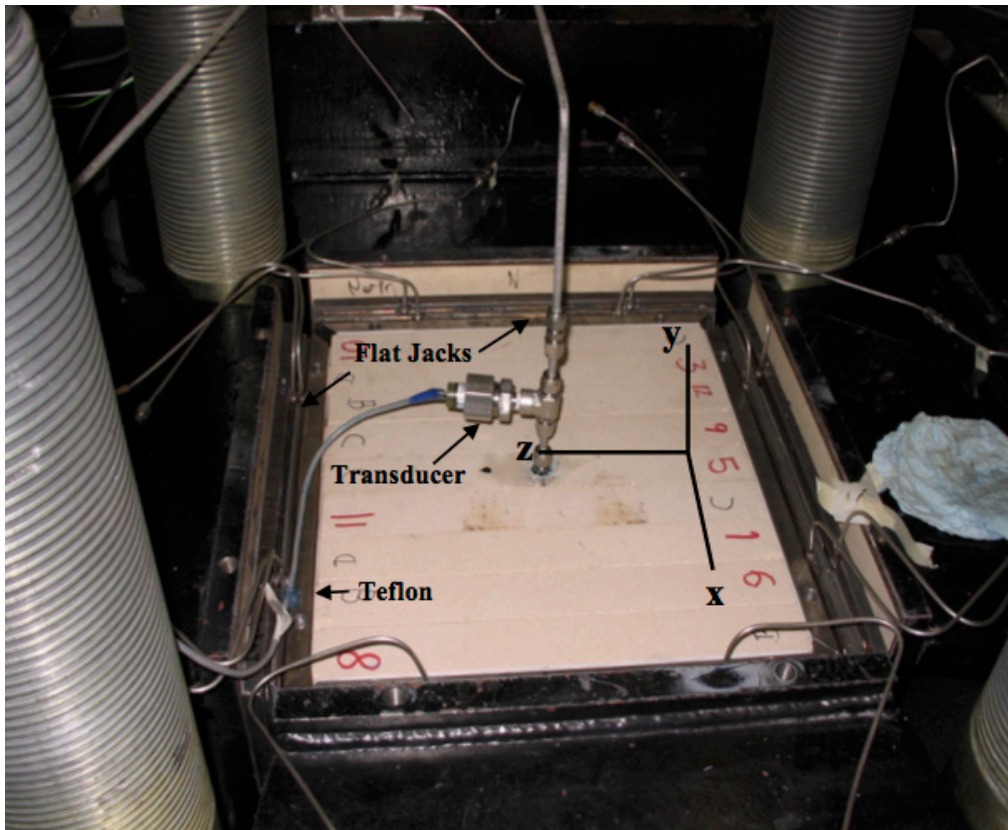
Figure 16. Biaxial experimental setup

The flat jacks used for the biaxial tests have two fluid fitting points which allow initial inflation of the jack via one port while bleeding air from the jack through the other. The flat jacks are pressurized using a Haskel air-over-water pump. Teflon sheets were used between the sample and the flat jacks to reduce shear stress that might be generated by compressing the stiffer steel shims against the softer rock sample. Use of a flat jack loading system further reduces the possibility of generating such shear stress. An initial load, applied before placing the injection tool in the borehole, allowed testing of the flat jacks. No leakage in the flat jacks was allowed in order to guarantee that the load could be held constant at the target stress values during each test. The desired load applied to the test block was increased once the conditions to start the test were achieved.

2.2.5 Pressure and Temperature Monitoring

A 35 MPa pressure transducer was located as close as possible to the top of the borehole for injection pressure measurements. A temperature sensor was located at the outlet of the cylindrical vessel. The National Instruments PC board installed in the computer operates as a

data logger for instrumentation and also controls the PDP. Labview software was used to control the pump, record data and display the data for monitoring the progress of the test.

2.3 Test Procedure

In the uniaxial experiments carried out for this thesis, σ_x is the applied confining stress across the frictional discontinuities, which, in these tests are represented by the contact generated between two adjacent slabs. Figure 15 shows that σ_y was zero. Therefore, the R & P (1995) crossing criterion (equation 1, section 1.5) was used to estimate the value of σ_x required for crossing to occur and, at the same time; the experimental results test the validity of equation 1 when applied to hydraulic fractures.

A constant uniaxial stress was applied normal to the slab layering. Once the target stress loads were stabilized a honey-based Newtonian fluid was then injected to pressurize the notch and initiate and propagate a fracture. The applied load, fluid temperature and injection pressure were recorded throughout each test. The results from varying loading stress levels were recorded in terms of whether the hydraulic fractures crossed or did not cross the frictional discontinuities between the slabs.

Crossing refers to a case where the fracture propagates across the central block and into the surrounding slabs. On the other hand, non-crossing refers to a test where the fracturing fluid enters into the interface of the central block and the hydraulic fracture does not continue to propagate into the adjacent blocks.

Figure 17 represents a case where the hydraulic fracture grew through the rock plates of the sample; that is all the discontinuities were crossed. In contrast, Figure 18 depicts a case where the injected fluid only fractured the middle slab without crossing any discontinuity.
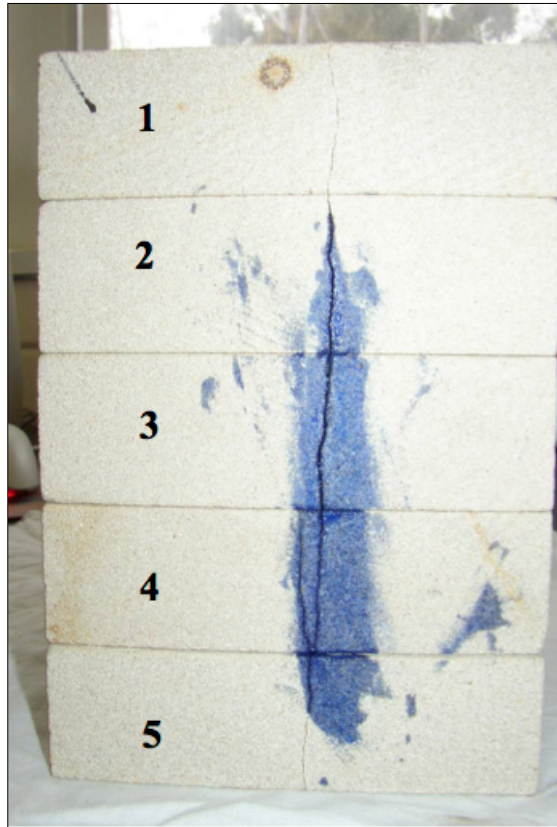
Figure 17. Crossing case – lateral view

Figure 18. Non crossing case – lateral view

42

The loading under which crossing was first observed provided an estimate of the stress needed for crossing to occur and was used to establish stress conditions for the biaxial tests (Figure 16). The stress in the y direction was maintained at zero in the biaxial tests while controlling the stresses in x and z directions. Once the target stress conditions were stabilized, the same injection procedure as for the uniaxial tests was followed. In the same way, the total injection volume was held constant throughout the biaxial tests and the applied load, fluid temperature and injection pressure were recorded. For both the uniaxial and biaxial experiments, injection fluids of different viscosities and sample loading to produce different stress values were used. The fracture growth and final shape of the propagated fracture were measured as a function of applied stress by removing and examining the samples after the tests (Figure 19).

Figure 19. Fracture growth through discontinuities

2.4 Summary

This current chapter describes the setup and procedure followed in the laboratory in preparation for presenting the results in Chapter 3. A series of uniaxial and biaxial tests were carried out using a honey-based Newtonian fluid of different viscosities as the injection fluid for fracturing stacks of Donnybrook sandstone plates subjected to different stress conditions.

The initial trials included the use of thin slabs, which developed stress concentrations around the borehole affecting the crossing behaviour. It was observed that this concentration affected the stress on the nearest discontinuities. The test method was then modified to prevent this effect by using thicker central slabs that contained the borehole. In addition, each central slab used for the

biaxial setup contained two notches to control fracture initiation location allowing two tests in the same block, maintaining rock properties and layer details constant for these two tests. The setup used for the uniaxial tests only allowed one test per sample block.

In their work, Renshaw and Pollard (1995) assumed unbounded discontinuities and did not consider surface curvature and roughness, or any features that could result in a stress concentration and promote or retard crossing. On the contrary, Gu et al. (2011) experimentally validated the e - R & P (2010) criterion using ground smooth and flat rock samples. In this thesis, the preparation of the rock plates also underlined the effect that curvature and local imperfections on the plate surface (or discontinuity in nature) can play in producing stress concentrations that can affect crossing. Small areas of lower or higher contact stress can inhibit or aid fracture initiation. The discontinuities must be smooth and flat in order to control the contact stress and frictional strength and to obtain valid experimental comparisons for the other parameters controlling crossing.

The procedure followed for the experiments started with the use of the R & P (1995) criterion for estimating the stress required for crossing to occur in the uniaxial setup. This type of experiments allowed testing the validity of the R & P (1995) criterion for hydraulic fracturing as well. The estimated stress required for crossing to occur was then used to establish initial stress conditions for the biaxial tests. Neither Renshaw and Pollard (1995) nor Blanton (1986) considered fluid viscosity effects on crossing behaviour.

For this thesis, the only testing parameters that varied between tests were the fluid viscosity and the confining stress. Two propagation regimes as described by Detournay (2004) were here reproduced by means of changing the injected fluid viscosity as discussed further in the next chapter. The data recorded during the experiments included applied load, the fluid temperature, the injection rate and the injection pressure. After completion of the tests, the blocks were carefully cut to measure fracture shape and extent and fracture surface features. A comparison of fracture shape with interface location and stress was made to investigate the resulting hydraulic fractures geometry.

Chapter 3

LABORATORY RESULTS AND DISCUSSION

This chapter starts with a summary of the experimental data followed by a discussion of the effects of the applied loading stress and the viscosity. Next, the observations and discussion on the obtained hydraulic fracture geometry are presented. The chapter finishes with a comparison of the experimental results against the corresponding predictions published by Blanton (1986), Renshaw and Pollard (1995) and Gu and Weng (2010).

3.1.   Summary of Experimental Results

The R & P (1995) crossing criterion (equation 1, section 1.5) provides a "Crossing Stress Ratio" (CSR) (equation 3), left hand side of the equation, which predicts crossing to occur when the horizontal compressive stress (σ_x) acting across the interface is large enough in relation to the sum of the tensile strength (T_o) and the vertical compressive stress (σ_y) acting along the interface. In the laboratory tests carried out in this thesis $\sigma_y=0$ was used for all tests.

$$CSR = \frac{\sigma_x}{T_o + \sigma_y}$$

Eq. 3

For the uniaxial tests, using the R & P (1995) criterion and based on the coefficient of friction of the interfaces, crossing was expected if the CSR was greater than 0.9. The results from the uniaxial experiments using 1 Pa.s and 100 Pa.s fluid are summarized in Table 2 and Table 3 respectively. The data for the biaxial tests are gathered in Table 4. The last column in these tables shows which interface was crossed based on the visual inspection along the plane x-z where the fracture propagated after the completion of the tests.

Referring to Figure 20, if the fracture was contained in the central slab (solid thick green ellipse in sample number 4) the result was reported as non-crossing (none in the table). The geometry in the dotted red ellipse shows the third interface being crossed (3) while in fuchsia (dash) a case where the fracture grew further to the second plate (2,3) is illustrated. The solid thin blue ellipse depicts a case where growth was observed through interfaces 3 and 5. The final hydraulic fracture geometry obtained from these experiments is discussed in detail later in section 3.4.

Recalling Table 1 (section 2.1.1) the injection volume for the uniaxial tests was 12.5 ml. The biaxial experiments with 100 Pa.s injection fluid required 25 ml while for the 1 Pa.s cases, 40 ml was injected. The injection rate was kept constant for all experiments at 0.0158 ml/s.

Experiment	σ_x (MPa)	CSR	Interface crossed
D1	5	1.14	None
D2	6	1.36	None
D3	7	1.59	None
D4	8	1.82	3
D5	10	2.27	2,3
D6	12	2.73	2,3

Table 2. Summary of experimental data: uniaxial tests for fluid with 1 Pa.s viscosity

Experiment	σ_x (MPa)	CSR	Interface Crossed
D7	5.0	1.14	None
D8	5.5	1.25	2,3
D9	6.0	1.36	2,3
D10	8.0	1.82	2,3

Table 3. Summary of experimental data: uniaxial tests for fluid with 100 Pa.s viscosity

Experiment	μ (Pa.s)	σ_x (MPa)	σ_z (MPa)	CSR	Notch depth (cm)	Interface Crossed
D11	1	12.0	12.0	2.73	15	3,5
D12	1	8.0	8.0	1.82	25	3,5
D13	100	4.0	4.0	0.91	15	3,5
D14	100	8.0	8.0	1.82	25	3,5

Table 4. Summary of experimental data: biaxial tests
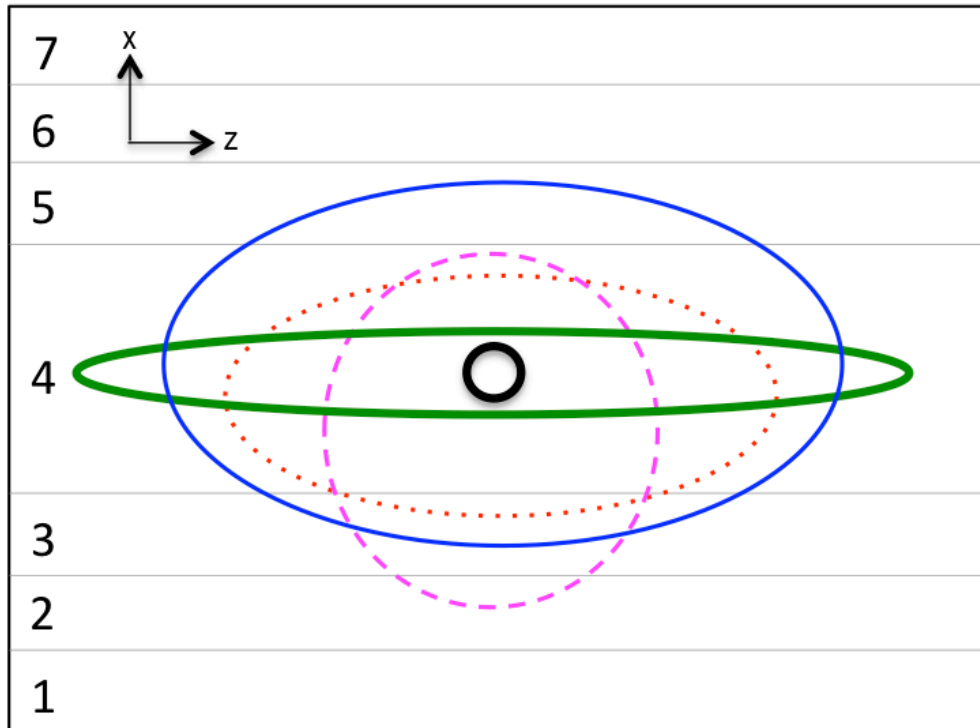
Figure 20. Possible interface crossing observed.

In all the experiments, the pressure increased during the injection of the fracturing fluid until reaching a peak followed by a declining pressure for the remaining of the test. The pressure behaviour for the biaxial tests is shown in Figure 21. The fractures were propagated at lower pressure (below 20 MPa) when using 1 Pa·s fluid and the pressure record displayed a slow pulsing of pressure during fracture growth. Lhomme (2005) noted pulsing in tests in permeable sandstone and attributed it to periodic fracture growth and high leakoff episodes, which acted together to cause the fracture to open and close during its growth. A similar process may be active here or the pulsing may indicate an interaction between the fracture and the interface. An interface interaction may, however, be less likely because the pulsing starts immediately after fracture initiation and it is unlikely that the interfaces were reached this quickly.

The higher fluid viscosity significantly reduced the fluid loss effect but also resulted in a significant fluid lag developing (since the stress across the fracture plane was zero). This is discussed in more detail in section 3.3.3. Figure 21 also contains the pressure record for the two tests run using 100 Pa·s fluid. In both cases the pressure follows a smooth decline with time and no pulsing is observed. This behaviour of the pressure was also observed by Bunger et al. (2015) in a series of experiments run under similar conditions in a different sandstone. However, the

pressure profile for both studies show no obvious inflection points that could be correlated with the hydraulic fracture crossing the natural fracture.
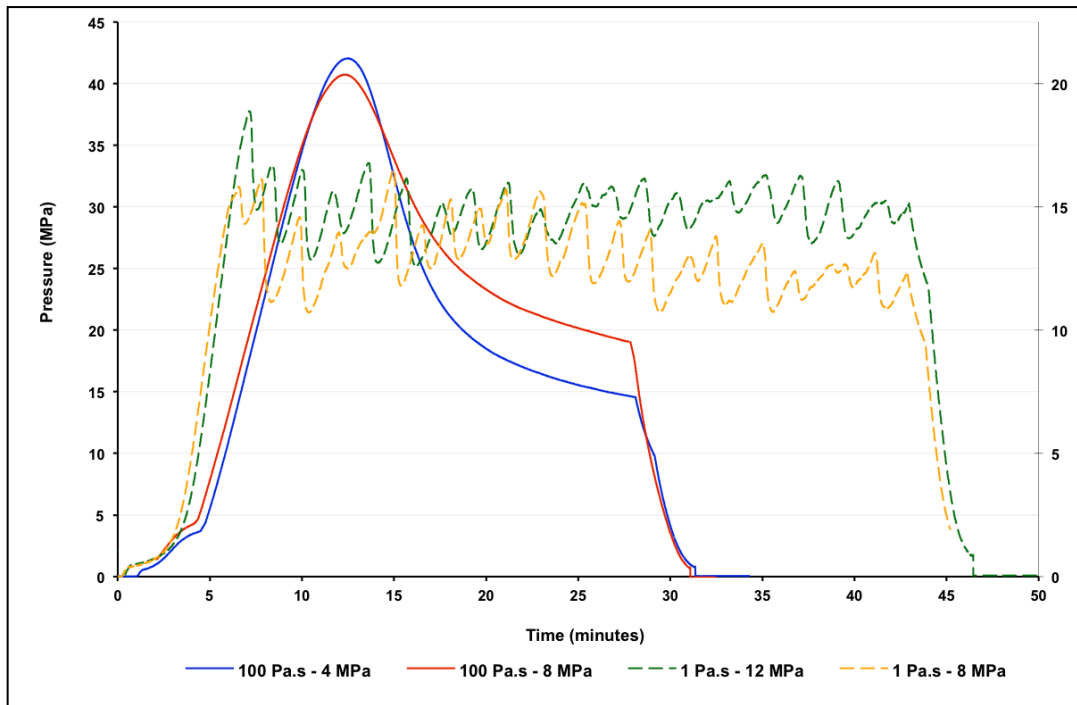
Figure 21. Injection pressure vs time behaviour

3.2. Applied Loading Stress Effect

3.2.1. Contact Stress and Surface Curvature

The nature of contact of the initially sawn plates used for the experiments carried out for this thesis was not only rough but also curved, as presented in Figure 10 (section 2.1.1). When two bodies with rough surfaces are pressed into each other, the contact area is much smaller than if the surfaces were smooth, i.e. without any asperities, mismatch or similar features. Additionally, when convex surfaces are under compression and in contact with other surfaces, compressive stresses both parallel and perpendicular to the line of contact in both members are developed. These high contact stress concentrations then resulted in hydraulic fractures crossing the natural fractures even for applied normal stress levels under which crossing was not expect to occur, as per the R & P (1995) criterion. Of course the criterion calculation assumes a uniform contact on a perfectly smooth surface. Consequently the slabs used for this thesis were ground flat to minimize non-uniform contact stress induced by the applied loading normal to the interfaces. Therefore the discussion on the results of the experiments carried out for this thesis only considers samples with flat slab surfaces.

3.2.2. Frictional Discontinuity Conditions

The experiments carried out as part of this thesis work used unbonded machined frictional interfaces and Coulomb's law (equation 4) can be used to express the shear strength of such an interface or natural fracture considering a nil cohesion. Therefore if the shear stress (τ) is less than the product of the frictional coefficient 'm' and normal stress 'σ_n,' there is no slip.

$$|\tau| < \sigma_n m$$
<div align="right">Eq. 4</div>

If the compressive stress changes because of the interaction of the hydraulic fracture with the frictional discontinuity, sliding may start or arrest at that local point. Once the hydraulic fracture is close to the discontinuity or the fluid invades the discontinuity the sliding status varies from point to point on the surface. Since slip occurs locally for hydraulic fractures crossing an interface, in this thesis crossing or not was controlled by the normal load (or stress) applied across the interfaces. The tests and analysis undertaken for this thesis project do not assume that slip prevents crossing.

3.2.3. Interface Hydraulic Conductivity and Effective Normal Stress

The ability of a fracture to conduct fluid is extremely sensitive to the fracture hydraulic aperture or opening (ϖ), a residual opening of a closed natural fracture, which provides it with residual conductivity. The residual hydraulic aperture itself does not contribute to stress changes. However, the apertures of fractures depend critically on the effective stress acting normal to the fracture plane. Equation 5 describes how the hydraulic aperture and the permeability (*k*) of a natural fracture are related.

$$k = \frac{\varpi^2}{12}$$
<div align="right">Eq. 5</div>

When the fracturing fluid infiltrates a closed natural fracture, without fully opening it, the hydraulic aperture can vary as a function of the fluid pressure. When the fluid pressure exceeds the normal stress acting on the fracture plane, the natural fracture will open completely and increase its hydraulic aperture further.

The dependency of the hydraulic aperture on the fluid pressure (P_l), at pressures below the far-field normal stress, can be described using a non-linear spring model (Zhang, 2011) as shown in equation 6. The constant χ is of the order of 1E-13 to 1E-11 MPa^{-1} and characterizes the compliance of a natural fracture with respect to pressure change. A measure of the relative volume change of a fluid or solid as a response to a change in pressure is the compressibility. Water has a much smaller compressibility than the pore or fracture compressibility. The compressibility of water at 20 °C is approximately 2.9 E-04 to 5.8 E-04 MPa^{-1} while for consolidated sandstones, pore compressibility varies between 2.2 E-04 to 2.9 E-03 MPa^{-1}.

$$\frac{d\varpi}{dP_l} = \chi\varpi$$

Eq. 6

3.3. Fluid Viscosity Effect

3.3.1. Viscous- vs. Toughness-Dominated Fracture Growth Regimes

The energy required to propagate a hydraulic fracture is consumed in overcoming fluid viscous dissipation and in fracturing the rock. The fracture growth process may be such that it is dominated by either one or the other of these two energy-consuming processes. In order to test the effect of the regime of propagation on the crossing behaviour, conditions were used in the laboratory tests that led to propagation of the hydraulic fracture either in the regime dominated by fluid viscous dissipation or by rock fracture toughness. A detailed discussion of these propagation regimes can be found in Savitski and Detournay (2002) and Detournay (2004) and the regimes are summarized as follows.

The value of the dimensionless fracture toughness K, given by equation 7, can be used to indicate the fracture regime that applies. For a penny-shaped fracture, K is given by:

$$K = \left(\frac{t}{t_{mk}}\right)^{1/9}$$

Eq. 7

where

$$t_{mk} = \left(\frac{\mu'^{5} Q_0^3 E'^{13}}{K'^{18}} \right)^{1/2} ; \qquad \mu' = 12\mu;$$

$$E' = \frac{E}{1-\nu^2}; \qquad K' = \left(\frac{32}{\pi} \right)^{1/2} K_{IC}$$

Eq. 8

and μ is the fluid dynamic viscosity, E and ν are the rock Young's modulus and Poisson's ratio, respectively, K_{IC} is the fracture toughness of the rock, and Q_0 is the volumetric injection rate.

When K is large, that is when t is significantly larger than the characteristic time, t_{mk}, the propagation occurs in the toughness-dominated regime. When K is small (t is significantly smaller than t_{mk}), the propagation is in the viscous dissipation regime. Toughness-dominated growth occurs when K is larger than about 3 and the fracture growth is dominated by viscous friction when K is smaller than about 0.5.

The parameters listed in Table 1 (section 2.2.1) were held constant except for the fluid viscosity and applied normal stress. The three viscosities (μ) used, after allowing for the temperature during each test, are 1.2, 20, and 135 Pa·s and from equation 7, the corresponding values of K are 2.2, 1.0, and 0.5 respectively for a time (t) of 100 seconds (Table 5). Therefore, the experiments using the 1.2 Pa·s fluid (rounded to 1.0 Pa.s) were just in the toughness-dominated regime while the thickest fluid (rounded to 100 Pa.s) produced conditions in the viscous-dominated regime.

K_{IC} (MPa m$^{1/2}$)	K' (MPa m$^{1/2}$)	E (MPa)	ν	ν^2	E' (MPa)
0.58	1.85	7000	0.28	0.08	7600
μ (MPa.s)	μ' (MPa.s)	Q (m^3/s)	t_{mk} (s)	t (s)	K
1.20E-06	1.44E-05	1.58E-08	0.10	100	2.2
2.00E-05	2.40E-04	1.58E-08	116	100	1.0
1.35E-04	1.62E-03	1.58E-08	13760	100	0.5

Table 5. Parameters for calculating values of K for a time of 100 seconds

During the propagation of a hydraulic fracture, a fluid lag (dry zone in the fracture near the tip) may develop (Garagash and Detournay, 2000). Such a fluid lag is often larger at early time during the propagation and can be of significant size in laboratory experiments. In order to check whether the fluid lag should be taken into account, the characteristic timescale associated with the disappearance of the fluid lag (t_{om}) is estimated from equation 9 (Bunger and Detournay, 2007; Bunger, 2005). This timescale is inversely proportional to the far-field confining stress cubed (σ_o^3). This means the higher the confining stress the smaller the timescale.

$$t_{om} = \frac{E^{'2}\mu^{'}}{\sigma_0^3}$$

Eq. 9

The experiments run for this thesis used biaxial stress loading with the minimum stress equal to zero. Therefore, equation 9 cannot be applied. Fluid lag was significant in some of the experiments, as discussed in the next section. It was not possible to determine whether fracture crossing occurred before or after fluid reached a particular interface in the experiments. Running a series of experiments under triaxial stress to study the effect of fluid lag on the crossing interaction is possible, but beyond the scope of this thesis. A new 2D hydraulic fracture method has recently been developed that allows direction observation of the fracture interacting with an interface and this method could be applied to a study of the effect of fluid lag on fracture-interface interactions (Jeffrey et al., 2015).

3.3.2. Penetration Effects

An unsuccessful attempt to investigate the possibility of detecting the fracture growth behaviour via electrical responses generated from streaming potential (Moore and Glaser 2005) was carried out in several biaxial tests (coloured wires on Figure 22). However since completing the tests for this thesis, ultrasound monitoring has been successfully proved to work by Bunger et al. (2015).

Visual inspection after testing was the only way used to make observations to determine the final fracture growth in the test samples. In this section observations along the z and negative y directions (as per Figure 22) are discussed. Measuring the fracture growth along the x-z plane was used to assess the hydraulic fracture final shape, as discussed later in section 3.4.
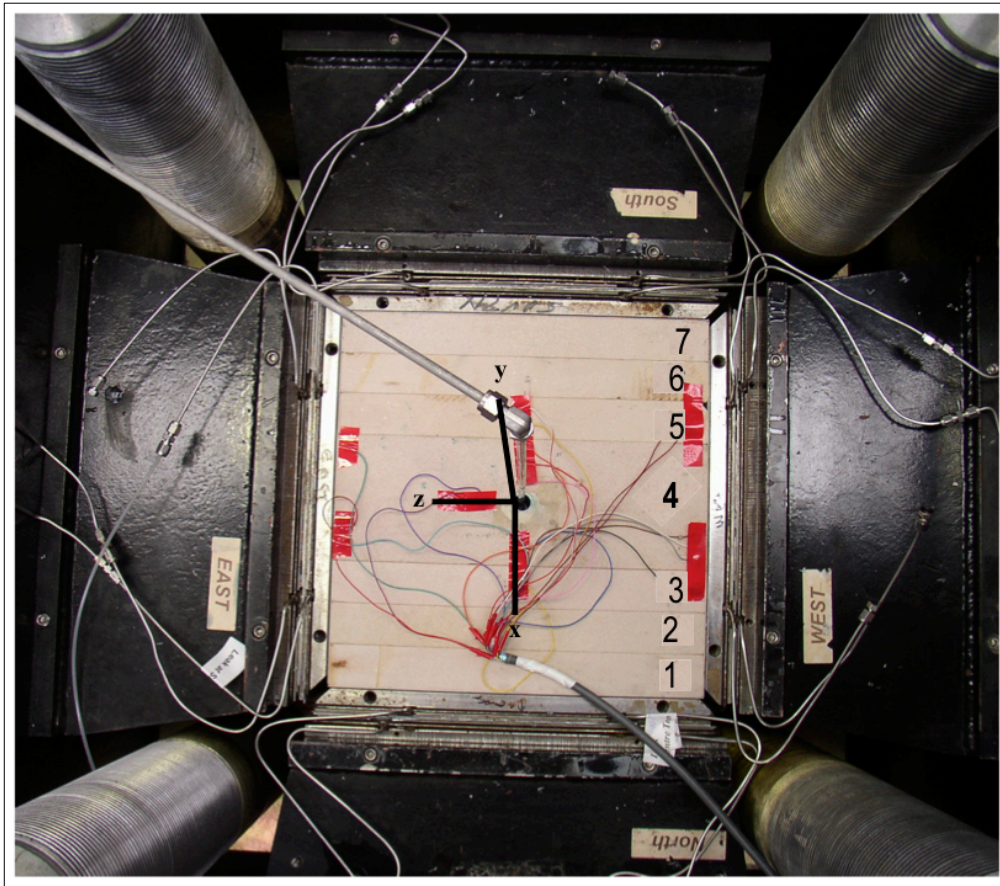
Figure 22. x-z Plane view of the biaxial setup.

The biaxial tests for the toughness-dominated cases were initially run by injecting 25 ml of a 1 Pa.s fluid viscosity, as designed. However, no fracture growth was observed and the injected volume was then increased to 40 ml. Figure 23 shows one side of the central thick slab and clearly depicts leakoff occurred. The fracturing fluid has entered the frictional interface which is similar to leakoff into natural fractures. Fluid leakoff into the sandstone pore space also occurred.

Garagash and Detournay (2000) concluded fluid lag is not relevant for toughness-dominated fractures. However, fluid lag became significant with the high viscosity fluid especially in the biaxial tests (partly because of σ_y being zero; Figure 16, section 2.2.4). For some cases, the lag zone extended through a discontinuity without fluid penetration across or into the interface.

Figure 24 shows an example of a centre slab with a lag zone present in the top and bottom fractures. It was observed that both fractures grew all the way to the left side edges of the sample. The fracture growth to the right side boundary stopped where the two vertical red lines are marked.
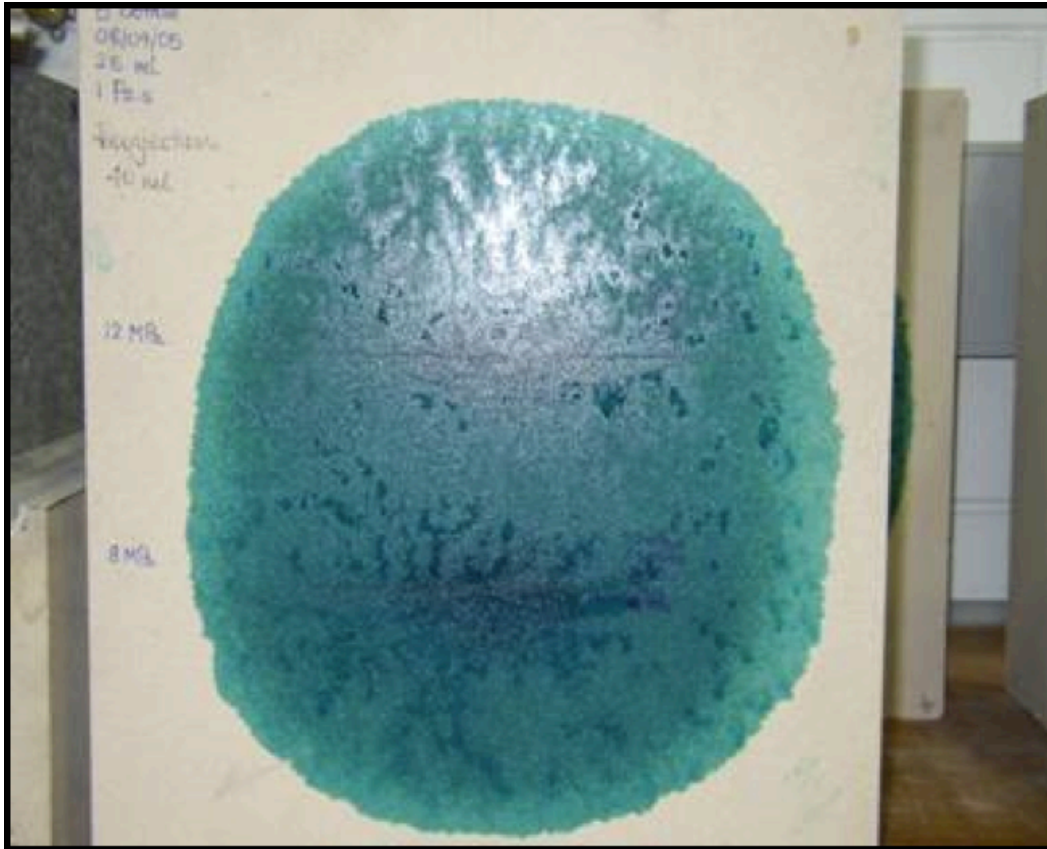
Figure 23. Fluid leakoff: Experiments D11 (top) and D12 (bottom)
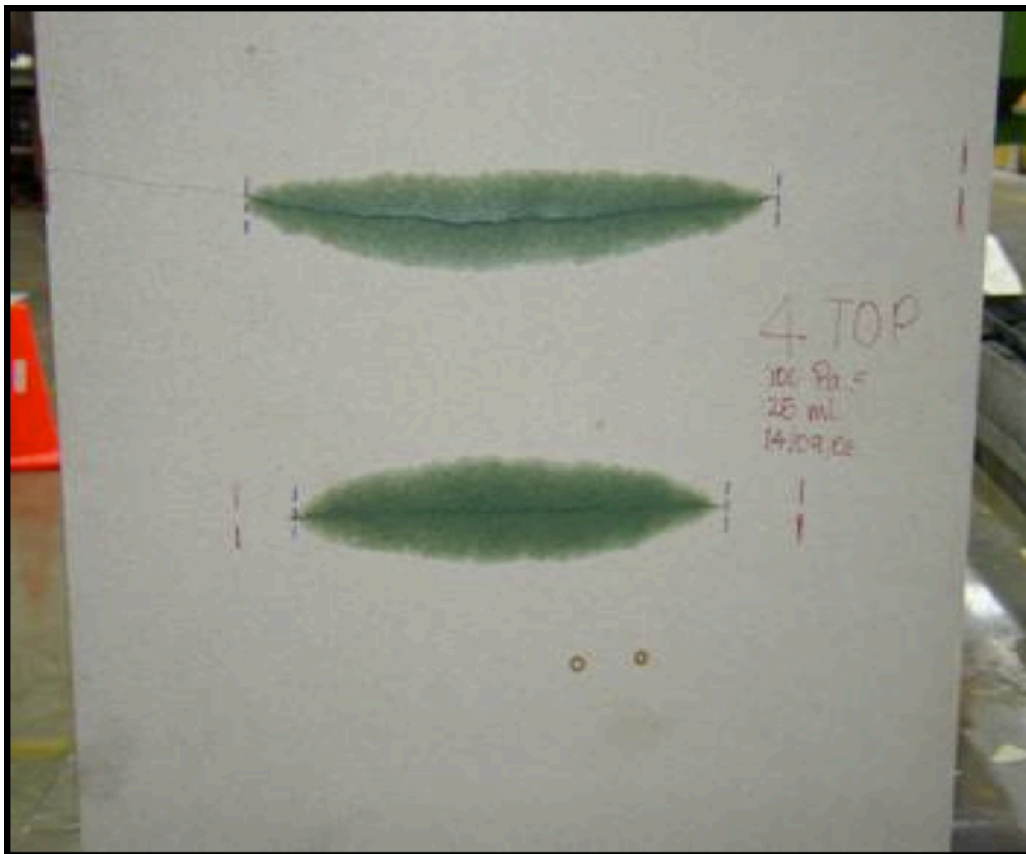
Figure 24. Lag zone extension with no fluid penetration: Experiments D13 (top) and D14 (bottom)

Both the top and bottom fractures (experiments D13 and D14) were generated using a fluid with a viscosity of 100 Pa s. The stress acting across the frictional interfaces was higher for the D14 experiment, producing a higher crossing stress ratio. The D13 fracture has extended further, as evidenced by the size of the fluid stained portion of the fracture trace, than the D14 fracture. This observation suggests that the hydraulic fracture growth may have been affected by local variation in the sample permeability. However, the larger of the two fractures broke through to the left edge of the block. This portion of the fracture is believed to represent a boundary effect rather than a fluid lag effect.

The size of the fracture produced in experiment D13 also became large compared with the distance to the top of the sample and some interaction of the fracture with the free surface occurred (Figure 25 and Figure 26). This interaction was associated with a slight curvature of the fracture toward the free surface of the block (Bunger, 2005).

Figure 25. Convex surface curvature (looking in negative y direction) : Experiments D13 (top) and D14 (bottom)

Figure 26. Convex surface curvature (looking in negative y direction) : Experiment D14 (bottom)

3.4.   Hydraulic Fracture Geometry

In this section observations on the fracture growth in the x-z planes are discussed. The laboratory results obtained for this thesis showed that a hydraulic fracture, provided it interacts with and crosses a similar number of natural fractures in either direction, will tend to grow more rapidly in the direction of the maximum stress or in the direction with fewer discontinuities.

As the normal stress acting on the interfaces was increased between tests, the ultimate fracture extent in that direction became larger. A slower growth was observed in the direction associated with fracture propagation through discontinuities compared with parallel to the interfaces. This preference in growth resulted in an elliptical shaped hydraulic fracture. Figure 27 is used as reference and it depicts a plan view of the setup used in the experiments carried out in this thesis. The effect of the increment of the loading stress on the final geometry shape (green ellipse) is summarized as follows:

- **Case A ($\sigma_{1A} > 0$; $\sigma_{2A} = 0$):**

The fracture crossed interfaces in the σ_{1A} direction but grew more quickly along the z-axis because there were no interfaces to cross in that direction. So it was elliptical in shape with short x-axis parallel to σ_{1A}.

- **Case B ($\sigma_{1B} > \sigma_{1A}$; $\sigma_{2B} = 0$):**

The hydraulic fracture crossed the interfaces perpendicular to σ_{1B} more easily, due to the higher loading stress in this direction. Therefore, the x-axis was larger in this ellipse, if compared to case A. The hydraulic fracture grew easily along the z-axis.

- **Case C ($\sigma_{1C} > 0$; $\sigma_{2C} \neq 0$):**

For the biaxial experiments carried out in this thesis the horizontal loading forces were identical (i.e. $\sigma_{1C} = \sigma_{2C}$) while the vertical stress was nil. The geometry obtained per regime is discussed in the following sections. Nevertheless it is possible to predict what will happen if $\sigma_{1C} > \sigma_{2C}$ and if discontinuities parallel to σ_{1C} are present. The hydraulic fracture will grow more easily in the direction of larger stress, σ_{1C}. In addition, it will grow to become elliptical in shape with its long axis parallel to σ_{1C}.
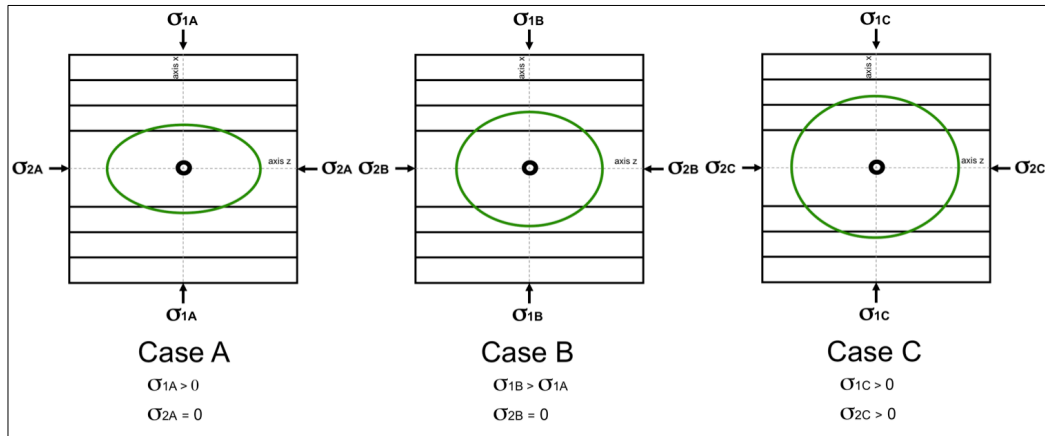
Figure 27. Effect of stress on hydraulic fracture geometry.

Figure 28 is a zoomed in view of a central plate along with two plate boundaries contained in the sample. The figure compares a circular geometry with the measured elliptical shape. The fracture extent was measured and is shown as a solid black line. The circular shape (dashed) is predicted by theory for a fracture growing in a homogeneous non-fractured material.
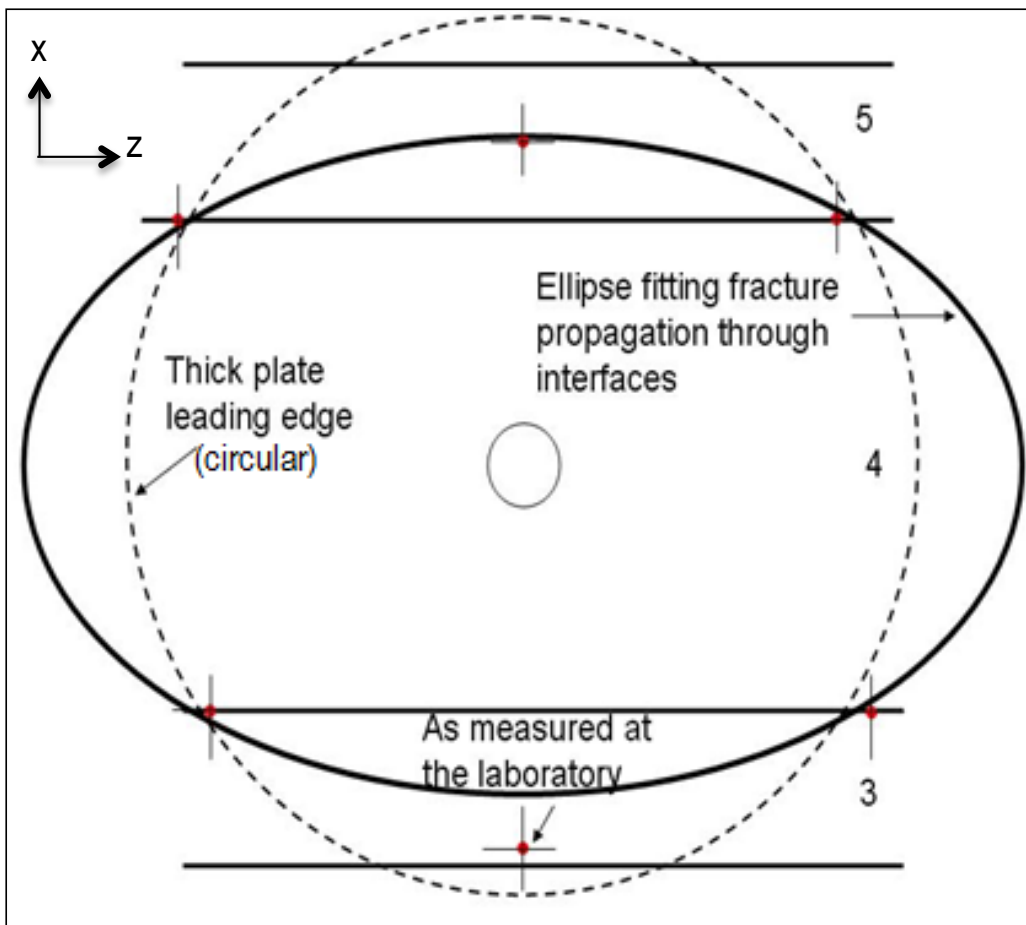
Figure 28. Fracture circular geometry vs. measured elliptical shape in central plate and two boundaries

Laboratory hydraulic fractures are expected to be initially circular in their plan view shape (Bunger et al., 2005) The elliptical shape results from the interaction of the hydraulic fracture with the frictional interfaces, which depends on the fluid viscosity and the conductivity of the interface, the frictional strength of the interface and the applied stress. As discussed next, in the biaxial experiments, the toughness-dominated hydraulic fracture exhibited an elliptical shape while a more circular shape was apparent in the viscosity-dominated cases.

Figure 29 and Figure 30 show the hydraulic fractures grew further in the z direction than in the x direction when two interfaces were crossed in the x-direction. The hydraulic fractures propagating in the toughness-dominated regime required a larger volume of fluid to obtain fracture crossing, suggesting the initial 25 ml injected was lost into the interfaces and the rock matrix. This fluid loss into interfaces could be an explanation for the reduced growth observed along the z-axis along the interface between slabs 3 and 4. This is more noticeable in Figure 30 (especially at the bottom left side) and may also explain why this axis of the ellipse was not as close to reaching the lower interface compared to the growth of the other end of the ellipse.

It is clear from the analysis of the results obtained from the experiments run under viscosity-dominated conditions that the applied stress had two distinctly different effects on the hydraulic fracture geometry. For a lower stress loading condition, the hydraulic fracture shape is less circular (Figure 31).

On the contrary, for cases under higher compressive loads (Figure 32), the fracture grew more circular. These tests suggest that if higher compression had been applied, the hydraulic fracture would have reached further in the x direction, i.e. it would have crossed more interfaces. The ultimate extent of the fracture growth without and with fluid lag is presented in both figures using black and red solid lines respectively.
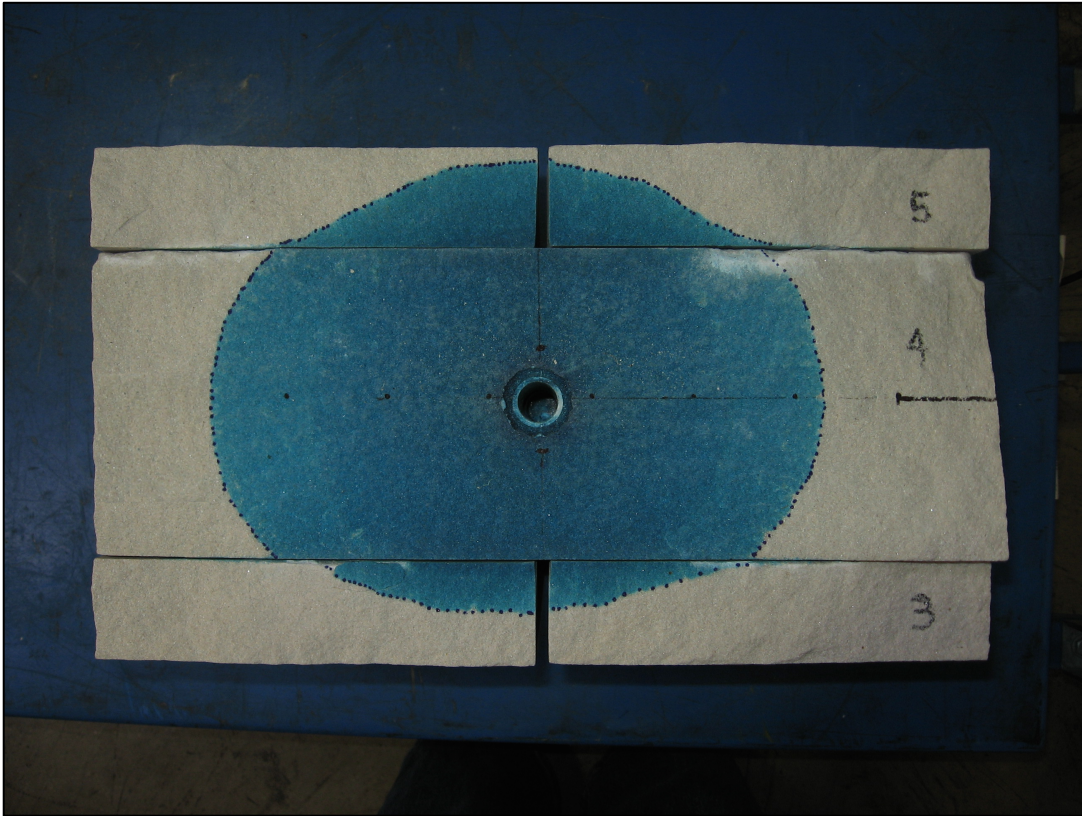
Figure 29. Experiment D11: 1 Pa.s 12 Mpa
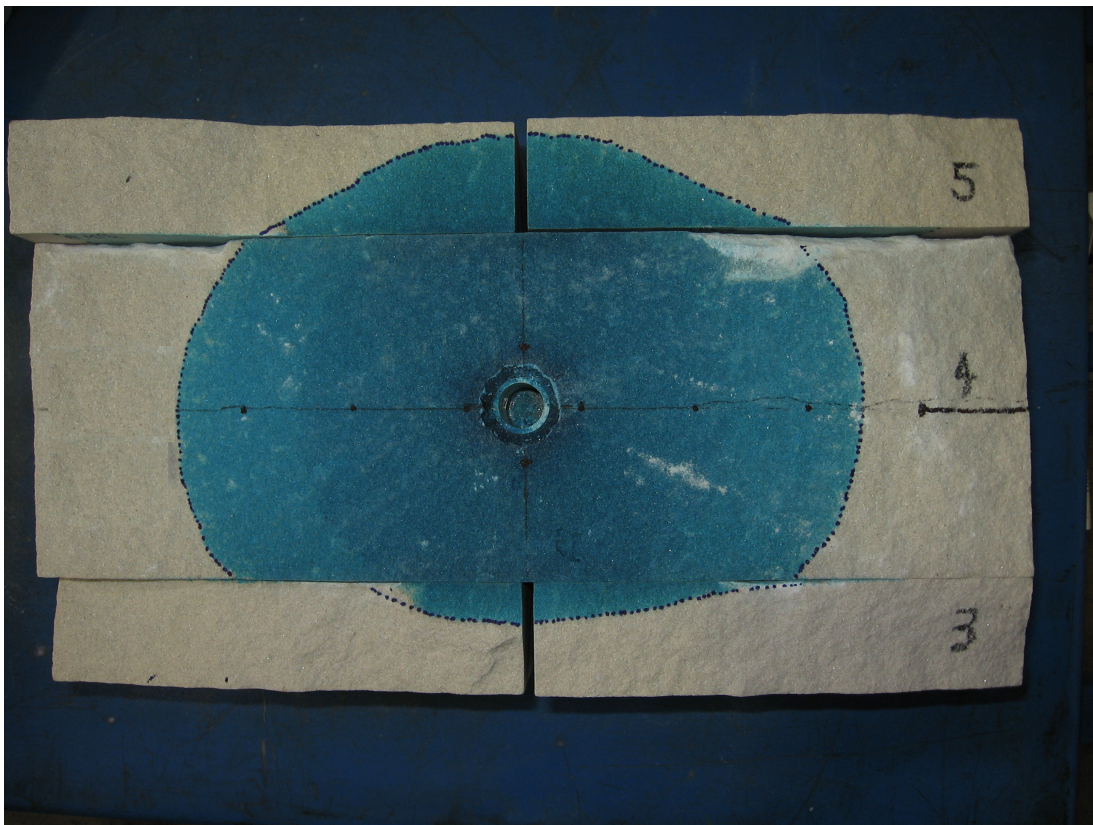
Figure 30. Experiment D12: 1 Pa.s 8 Mpa
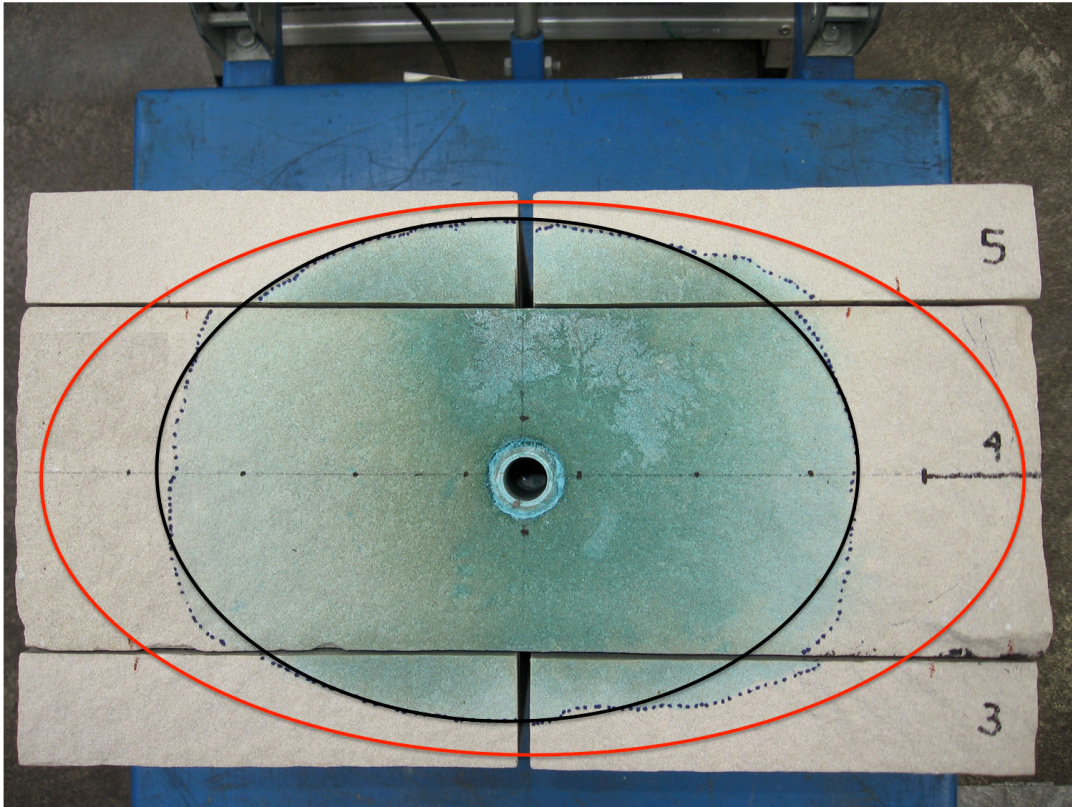
Figure 31. Experiment D13: 100 Pa.s 4 Mpa. Ultimate extent of fracture without and with fluid lag (black and red lines respectively)
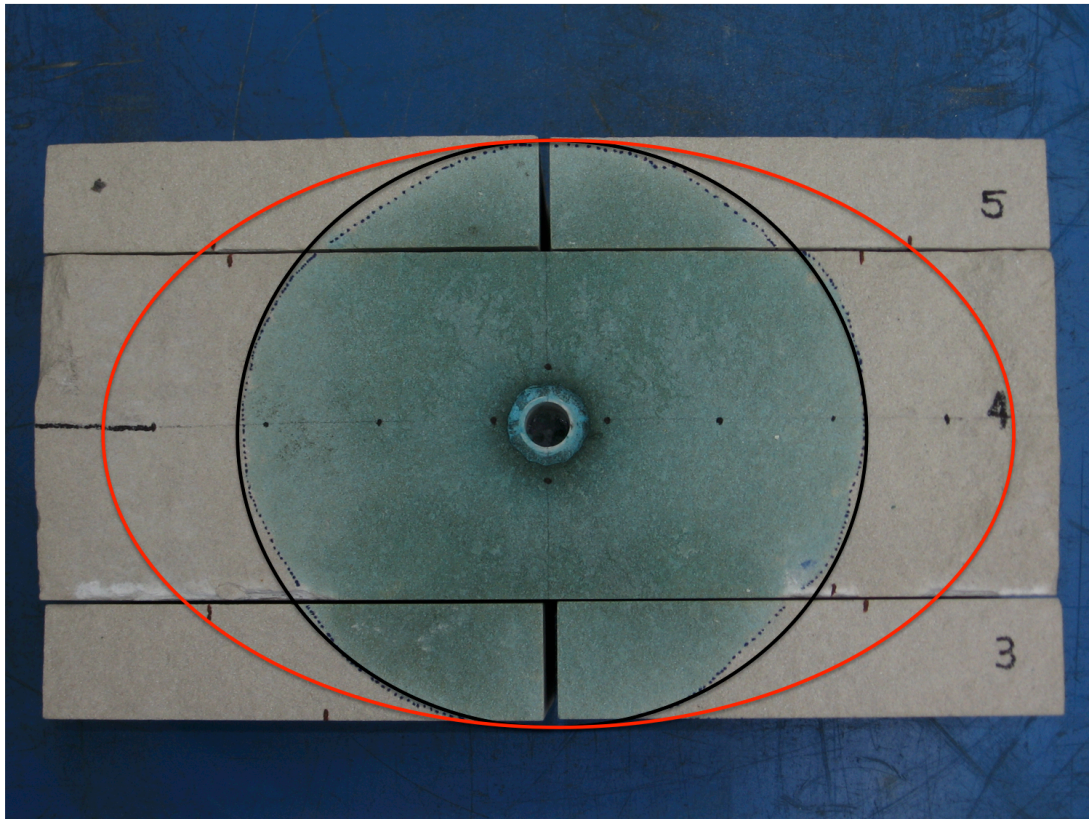
Figure 32 Experiment D14: 100 Pa.s 8 Mpa. Ultimate extent of fracture without and with fluid lag (black and red lines respectively)

3.5. *Crossing Criteria Comparison*

3.5.1. Uniaxial Tests Results vs. Crossing Criteria

Following the R & P (1995) and Gu and Weng (2010) criteria, the results of the experiments run for this thesis are plotted in a parametric space where one dimension is the interface friction coefficient and the other is the crossing stress ratio (Figure 33 and Figure 34).

The comparison of the laboratory results with respect to Blanton's (1986) criterion is shown by presenting the results in plots of differential stress vs. the angle of approach (Figure 35 and Figure 36).

The areas above and below the theoretical thresholds correspond to cases for which conditions would predict crossing and non-crossing respectively. Each test is represented by a dot and dots are colour coded as per a traffic light, i.e. the red represents non-crossing cases while the green dots symbolize crossing cases.

Some non-crossing cases are in the region where crossing is predicted by the criterion. Neither criterion fitted the data obtained from these tests; except for the results from the uniaxial tests ran under viscosity-dominated conditions, which seem to fit the R & P (1995) criterion well (Figure 34). The experimental data suggest a higher normal stress is needed to generate a crossing condition than what is predicted by either criterion.
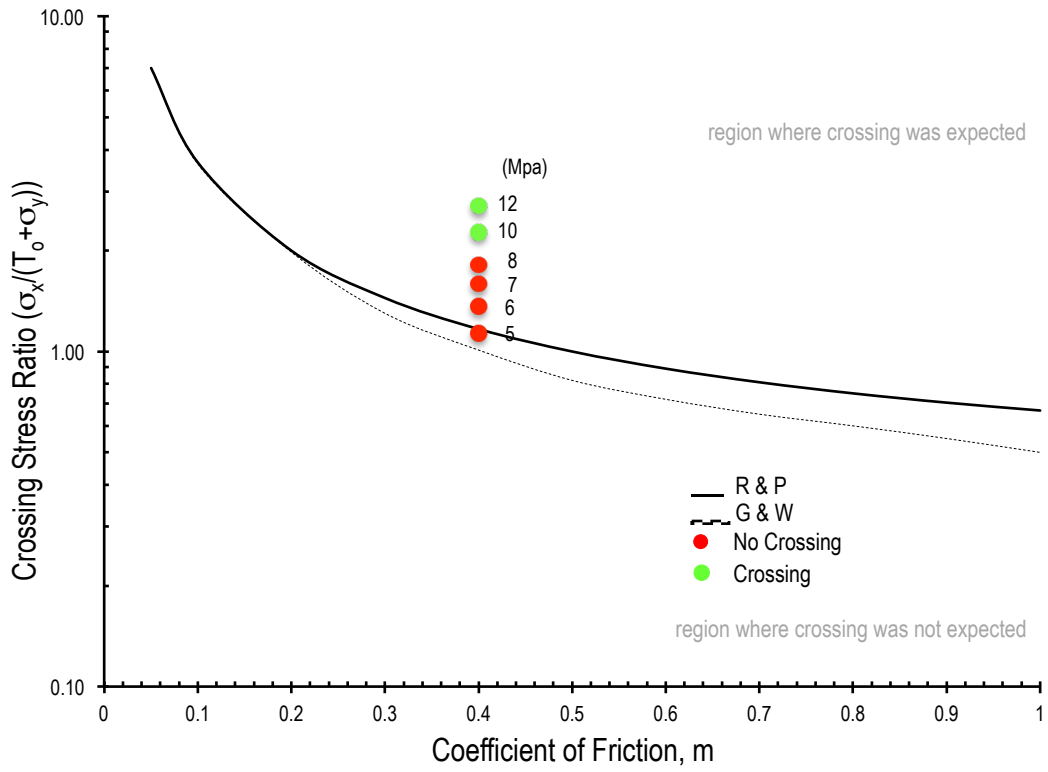
Figure 33. Uniaxial tests results for fluid with 1Pa·s viscosity compared to Renshaw and Pollard (1995) and Gu and Weng (2010) crossing criteria
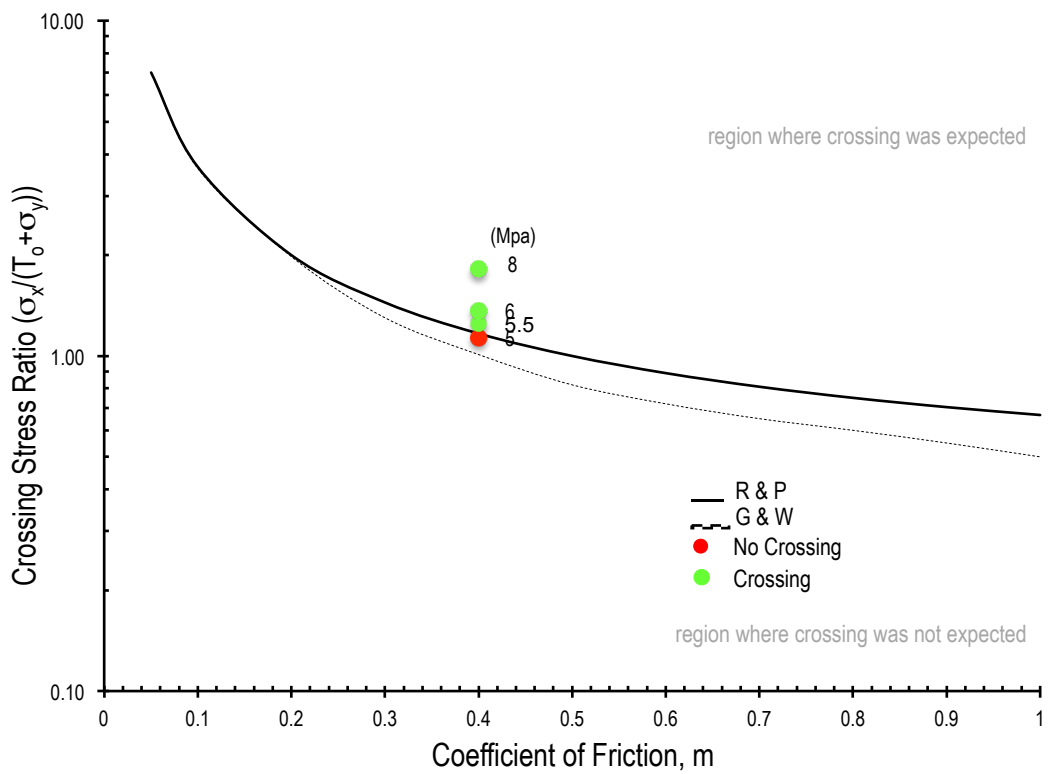
Figure 34. Uniaxial tests results for fluid with 100 Pa·s viscosity compared to Renshaw and Pollard (1995) and Gu and Weng (2010) crossing criteria
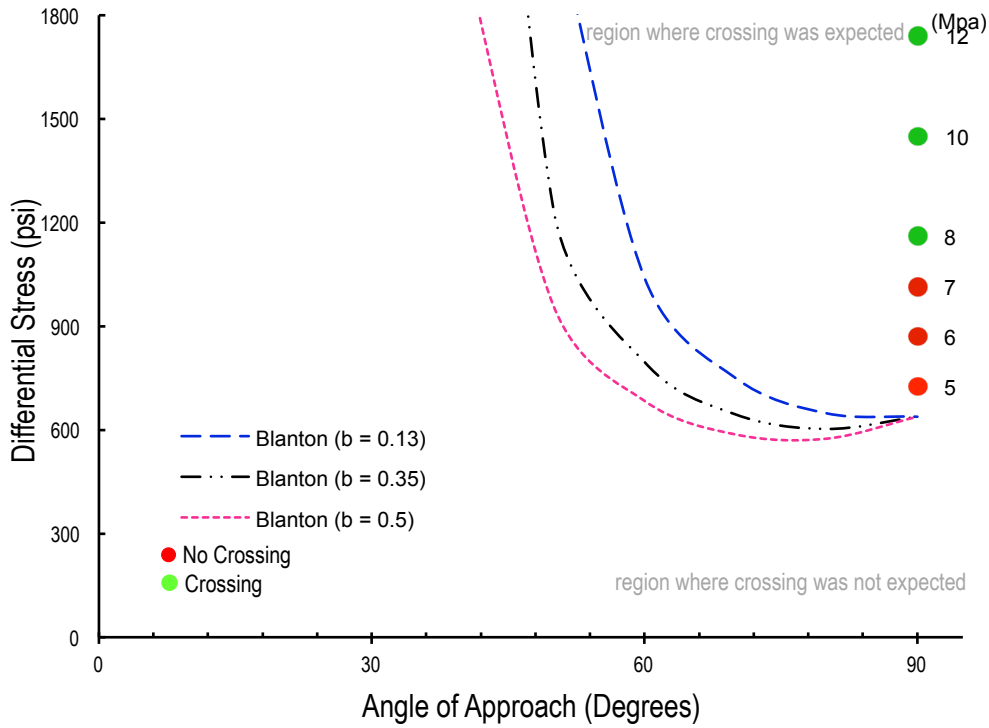
Figure 35. Uniaxial tests results for fluid with 1Pa·s viscosity compared to Blanton's (1986) crossing criterion
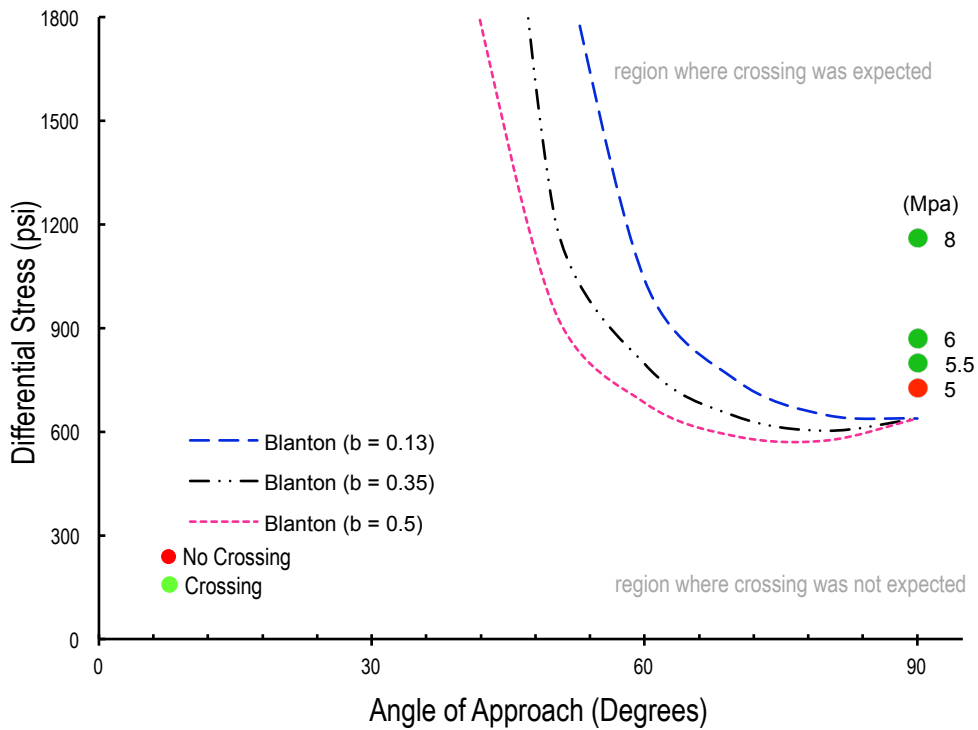
Figure 36. Uniaxial tests results for fluid with 100 Pa·s viscosity compared to Blanton's (1986) crossing criterion

3.5.2. Biaxial Tests Results vs. Crossing Criteria

In the larger blocks tested in the polyaxial frame, crossing occurred for all stress conditions so the non-crossing comparison cannot be made (Figure 37 and Figure 38). The biaxial experiments proved most useful in studying fracture growth and shape as affected by the crossing interactions. From the plots it can be concluded that consistency between crossing and non-crossing cases was not observed when comparing the uniaxial and the biaxial tests. The test conditions used by Renshaw and Pollard (1995) were uniaxial and the results of this thesis suggest that the intermediate principal stress plays a significant role in the crossing interaction. This study should be repeated considering different values of horizontal stresses.

The laboratory results obtained for this thesis support the existence of a viscosity effect since the higher viscosity fluid produces a crossing behaviour at a lower normal stress condition. The different stress states near the leading edge in a viscous-dominated fracture growth regime, which held for tests using the higher viscosity injected fluid, may induce slip on the discontinuity before the fracture reaches the discontinuity (Lecampion and Zhang 2005).

Nevertheless, any slip that occurs because of this does not necessarily result in fracture arrest. The higher viscosity fluid reduces the loss of fluid into the discontinuity that is associated with use of a low viscosity fluid. A low viscosity fluid can also more easily enter and pressurize the interface during the interaction, which serves to reduce the shear strength of the discontinuity and its ability to transmitted shear stress into the rock on the other side. This is an important finding of this thesis and points to the interface permeability and its interaction with the injected fluid viscosity as an important factor that needs to be accounted for in any crossing criterion. A similar suggestion has been published by Chuprakov et al., (2013a, b) and Bunger et al., (2015).
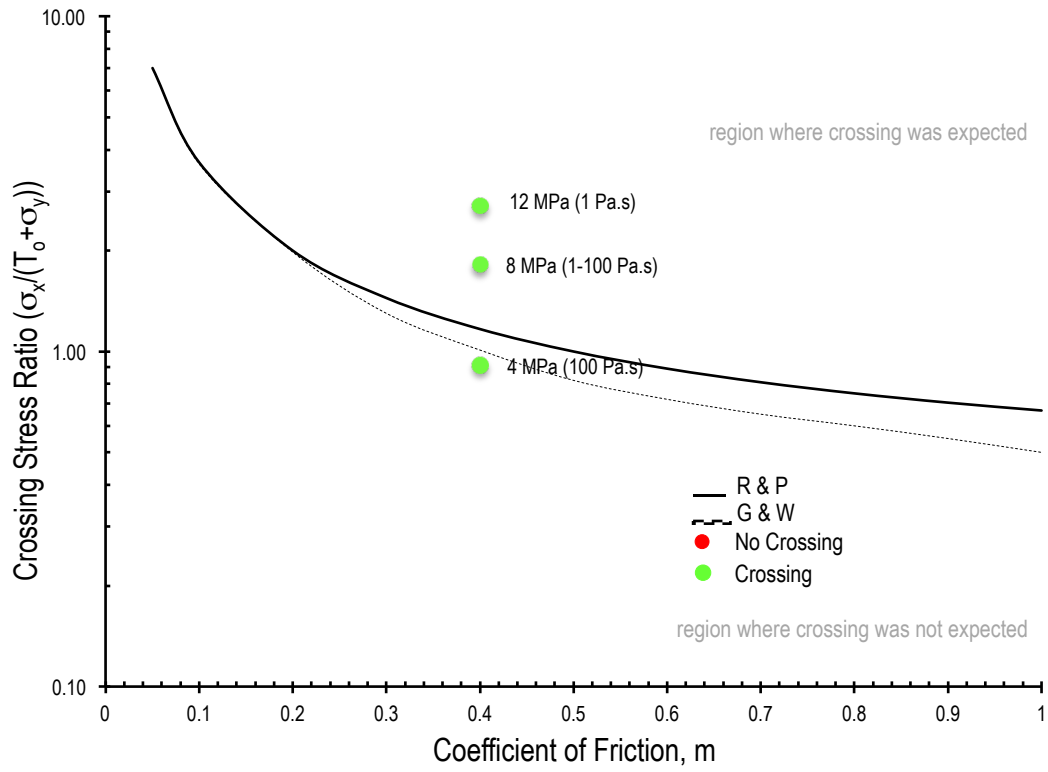
Figure 37. Biaxial tests results presented after Renshaw and Pollard (1995) and Gu and Weng (2010)
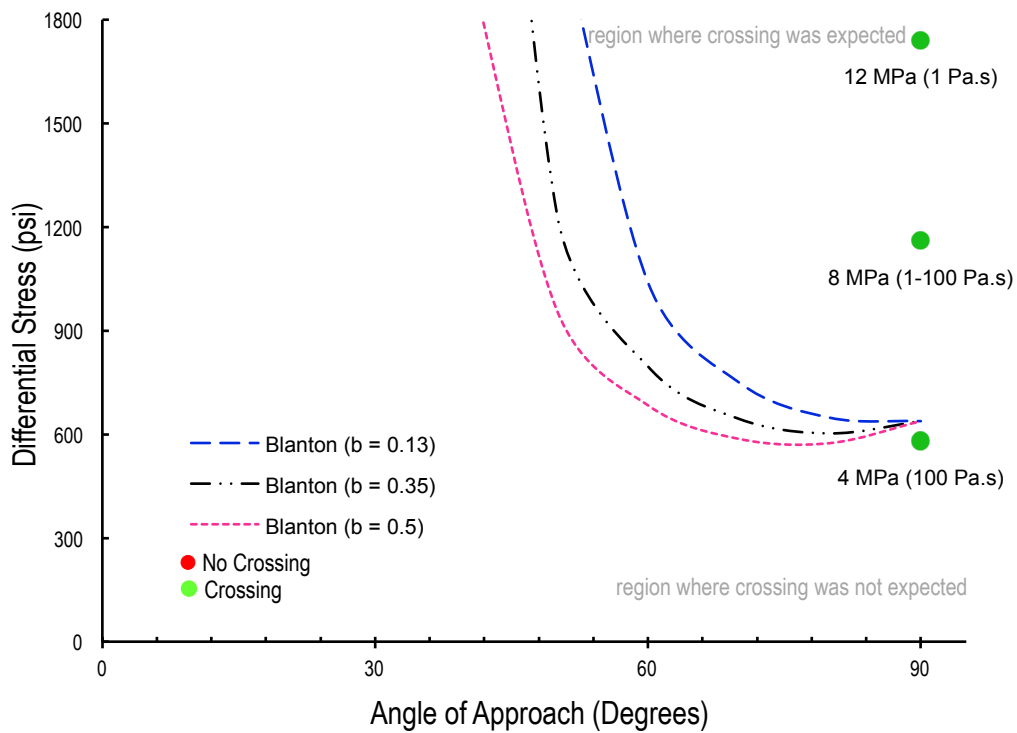
Figure 38. Biaxial tests results presented after Blanton (1986)

3.6. *Summary*

The uniaxial and biaxial laboratory experiments carried out for this thesis were designed to extend Renshaw and Pollard's (1995) work by using hydraulic fractures rather than the mechanical loading used by Renshaw and Pollard (1995). Although Blanton (1986) used fluids for the propagation, his work did not consider the effect of fluid viscosity in the crossing behaviour. Supported by the scaling theories, the inclusion of viscous fluids into the experimental approach used for this thesis, allowed recreating viscosity- and toughness-dominated scenarios. In this thesis, the hydraulic fractures were designed such that they intersect orthogonally at an unbonded machined frictional interface, which represented a natural fracture.

To measure the effect of stress, the R & P (1995) crossing stress ratio (CSR) was used as a reference point to predict whether a hydraulic fracture would cross or not the natural fracture. The fracture extent of each experiment was investigated via post-experiment visual inspection, which allowed assessment of the effect of the viscosity. Finally, the criteria of R & P (1995), Blanton (1986) and Gu and Weng (2010) were compared to the results obtained in the laboratory.

This chapter summarizes the results of fourteen experiments. In addition, the laboratory tests that were not presented here, which were carried out initially helped in defining the importance of having ground flat rock samples. Contrary to Renshaw and Pollard (1995) who ignored this factor, by removing curvature and local imperfections on the plates' surfaces, valid experimental comparisons for the other parameters controlling crossing were obtained. Otherwise, the high contact stresses could well have resulted in a false crossing interaction. Additionally, the initial trials contributed to improving the final setup, mainly by highlighting the need for the sample plate that hosts the borehole to be wide enough to prevent stress disturbances onto the first set of interfaces.

The laboratory work undertaken for this thesis produced four findings:

Firstly, in reference to the normal stress acting across the interfaces, in general it can be concluded that the higher it is the more likely the fracture will cross the interface. Additionally, although more complicated to carry out, running experiments that include a non-zero minimum stress would allow minimising fluid lag and the free-surface effect when using a high viscosity fracturing fluid.

Secondly, the results discuss in this chapter support the existence of a viscosity effect. Contrary to Renshaw and Pollard (1995), the viscosity-dominated hydraulic fractures crossed the natural fractures more easily than the toughness-dominated fractures. A hydraulic fracture propagating in a toughness dominated regime is more likely to enter and pressurize a natural fracture during the interaction, which serves to reduce the shear strength of the discontinuity and its ability to transmit shear stress into the rock on the other side. A viscosity-dominated fracture is more likely to cross a discontinuity because the fluid is less likely to enter into a discontinuity. Thus, both the fracturing fluid viscosity and the permeability of the discontinuity are parameters that need to be considered in developing criteria for predicting crossing interaction behaviour.

Thirdly, the effect of discontinuities on hydraulic fracture propagation was observed as a retarded but stress-dependent growth associated with the propagation through the discontinuities. The fractures grew further for cases where a higher normal stress was applied across the discontinuity direction. As normal stress acting on the discontinuities was increased, the ultimate fracture length in that direction becomes larger. The biaxial experiments proved most useful in studying fracture growth and shape as affected by the crossing interactions.

Finally, in reference to the hydraulic fracture growth, Renshaw and Pollard (1995) predict crossing to occur for cases where arresting was the result obtained by uniaxial experiments carried out as part of the work of this thesis. Additionally, consistency between crossing and non-crossing cases was not observed when comparing the uniaxial and the biaxial tests. The biaxial tests showed that crossing occurred for all stress conditions so the non-crossing comparison cannot be made.

The interpretation of these findings leads to the following conclusions:

- The observations on the fracture geometry allow confirmation of the hypothesis presented in the introductory chapter: "When applied to hydraulic fracturing, the work of Renshaw and Pollard (1995) and Thiercelin et al. (1987) and as suggested by van As and Jeffrey (2002), the hydraulic fractures may grow more quickly in the direction of the maximum stress or fewer discontinuities. An elliptical fracture shape, with the long axis along the direction of higher stress or fewer discontinuities, may develop as a result", an

important finding for the design of hydraulic fracture treatments in naturally fractured rocks.

- Crossing of the discontinuities was enhanced by the use of higher viscosity fluids, in part because the high viscosity fluids were not lost into the frictional discontinuity as easily as lower viscosity fluids. The fluid viscosity and the permeability of the interface that the hydraulic fracture is interacting with are important parameters in determining if crossing will occur or not. However, the viscosity-dominated hydraulic fractures exhibited fluid lag. A lower fluid viscosity could have been used for the toughness-dominated tests, but high leakoff of fluid into the sandstone precluded its use for these tests. Additionally fluid lag should be minimised and the free surface effect avoided by applying stress along the y direction. The experiments run for this thesis suggest work with this test geometry should be undertaken using a rock material with lower permeability so that fluid loss and lag do not limit the range of parameters that can be considered in obtaining experimental results. This is exactly what Bunger et al. (2015) did with further improvements and analysis including an extension of this type of work to non-orthogonal cases.

- From the sample preparation step, the laboratory results of this thesis and from measuring fracture growth in field experiments, it seems that the R & P (1995) and Gu and Weng (2010) criteria provide a lower limit on discontinuity strength that result in hydraulic fractures crossing geological discontinuities. A higher normal stress is needed to generate a crossing condition than what is predicted by the either of these criteria.

- The crossing behaviour observed in the experiments carried out for this thesis combined with Bunger et al. (2015), contributes to a new perspective in the hydraulic fracture growth through orthogonal discontinuities: it does not depend only on the friction coefficient of the interface. This result contradicts the current models in which interface plasticity plays a key role for understanding the crossing interaction between a hydraulic and a natural fracture. Should further studies in other rock types provide a similar outcome, a new mechanism should be sought and defined.

- The results from this thesis together with the work by Bunger et al. (2015) suggest that the numerical work of Chuprakov et al. (2013) on the effect of natural fracture permeability on the crossing interaction should be acknowledged with higher importance than the friction itself.

- Renshaw and Pollard (1995) and Gu and Weng (2010) do not allow for crossing after slip has occurred but the laboratory results obtained for this thesis suggest that hydraulic fractures can cross discontinuities after some fluid penetration into the interface. Some slip is likely to have occurred in such cases although no direct measurements of slip on interfaces were made. This result creates the need to understand the mechanics surrounding frictional crossing interactions with permeable discontinuities. Therefore, the effect of slip prior to intersection was studied theoretically using the procedure presented in the next chapter

Chapter 4

MATHEMATICAL MODEL AND SCALING

The validity of the R & P (1995) and Blanton's criteria (1986) has been examined in light of laboratory experiments as presented in the previous chapter. In developing their criterion, Renshaw and Pollard (1995) assume fracture re-initiation is not possible after the occurrence of slip along the natural fracture. However, even though a natural fracture is in a partially sliding stage, tensile stress parallel to the natural fracture at some points can be generated. Only after the entire natural fracture is in slip, will the stress concentration disappear, as studied by Dollar and Steif (1988). Hence, there is potential for fracture re-initiation during the time interval between the start of slip and the full sliding of the natural fracture. Furthermore, a flaw may exist in the rock on the far side of the natural fracture, which would allow a hydraulic fracture to re-initiate without requiring generation of a tensile stress equal to the tensile strength of the intact rock. Such a variation of tensile strength is not considered further in this thesis, but it must be recognised as a factor that can influence laboratory and field scale results on fracture crossing and interaction.

It is natural to discuss the fracture re-initiation from the natural fracture within the framework of fracture mechanics. The presence of fractures in a structure weakens it. The stress at the fracture tip increases during loading, which may lead to fracture growth and structural failure. Therefore, it is of high importance to account for the presence of fractures in a material and to understand the stress distribution around the fracture tip. The theory of Linear Elastic Fracture Mechanics (LEFM) has been widely used for studying fracture propagation problems. This theory is based on linear elasticity, i.e. the mathematical study of how solid bodies deform elastically and become internally stressed as a result of loading conditions. According to LEFM, a fracture will propagate when the stress intensity factor (K) at the fracture tip reaches a critical value (Kc) known as the fracture toughness of the material. The stress intensity factor is a function of the loading parameters and of the geometry of the fracture and body. The fracture toughness is taken to be a material property that is evaluated experimentally.

The fracture propagation criterion of LEFM is associated with the Griffith theory of fracture and, to be valid, plastic flow is limited in a small region very near the tip. In developing the LEFM model, it is assumed that no plastic deformation or energy absorption takes place at the fracture tip. Instead, the material is elastic everywhere and energy is used either to elastically deform the material all around the fracture or break the material at the tip. A restriction to the validity of LEFM

is the requirement that any plastic deformation, occurring in real materials, be confined to a small zone at the tip that is encompassed by the region dominated by the elastic stress singularity zone near the fracture tip.

Renshaw and Pollard (1995) employed the LEFM-based solutions for the associated singular near-tip elastic stress fields; hence many geometric lengths such as finite fracture length are not included in their criterion. They calculate the stress on the interface at a point on the edge of the elastic stress singularity dominated zone. Furthermore, their criterion was compared to experiments using mechanical fracture loading rather than fluid-driven fractures. The associated simplification can certainly cause some mismatch between the predictions and the experimental and field scale results.

Alternatively, Blanton (1986) neglected the stress induced by the hydraulic fracture itself and assumed that a simplified shear stress distribution exists on the pre-existing geological discontinuity (Zhang, 2007). Blanton's (1986) criterion is possibly more correct for fracture initiation from a fault, where slip is remote from any pressurized hydraulic fracture.

In addition, the effect of fluid viscosity on the stress field around a hydraulic fracture has been shown to be significant by Lecampion and Zhang (2005) who analysed the onset of slip on a frictional natural fracture interacting with an approaching finite-length hydraulic fracture driven by a viscous fluid. The analysis of Lecampion and Zhang (2005) indicated that the fracture propagating in the viscosity-dominated regime would induce slip on the natural fracture more easily than a hydraulic fracture propagating in the toughness-dominated regime. This conclusion suggests that crossing, according to Renshaw and Pollard (1995), should be more difficult for viscous-dominated hydraulic fractures. As presented in chapter 3, this prediction is not supported by results from the experiments undertaken for this thesis (Llanos et al., 2006).

Therefore the effect of viscosity on the crossing interaction is more complicated and cannot be predicted based only on whether or not slip occurs on the natural fracture before the hydraulic fracture intersects it. However, in order to understand the mechanics of fracture crossing through the frictional geological discontinuities, the effect of slip prior to and post intersection should be investigated, especially for the finite-length fracture geometry.

In this chapter, the incipient point of frictional slip is determined by reformulating the problem and grouping some parameters to form dimensionless terms so as to reduce the number of parameters in the analysis. This dimensional analysis is important for developing mathematical models of physical problems as well as for understanding existing models. This analysis is followed by results obtained by solving the proposed problem, by using both an analytical and a numerical method.

The procedure to obtain the stress changes in the presence of a finite-length fracture is next discussed in detail. The stresses at the points along the natural fracture, prior to the occurrence of frictional slip, can be obtained using analytical solutions to include the effect of fracture length (Sneddon, 1995; Weertman, 1996). With an appropriate failure criterion, the governing equations for determining the incipient slip points can be solved analytically, the solution of which provides universal curves for the initiation of slip. Through those curves, presented in chapter 5, the incipient sliding points can be found without the need of additional analysis. This approach takes account of the stress generated by the entire pressurised fracture in predicting slip, in contrast to Renshaw and Pollard (1995) who only consider the stress fields near the tip of a mechanically loaded but unpressurised fracture.

The numerical modelling was undertaken using MineHF2D (Mining Hydraulic Fracture 2D), CSIRO's hydraulic fracturing model, a 2D plane-strain boundary element–based computation code. The program has been developed by Xi Zhang and Robert Jeffrey from CSIRO and Emmanuel Detournay from the University of Minnesota. This in-house research program has been applied to studies of the impact that pre-existing geological discontinuities have on hydraulic fracture propagation, as reviewed in section 1.4.

MineHF2D allows investigating various interaction cases including the mechanisms of fracture re-initiation (Zhang et al., 2008). Also, the numerical model can consider frictional slip, which allows the evolution of the zone of slippage on the natural fracture as a hydraulic fracture grows towards it.

4.1 Scaling

4.1.1. Problem Definition

A uniformly pressurized finite-length fracture approaching perpendicularly to a frictional interface is considered as depicted in Figure 39. A uniform pressure distribution in a hydraulic fracture is equivalent to using an inviscid fluid or assuming zero viscous dissipation. This pressure distribution is used here because it allows use of a closed-form analytical solution for stresses around the pressurised fracture.

Let *H* denote the distance between the closest tip of the hydraulic fracture, drawn as a blue line, and the discontinuity (drawn as a brown line). *L* denotes the distance between the other tip of the hydraulic fracture and the discontinuity.
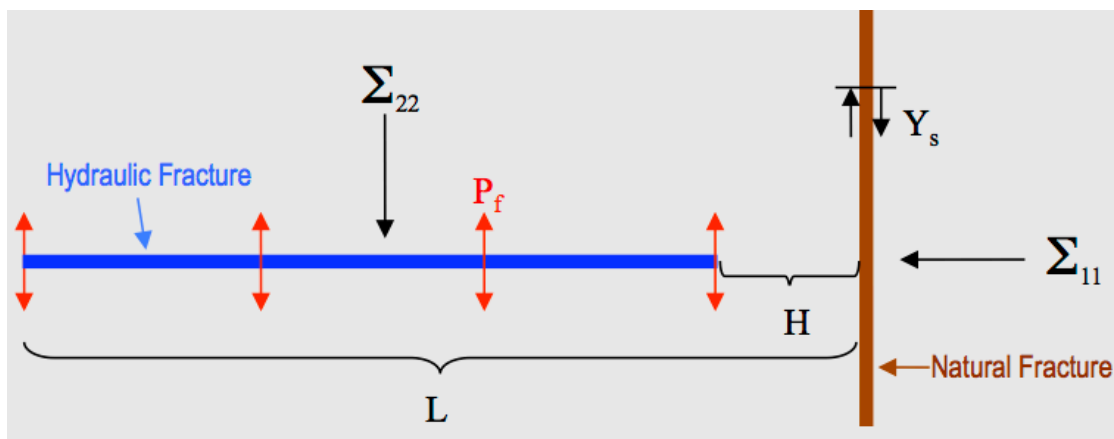
Figure 39. Geometry for the scaling problem definition

For this analysis, the distance *H* is considered as fixed and L is increased to study the effect of fracture size. This process generates stresses on the interface that are identical to those produced by moving the near tip closer to the interface. When the fracture tip moves closer, the stress levels on the discontinuity increase. In addition, the length of the discontinuity is infinite so that incipient slip can occur at any distance to the fracture plane.

However, the pressure in the hydraulic fracture is adjusted to ensure the fracture is always in critical equilibrium at both tips, i.e. $K_I=K_{IC}$ (the subscript I stands for tensile or mode I fracture), i.e., the internal pressure P_f is computed so that $K_I=K_{IC}$ is satisfied. In general, the internal pressure will then decrease with fracture growth.

The parameters used for the problem under the plane-strain conditions are therefore:

- Geometry: H and L
- Discontinuity: *m* (friction coefficient)
- Stress: Σ_{11} and Σ_{22}
- Rock properties: E' (Young modulus)

    ν (Poisson ratio) and

    K_{IC} (critical stress intensity factor).

Evolution is considered in terms of the change in geometry, namely H is adopted as the evolution parameter. Time is not a parameter of the problem but the evolution in time can be readily computed *a posteriori* by dividing the fracture volume by any given constant injection rate *Qo*.

Besides the stress and displacement fields (U, V), the solution *S* of the problem consists in particular of:

- Net fracture pressure: $P = P_f - \Sigma_{22}$
- Slip front location: Y_s
- Maximum tensile stress Σ_{Imax} (or maximum K_I) along the other side of the discontinuity, where Σ_I is the most tensile principal stress.

Thus the solution is of the form $\quad S = \mathscr{F}\left(H; L, E', \nu, K_{IC}, m, \Sigma_{11}, \Sigma_{22}\right)$
<div align="right">Eq. 10</div>

Following the scaling used by Detournay (2004) and Bunger et al. (2005), it is convenient to introduce the following characteristics quantities:

- Characteristic length: $L_* = H$
<div align="right">Eq. 11</div>

- Characteristic stress: $\Sigma_* = \dfrac{K_{IC}}{\sqrt{H}}$
<div align="right">Eq. 12</div>

Hence the scaled quantities are:

$$h = \frac{2H}{H+L} \qquad x_j = \frac{X_j}{H} \qquad \varepsilon = \frac{\Sigma_*}{E'}$$

$$\sigma_{jj} = \frac{\Sigma_{jj}}{\Sigma_*} \qquad \sigma_{\mathrm{Im}ax} = \frac{\Sigma_{\mathrm{Im}ax}}{\Sigma_*} \qquad p = \frac{P}{\Sigma_*}$$

$$y_s = \frac{Y_s}{H} \qquad u = \frac{U}{\varepsilon H} \qquad \upsilon = \frac{V}{\varepsilon H}$$

So that
$$\{y_s, p, \sigma_{\mathrm{Im}ax}\} = \Phi(h; \varepsilon, \sigma_{11}, \sigma_{22}, \nu, m). \qquad \text{Eq. 13}$$

It is possible to see the reduction in the number of controlling parameters by 2 after comparing equations 10 and 13.

The effect of σ_{22} is expected to enter only via its influence on the net pressure and in the computation of σ_{Imax}. The evolving non-dimensional parameter in equation 13 is h to highlight how close the fracture tip is from the discontinuity. In addition, the effect of ν is not significant, as it is only included in the plane-strain modulus E'.

4.1.2. Objective

The end of the elastic regime corresponds either to the onset of slip or opening on the discontinuity and it is computed, as was done by Lecampion and Zhang (2005), but is recast using the dimensionless formalism presented above. The elastic regime corresponds to the range for the evolving parameter $h_p < h < 1$ where the elastic limit is of the form presented below. The subscript p when applied to h stands for plastic.

$$h_p = h_p(\sigma_{11}, m)$$

In this thesis only the onset of slip (plastic deformation) is evaluated, and therefore the method is valid if $m < m_s$ (σ_{11}) (initial slip regime). The determination of the critical value of the evolving parameter becomes important in the analysis of fracture crossing. The numerical simulations carried out for this thesis allow finding the critical value for different stress conditions.

4.2 Analytical Solution Method

4.2.1. Problem Definition

For this thesis the behaviour of the onset of slip is estimated analytically using the geometry illustrated in Figure 39. The stress components for a uniformly pressurized fracture are considered (equations. 14 - 16; Weertman, 1996). These equations are valid for a mode I fracture in an infinite linear elastic solid, or when there is no relative displacement along the discontinuity. In this chapter the results using the physical variables are presented. The dimensionless formulation of the required results in terms of the evolving parameter will be presented in next chapter. In the following, the subscripts L and R refer to the left and right hand fracture tip, respectively, while the C stands for the centre of the fracture (see Figure 40).
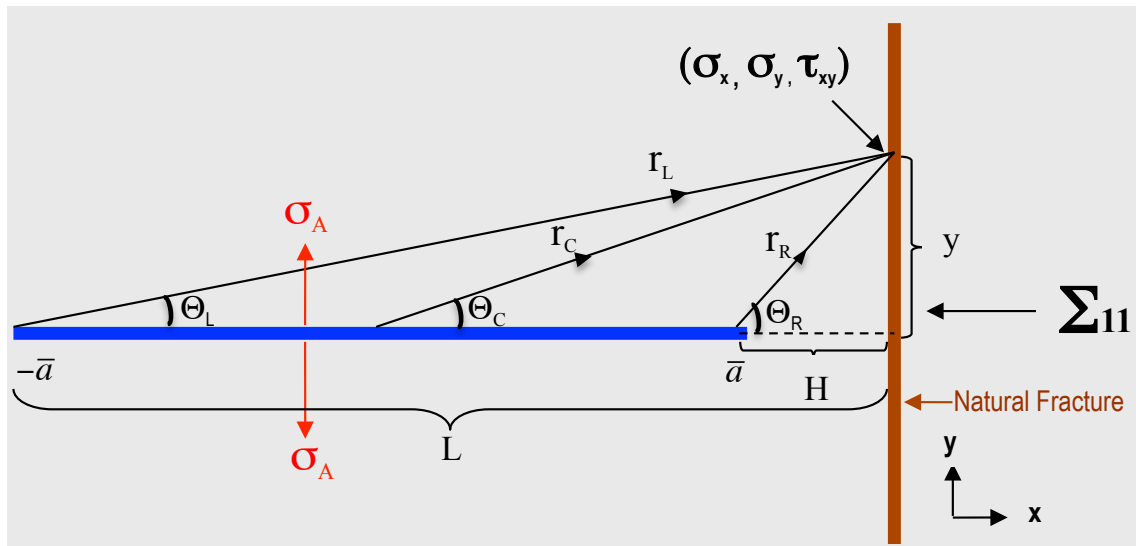
Figure 40. Geometry of the problem for the analytical calculation of h_p

$$\sigma_x = -\sigma_A + \sigma_A \left[r_c / 2r^* \right] \begin{Bmatrix} 2\cos\left(\theta^* - \theta_C\right) + 2\sin\theta_C \sin\theta^* \\ -\sin\theta_R \sin\left(\theta^* + \theta_R - \theta_C\right) - \sin\theta_L \sin\left(\theta^* + \theta_L - \theta_C\right) \end{Bmatrix}$$ Eq. 14

$$\sigma_y = \sigma_A \left[r_c / 2r^* \right] \begin{Bmatrix} 2\cos\left(\theta^* - \theta_C\right) - 2\sin\theta_C \sin\theta^* \\ +\sin\theta_R \sin\left(\theta^* + \theta_R - \theta_C\right) + \sin\theta_L \sin\left(\theta^* + \theta_L - \theta_C\right) \end{Bmatrix}$$ Eq. 15

$$\tau_{xy} = \sigma_A \left[r_c / 2r^* \right] \begin{Bmatrix} \sin\theta_R \cos\left(\theta^* + \theta_R - \theta_C\right) \\ +\sin\theta_L \cos\left(\theta^* + \theta_L - \theta_C\right) - 2\sin\theta_C \cos\theta^* \end{Bmatrix}$$ Eq. 16

Where: the net pressure is defined as $\sigma_A = p_f - \Sigma_{22}$ and

$$r^* = \sqrt{r_L r_R},$$

$$r_C = \sqrt{x^2 + y^2},$$

$$r_L = \sqrt{(x+\bar{a})^2 + y^2},$$

$$r_R = \sqrt{(x-\bar{a})^2 + y^2},$$

$$\theta^* = \frac{1}{2}(\theta_L + \theta_R),$$

$$\theta_C = \tan^{-1}[y/x],$$

$$\theta_L = \tan^{-1}[y/(x+\bar{a})],$$

$$\theta_R = \tan^{-1}[y/(x-\bar{a})],$$

Eq. 17

and $-\pi \le \left\{\theta_C, \theta_L, \theta_R, \theta^*\right\} \le \pi.$

4.2.2. Failure Criterion and Solution Method

In order to find the incipient slip location, the effective normal stress and the corresponding net frictional stress are calculated based on Coulomb's frictional law at any position y along the discontinuity in terms of equations 18 and 19 as follows,

Effective normal stress: $\qquad f_x\left(\sigma_A, \Sigma_{11}, \bar{a}, y\right) = \sigma_x - \Sigma_{11}$

Eq. 18

Net frictional stress: $\qquad g\left(\sigma_A, \Sigma_{11}, \bar{a}, y, m\right) = \tau_{xy} - m f_x\left(\sigma_A, \Sigma_{11}, \bar{a}, y\right)$

Eq. 19

where σ_x and τ_{xy} are known from equations 14 and 16 and $\bar{a} = \dfrac{(L-H)}{2}$.

However, equation 19 contains two variables ($\bar{a}$, y) and can only be solved numerically at a given H. An alternative way is to find the location of the maximum in net frictional stress along the discontinuity. The slip should occur first at this location prior to extending along the discontinuity. Therefore the incipient slip location can be found. In particular, this approach leads to

$$h\left(\sigma_A, \Sigma_{11}, \bar{a}, y, m\right) = \partial_y g\left(\sigma_A, \Sigma_{11}, \bar{a}, y, m\right) = 0$$

Eq. 20

Additionally, the stress field depends on the net pressure in the hydraulic fracture. Based on the failure criterion, the net pressure can be calculated as

$$\sigma_A = \frac{K_{ic}}{\sqrt{\pi \bar{a}}}$$

Eq. 21

Moreover, the solutions on y are only dependent on the stress ratio Σ_{11} / σ_A. Particularly, another dimensionless parameter for this stress ratio is introduced as

$$S = \frac{\Sigma_{11}}{\sigma_A} \sqrt{\frac{2H}{\pi(L-H)}}$$

<div align="right">Eq. 22</div>

The software Mathematica was used for solving the above equations and the script is presented in Appendix C.

4.3 Numerical Solution Method

MineHF2D is useful for analysing the problem posed in this thesis as it allows investigating various interaction cases. Of special interest, MineHF2D allows modelling the zone of slippage on the natural fracture as a hydraulic fracture grows towards it. The model checks the slippage condition based on Coulomb's friction law. Recalling equation 4 from section 3.2.2 and presented below, the friction law is simplified by setting the cohesion (*C*) to zero.

$$|\tau| < C + \sigma \tan\phi \qquad \text{(But C is zero)}$$

<div align="right">Eq. 4</div>

Explicitly, if the shear stress (τ) reaches the critical value that is equal to the product of the coefficient of friction (*tanϕ*, ϕ being the angle of friction) and the effective normal stress (σ), a sliding mode is present at that point on the natural fracture. The shear strength varies with the normal stress at each position, since the normal stress is dependent on the hydraulic and natural fracture interaction.

For the numerical simulations, the material information such as Young's modulus, Poisson's ratio and fracture toughness were chosen to represent those of the rock materials used in the laboratory as presented in the following chapter. Likewise, the boundary conditions imposed, such as constant injection rate and stresses normal to the hydraulic and natural fractures were as used in the laboratory. Finally, a sufficiently small element size must be used to obtain accurate numerical results. A sensitivity study checking for suitable element size has therefore been done and is presented in Appendix D.

Furthermore, for problems involving hydraulic fracture propagation, an additional boundary condition is needed in the form of a fracture propagation criterion. To comply with the assumptions used in this thesis, in MineHF2D, the fluid flow in the fractures is based on the uniform pressure assumption. And the propagation criterion is expressed as $K_I=K_{Ic}$. By satisfying this condition, the hydraulic fracture satisfies the propagation criterion and the energy is only dissipated in the creation of new fracture surface in the rock medium.

4.4 Summary

The experiments by both Renshaw and Pollard (1995) and Blanton (1986) were carried out for toughness-dominated conditions and their crossing criteria do not consider fluid viscous dissipation in a hydraulic fracture. The effect of viscosity on the interaction of the hydraulic and frictional natural fractures was evaluated in this thesis through uniaxial and biaxial tests. An important result is that the laboratory experiments carried out as part of this thesis suggest crossing can occur after slip on the interface. To investigate the mechanics of slip generation, this thesis combines a numerical and analytical analysis as described in this chapter. The numerical results are presented next in Chapter 5 followed by a comparison of the experimental data to the numerical and analytical data as presented in Chapter 6.

Both the hydraulic fracturing model used, called MineHF2D, and the scaling method were developed at CSIRO. The scaling was designed for toughness-dominated cases, which MineHF2D can also reproduce. In addition, the scaling considers the hydraulic fracture to be uniformly pressurized, which is also known as a Griffith-Inglis fracture problem.

Weertman's analytical solution (1996) has been applied to the same problem to verify the numerical results. The solution for stress around a uniformly pressurised fracture given by Weertman (1996) has been adapted to the problem geometry used with the scaling. The difference between the approach used in this thesis and that used by Renshaw and Pollard (1995) is that they used the fracture-tip singular stress solution. This means their analysis does not include the effect of finite fracture length and the non-singular stress changes induced by the entire pressurised fracture. The approach used for this thesis is therefore an improvement to their analysis. This approach allows finding universal curves for the locations of slip starting points, an important aid for hydraulic fracture design.

Chapter 5

MODELLING RESULTS AND DISCUSSION

In their results for large toughness cases, Lecampion and Zhang (2005) indicate that natural fractures that are oriented orthogonally with respect to the hydraulic fracture are more stable to induced shear and this increases the chances of crossing. Lecampion and Zhang (2005) also investigated the governing parameters controlling the beginning of the interaction between a single pre-existing discontinuity and an approaching hydraulic fracture. The onset of the interaction was defined as the first occurrence of plasticity, i.e. frictional shear strength exceeded by shear stress at a point along the natural fracture. Lecampion and Zhang (2005) do not consider displacement and stress conditions after sliding initiates. Fracture re-initiation may occur after the hydraulic fracture reaches the natural fracture.

Studying cases with non-orthogonal angles of approach between the hydraulic and natural fractures were out of the scope of the experimental, numerical and analytical works carried out for this thesis. The elastic limit corresponding to the onset of slip (plastic deformation) along the discontinuity is determined for toughness-dominated conditions as per the dimensionless analysis described in the previous chapter.

In order to verify the dependence on the evolving parameter, several runs with different fracture geometries were explored. For the modelling work carried out for this thesis the definition of the onset of the interaction as described by Lecampion and Zhang (2005) is followed. This chapter reports on the numerical and analytical results for the onset of slip. The evolution parameter h_p defining the beginning of the interaction is graphically presented as a function of two dimensionless parameters: the stress ratio and the discontinuity friction coefficient.

5.1 Numerical Results

The MineHF2D results plotted in Figure 41 display the evolution of h_p with respect to the coefficient of friction (m) of the discontinuity for different values of dimensionless stress (S), refer to equation 22 (section 4.2.2). Recall that $h = 2H/(H+L)$ where H and L denote the distances between the closest and furthest tips of the hydraulic fracture and the discontinuity respectively. The subscript p stands for plastic. A small h_p value indicates that for slip to occur, the hydraulic fracture's total length must be large compared to the distance from the closest tip to the

discontinuity. As h_p increases to 1 the hydraulic fracture's length relative to H decreases to zero. Conversely, when h_p = 0 the hydraulic fracture's length is infinite. Table 6 shows a range of values of L with regard to H and the corresponding scale quantity h.
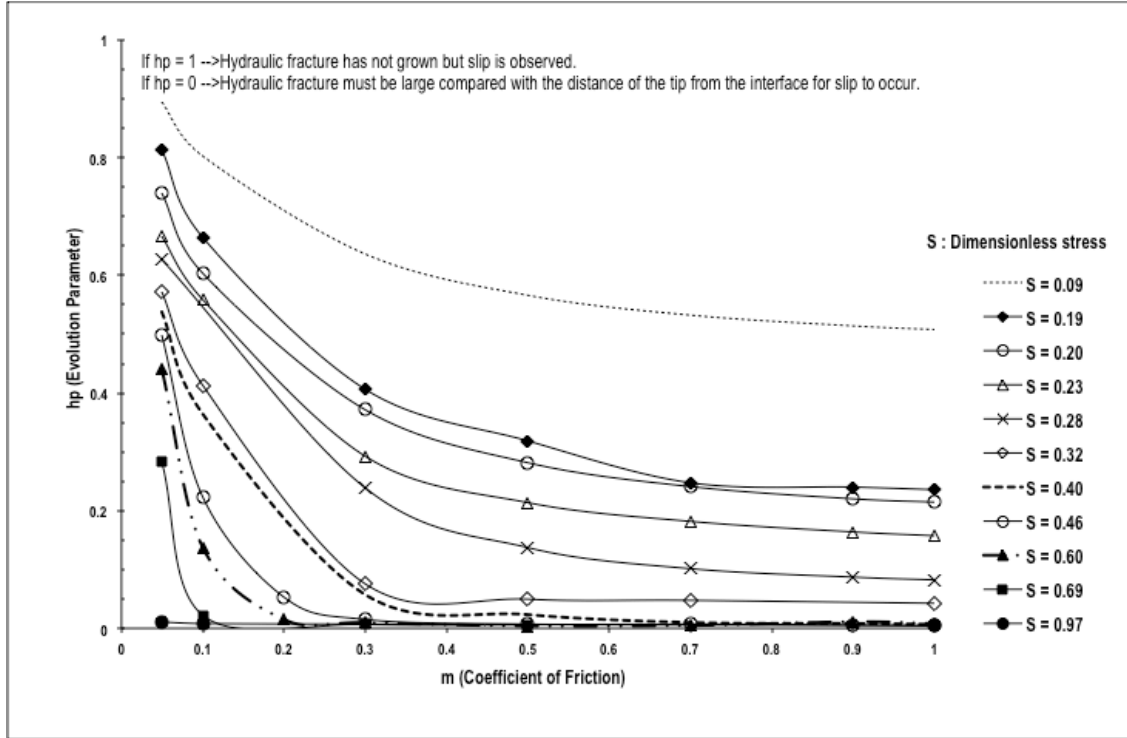
Figure 41. Evolution of h_p with respect to m for different values of S – numerical results.

L =	H	1.2H	1.5H	1.8H	2.5H	3H	4H	5H	8H	19H
h =	1	0.9	0.8	0.7	0.6	0.5	0.4	0.3	0.2	0.1

Table 6. Values of h for different values of L with regard to H

As expected, plasticity occurs more easily for low stress values and for low values of the friction coefficient in which cases the hydraulic fracture does not need to grow much before slip occurs. As S, the dimensionless stress, increases, the likelihood for slip to develop decreases.

The results in Figure 41 also depict a region where the slope of the curves seems to be insensitive to the coefficient of friction. For the higher dimensionless stress down to S=0.32, an h_p value does not decrease further as m is increased after a critical point. This indicates that for S greater than 0.32, h_p does not depend on m provide m is larger than about 0.5 in value. For values of S less than 0.32 and friction values higher than 0.5, which involve sandstones, granites

and gneiss, the data vary slowly with m and fall nearly on straight lines indicating a more or less linear behaviour in the h_p versus m curves. Values of m higher than 1.0 were not considered because they are not representative of frictional measurements on rock.

The independence of h_p on m becomes more obvious when presenting the results with respect to the dimensionless stress for different values of friction, as in Figure 42. For S higher than 0.4 and coefficients of friction higher than 0.5 the results indicate slip is prevented by frictional strength developed under high loading conditions since h_p is zero. Also, unless the values of m are very small, for values of S higher than 0.4 the chances for slipping occurring are small since H must be very small or L must be very large to produce a nearly zero h_p. This implies that for these conditions incipient slip can only occur when the fracture tip is very close or touches on the natural fracture.
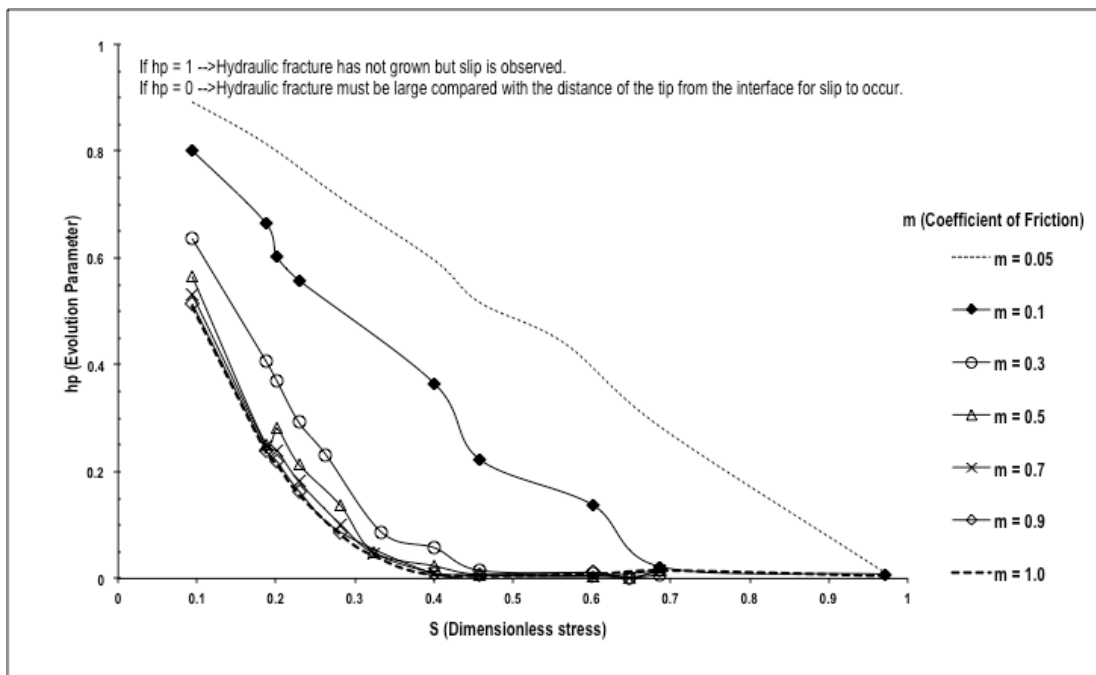
Figure 42. Evolution of h_p with respect to S for different values of m – numerical results

5.2 Analytical Results

When verifying the numerical results by applying Weertman's (1996) analytical solution, Mathematica software was used. By using the analytical method more data can be calculated and therefore smoother curves were obtained. Similar to the numerical results, the results plotted in Figure 43 and Figure 44 show the conditions for sliding of the natural fracture become more

favourable as far-field stress decreases and *vice versa*. When the stress is close to zero, slip is observed with no growth of the hydraulic fracture, regardless of the friction coefficient used. The higher the frictional coefficient along the natural fracture, the longer the hydraulic fracture needs to be for slip to occur.
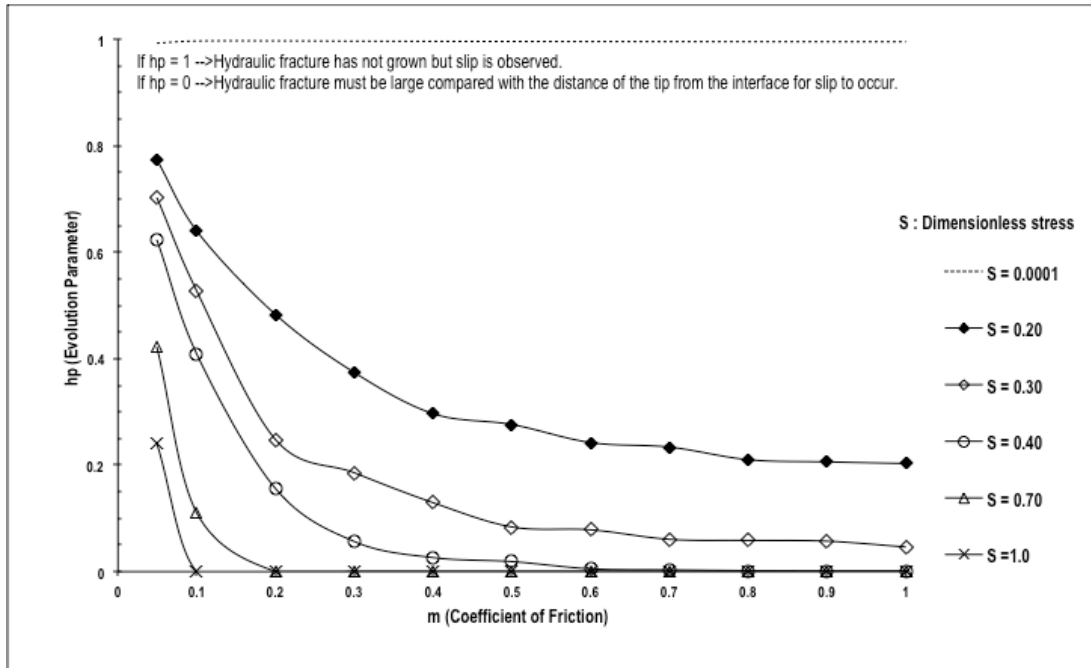
Figure 43. Evolution of h_p with respect to m for different values of S – analytical results
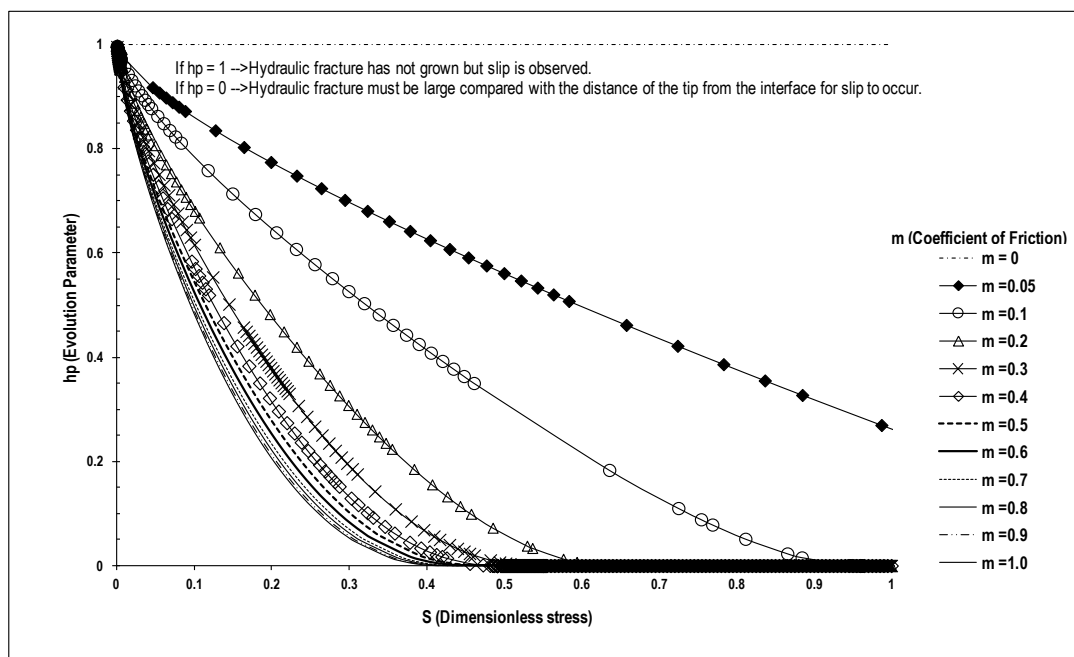
Figure 44. Evolution of h_p with respect to S for different values of m – analytical results

5.3 Comparison between Numerical and Analytical Results

When plotting together the numerical and analytical results, as in Figure 45 and Figure 46, a reasonable match is observed, and the curves show a power-law relationship. The data treatment will be discussed in the next section. Especially, the analytical results, which provide more accurate results at small values of m.
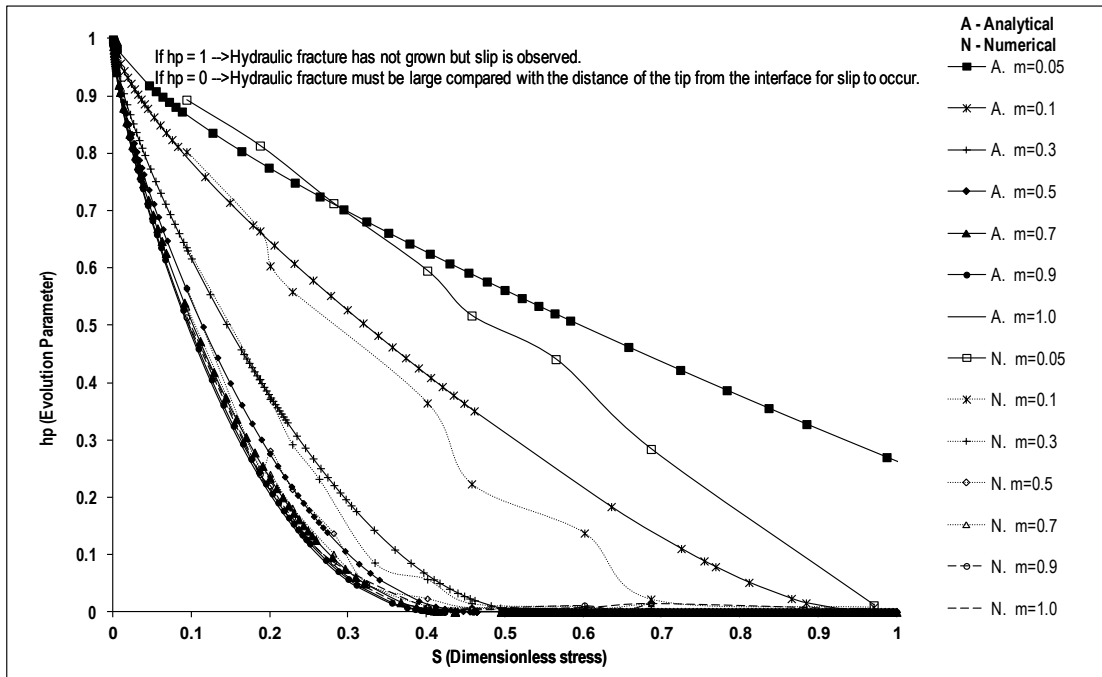
Figure 45. Evolution of h_p with respect to S for different values of m – Comparison between analytical and numerical results
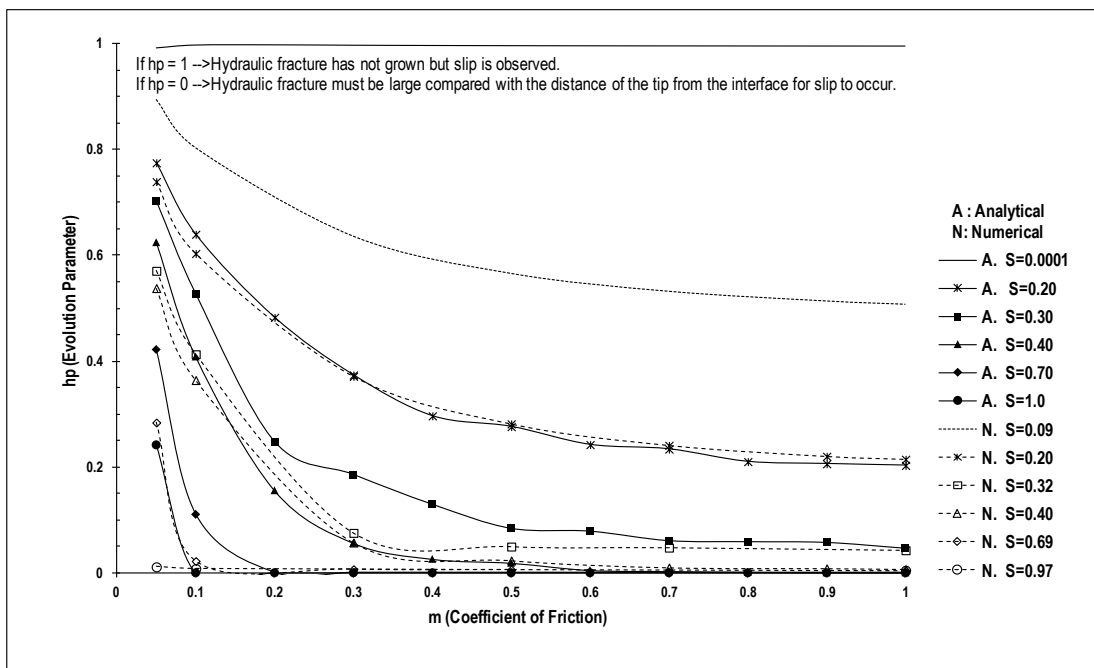
Figure 46. Evolution of h_p with respect to m for different values of S – Comparison between analytical and numerical results

5.4 Universal Curves

The curves in Figure 45 show trends that can be easily fitted by least squares methods. To reduce the computational burden, the universal curves for h_p were fitted to curves. Therefore, SigmaPlot software has been used to fit these curves in Figure 45 and the results are presented in Appendix E. The universal curves allowed obtaining equation 23 which will help designers of industrial hydraulic fractures to find methods to promote or predict fracturing crossing, provided dimensionless friction (m) and stress (S) are given, and if that is the aim of the treatment. This industrial application could be possible once a numerical study similar the one undertaken in this thesis is carried for the opening of the interface. By doing this, a connection can be made between sliding of the interface and whether there is a propensity for the hydraulic fracture to cross the interface. The values of the fitting coefficients *a*, *b*, *c*, *d*, *e* and *f* corresponding to the friction cases used for producing Figure 44 are given in Table 7.

$$h_p = \frac{\left(a + bS + cS^2\right)}{\left(1 + dS + eS^2 + fS^3\right)}$$

Eq. 23

m ↓	a	b	c	d	e	f
0	1	0	0	0	0	0
0.05	0.989500	-1.09520	0.298100	0.239400	-1.02830	0.504400
0.1	0.990112	-1.64810	0.649261	1.049084	-4.36092	4.939399
0.2	0.981776	-2.56899	1.645566	1.705347	-9.55252	18.97925
0.3	0.984751	-2.82950	1.967569	3.045700	-17.9869	52.34666
0.4	1.003887	-3.15526	2.362533	4.382706	-27.1852	83.31532
0.5	0.985954	-3.19942	2.474528	4.247058	-25.1014	94.07905
0.6	0.985585	-3.24377	2.546011	4.703988	-27.7665	114.0495
0.7	0.985366	-3.29767	2.631914	5.032807	-30.0283	129.9824
0.8	0.984056	-3.31565	2.665303	5.213019	-30.5647	139.3449
0.9	0.985049	-3.34779	2.713770	5.477470	-32.7733	152.5022
1.0	0.984991	-3.40850	2.809477	5.594832	-34.0346	159.1824

Table 7. Values of fitting coefficients for given values of m.

However if required, equation 24 can be used to calculate the fitting coefficients, with a mathematical relationship derived based on the fitted curves estimated with SigmaPlot. The

curves depicted in Figure 47 to Figure 49 reflect the accuracy of equation 24 for estimating the fitting coefficients. In the figures the symbols are the values of the fitting coefficients corresponding to the friction values as used in Table 7, while the solid lines are calculated using equation 24. The fitting parameters Xo, Yo, A and B are summarized in Table 8.

$$coefficient(a,b,c,d,e,f) = Y_0 + \frac{A}{\left(1 + \left(\dfrac{m}{X_0}\right)^B\right)}$$

Eq. 24
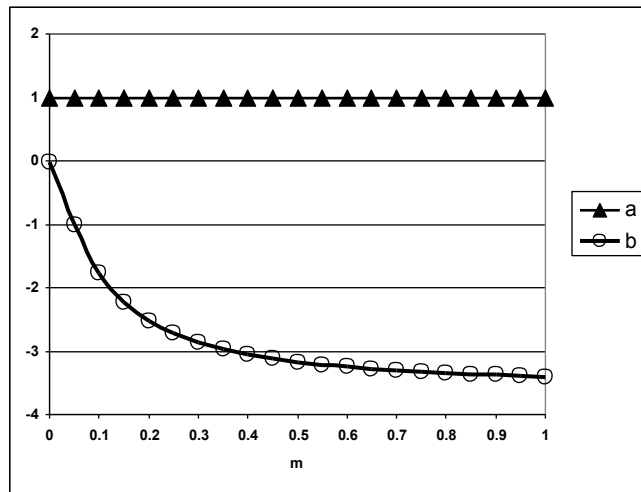
Figure 47. Behaviour of fitting coefficients (a,b) with respect to m.
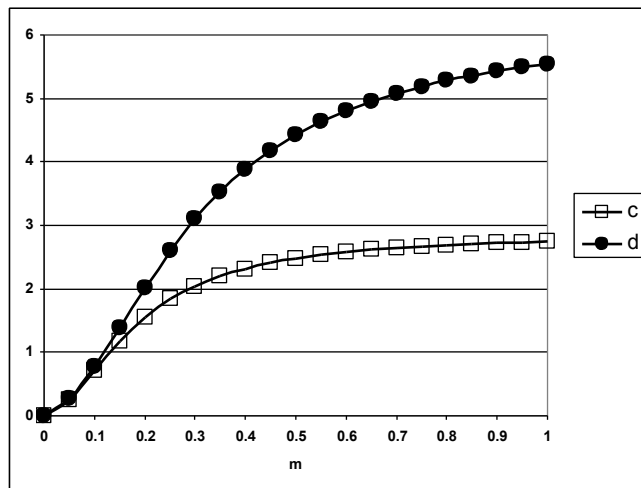
Figure 48. Behaviour of fitting coefficients (c,d) with respect to m
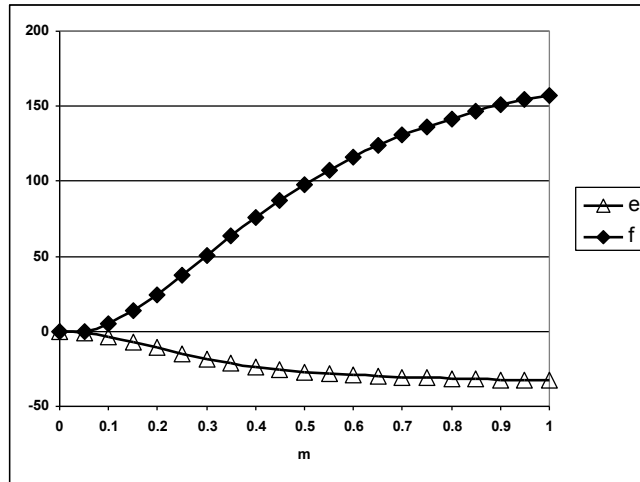
Figure 49. Behaviour of fitting coefficients (e,f) with respect to m

	a	b	c	d	e	f
A	0.0000001	3.564932	2.864705	6.082595	34.67183	196.0379
B	0.0000001	1.299716	-1.82130	-1.83157	2.171063	-2.06646
X_0	0.0000001	0.102898	0.183256	0.299919	0.289484	0.491851
Y_0	0.9884000	-3.57958	0.008881	0.060368	-34.9528	-1.68097

Table 8. Values of fitting parameters.

5.5 Summary

This thesis is a study to develop new understanding of the problem of the interaction between a hydraulic and a natural fracture. This objective was first approached by means of experimental work whose results suggested crossing after slip, a topic that was further addressed by numerical and analytical calculations. These analyses were designed to determine the incipient point of frictional slip. The geometry of the problem involved a uniformly pressurized finite-length hydraulic fracture approaching a natural fracture under toughness-dominated conditions. In this chapter the results have been plotted in a non-dimensional form. Evolution is considered in terms of the change in fracture geometry. The findings of the modelling work undertaken in this thesis suggest a hydraulic fracture propagating in a toughness-dominated regime does not need to grow much before easily inducing irreversible slip on the discontinuity with low coefficient of friction and under low stress loading conditions. As the stress increases a longer hydraulic fracture is required for slip to occur. Plasticity is limited for discontinuities with friction coefficients higher than 0.5. These observations allowed finding universal curves and an analytical expression for the values of S and m associated with initiation of slip.

Chapter 6

COMPARISON OF EXPERIMENTAL DATA TO MODELLING CALCULATIONS

Laboratory tests represent a significant simplification of the problem compared to the full-scale reservoir environment. The difference in scale and the different processes acting in the field mean that laboratory experiments can only consider a part of the overall process. The uniaxial and biaxial tests carried out for this thesis offered an insight into the effect of the viscosity on the hydraulic and natural fracture interaction problem. One outcome suggested crossing after slip and therefore numerical and analytical approaches were used to study this issue in depth. The novelty of the approaches used in this thesis is associated with having considered the effect of non-singular stresses existing around a pressurised finite-length fracture. This lead to the development of a criterion that allows determining the onset of slip (plastic deformation) along the discontinuity for toughness-dominated conditions.

In order to complement the analysis of the effect the parameters studied in this thesis have on the fracture interaction problem, the outcomes of this thesis are compared to the results provided by the works by Chuprakov et al. (2010) and the OpenT model (Chuprakov et al., 2013a, 2013b). Therefore, this chapter presents a description of any similarity or difference found for each stage of the propagation of the hydraulic fracture as per Chuprakov et al. (2010), i.e. approaching, contacting and infiltrating a discontinuity.

6.1.   Propagation Stages

6.1.1 Geometry of the Problem

The problem addressed by Chuprakov et al. (2010) considers a hydraulic fracture propagating with a uniform profile of inner pressure (P_f) towards an initially closed discontinuity in an impermeable elastic rock medium (Figure 50). The far field stresses, Σ_{11} and Σ_{33}, act parallel and perpendicular to the hydraulic fracture respectively. The angle of the hydraulic fracture and Σ_{11} with respect to the discontinuity (Θ) varied from 0° to 90°. Similar to the geometry used in the modeling carried out for this thesis (Figure 39 and Figure 40), the length of the discontinuity was considered infinite. Contact occurred once the hydraulic fracture touched the discontinuity, i.e. when the distance separating them (H) was zero.
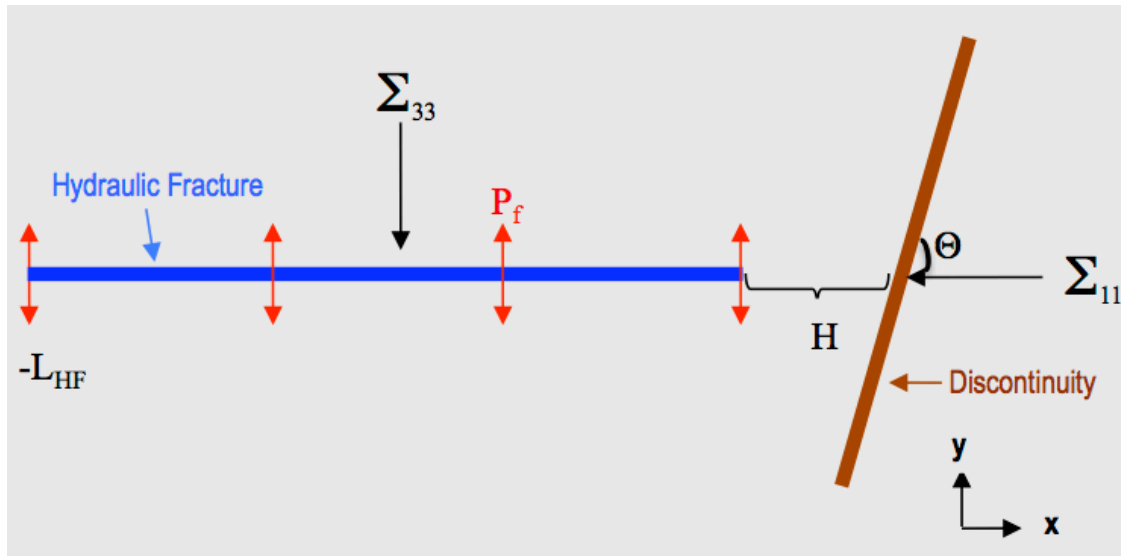
Figure 50. Geometry of the problem by Chuprakov et al. (2010).

OpenT considers the hydraulic fracture as semi-infinite. The approach used in this thesis considers a finite-length hydraulic fracture and takes account of the stress generated by the entire pressurised fracture in predicting slip. Renshaw and Pollard (1995) used the LEFM-based solutions for the associated singular near-tip elastic stress fields; hence geometric lengths such as finite fracture length are not included in their criterion. Blanton (1986) neglected the stress induced by the hydraulic fracture itself and his criterion is possibly more correct for fracture initiation from a fault, where slip is remote from any pressurized hydraulic fracture.

6.1.2 Hydraulic Fracture Approaching a Discontinuity

In this initial stage, Chuprakov et al. (2010) focused on opening and/or slippage along the discontinuity. As described in chapters 4 and 5, in this thesis only the onset of slip was studied and slip was considered possible before the hydraulic fracture contacts the discontinuity. In their very recent work Chuprakov and Prioul (2015) offer an explicit formula for the length of the slip zone, which they consider only once contact has occurred.

Chuprakov et al. (2010) observed that once the fault slips the tensile stress on the opposite side of the interface quickly increases, as the hydraulic fracture gets closer. Their model is able to predict the onset of a new tensile fracture, generated at the tips of the open zone. This open zone requires fluid infiltration to occur before it can grow further. However, Chuprakov et al. (2010) assumed no fluid pressurization in the fault once it opens as the hydraulic fracture approaches it. The reason for this has to do with leakoff not being considered in the model. The issue of leakoff

has been addressed by Chuprakov and Prioul (2015).

As presented in chapter 3, a hydraulic fracture propagating in a toughness-dominated regime is more likely to enter and pressurize a discontinuity during this phase, which serves to reduce the shear strength of a discontinuity and its ability to transmit shear stress into the rock on the other side. Similarly, the script presented in Appendix C of this thesis allows determining the initiation of slip if desired. This value would correspond to a potential offset to develop. The fracture re-initiation site must be found using a model such as MineHF2D or OpenT assuming the conditions are favorable for the fracture to keep propagating in the original direction.

Contrary to Blanton (1986), the study by Chuprakov et al. (2010) suggests the normal and shear stress profiles along the discontinuity during the interaction are more parabolic than linear. The same feature was observed in the numerical study carried out for this thesis, as presented in Figure 58 in Appendix D.

6.1.3 Hydraulic Fracture Contacting a Discontinuity

Chuprakov et al. (2010) considered a uniformly pressurized hydraulic fracture, as has been done in this thesis, which implies the stress perturbation near the hydraulic fracture tip increases proportionally to increments of the applied pressure. This enlarges the open zone and positions the tensile stress peak at the end of the open zone along the discontinuity. At this point in the process the authors found that the tangential stress reaches its maximum possible values. This point also corresponds to the most likely point for a tensile fracture to be created on the far side of the discontinuity. The authors also assumed that at this stage, the hydraulic fracture touches the fault without crossing it directly.

With regards to the coefficient of friction of the natural fracture, Chuprakov et al. (2010) concluded that it plays a role on the fracture interaction problem only when it is low enough (less than 0.6) for a shear zone to develop ahead of the tensile zone. For values of coefficients of friction higher than 0.6 they concluded only a tensile fracture propagates and the fracture offset is small.

Figure 51 displays results by Chuprakov et al. (2013b) compared to the predictions by Blanton (1986) and the extended R & P (1995) criterion by Gu et al. (2011). The areas of crossing and arresting correspond to the spaces above and below the lines respectively. According to OpenT, the chances of a discontinuity with a coefficient of friction of 0.5 being crossed by a hydraulic

fracture are directly proportional to the hydraulic fracture's length and normal crack displacement (opening). This is valid for fractures oriented at angles between 55° and 70°. Likewise, the shorter the hydraulic fracture's length and opening at the contact with the discontinuity, the more difficult it will be for the crossing behavior, even at 90°.

The laboratory results obtained from the tests carried out for this thesis do not tell a story if plotted in Figure 51 or a modification of it. The reason lies on the biaxial stress conditions used ($\sigma_x = \sigma_z$ and $\sigma_y = 0$) which implies a constant value of 1 for a modified stress difference like ($\sigma_x - \sigma_y$)/ σ_x if compared to ($\sigma_x - \sigma_y$)/ σ_y which was used by Chuprakov et al. (2013b), which would be an undefined results associated to the division by zero.
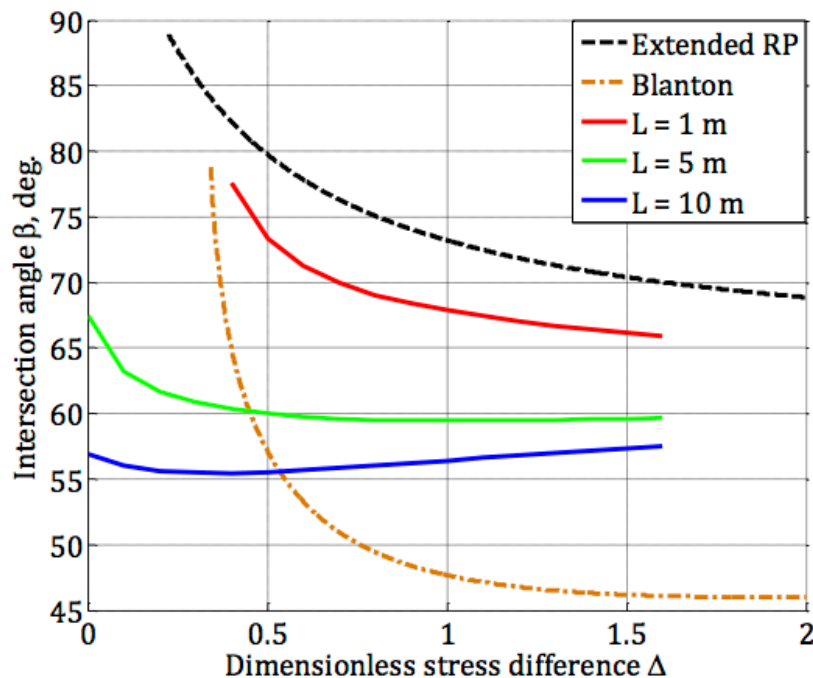
Figure 51. OpenT results as function of intersection angle and dimensionless stress difference (from Chuprakov et al., 2013b).

OpenT results for a 1-metre length hydraulic fracture at contact with the discontinuity are presented in Figure 52. The plot indicates that for orthogonal crossing (red lines) the differential stress contrast for crossing decreases with the coefficient of friction and becomes zero for values higher than 0.6. This prediction is similar to Gu et al. (2011) and their extended R & P (1995) criterion but rather different from Blanton's (1986) criterion, which seems to remain unaffected by the coefficient of friction.

As discussed in section 1.5, the parameter 'b' in Blanton's (1986) criterion depends on the

coefficient of friction and the lengths of the opening and slippage zones along the discontinuity. The parameter 'b' affects the form of the criterion as when there is no slippage it goes to infinity and crossing will always be satisfied.
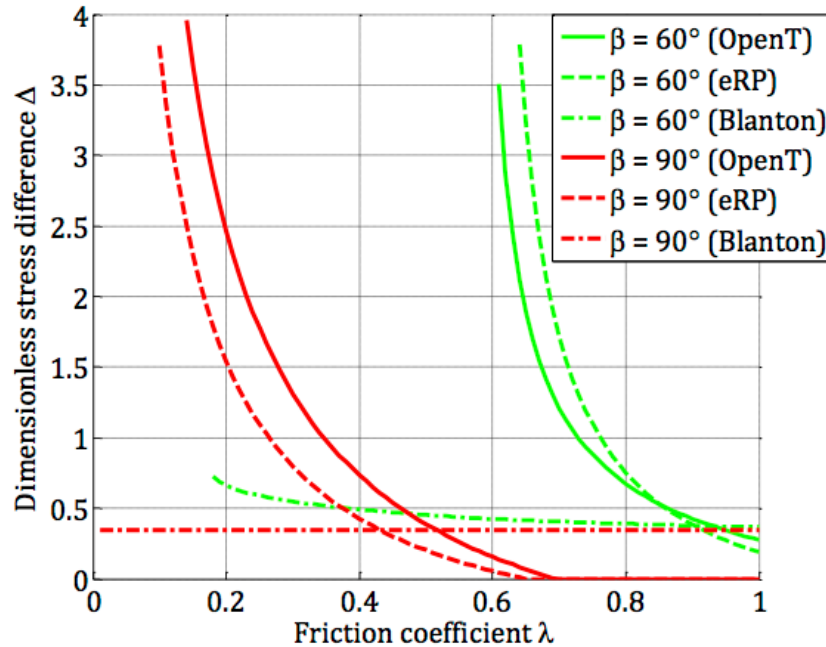
Figure 52. OpenT results as function of dimensionless stress difference and coefficient of friction (from Chuprakov et al., 2013b).

The impact of the coefficient of friction, fracture length and stress on the interaction problem were analysed in the modelling work undertaken in this thesis. The outcome indicates a toughness-dominated hydraulic fracture does not need to grow much before inducing irreversible slip on a discontinuity with a coefficient of friction below 0.5 and under low normal loading conditions. As the stress increases a longer hydraulic fracture is required for slip to occur.

6.1.3 Hydraulic Fracture Infiltrating a Discontinuity

Chuprakov et al. (2010) studied two cases for this stage of the process: fluid leaking into the fault with lag possible and secondly no fluid allowed into the discontinuity. The authors found that at sufficiently small injection rates the induced fracture is arrested for conditions that allow fluid to infiltrate into the discontinuity. For larger injection rates the hydraulic fracture reinitiates at the fault after the contact.

Additionally, Chuprakov et al. (2013a, 2013b) found that as the fracturing fluid viscosity increased the crossing limit for both OpenT and MineHF2D and crossing was predicted for higher viscosity

with less sensitivity to the relative stress difference. This result is in line with the findings of the experimental component of this thesis where viscosity-dominated fractures seemed to cross the discontinuities more easily than toughness-dominated fractures especially as the loading stress increased.

6.2.   Application

Kaiser et al. (2013) conducted a literature survey on hydraulic fracturing treatments in mining, deep geothermal and the hydrocarbon industries. The survey included geomechanics, fluid injection parameters and the observed activation mechanisms. It was found that in deep geothermal projects high rates and long duration injections are performed. Figure 53 displays the maximum pressure reached during an injection against the local estimate of the minimum principal stress magnitude as well as the predominantly activated mechanism.

It is often assumed that in Enhanced Geothermal Systems (EGS) stimulation occurs mainly through induced slip on pre-existing discontinuities and that propagation of new fractures plays a minor role. McClure and Horne (2013, 2014) refer to this concept as 'pure shear stimulation' (PSS) in their review of ten historical EGS projects. PSS is possible if the fluid pressure is maintain below the minimum principal stress during the stimulation. In order for this to happen the discontinuity must have an adequate storativity and initial transmissivity. McClure and Horne (2013, 2014) found that high injection rates help the hydraulic fractures propagate through the formation. They also concluded that the chances of PSS is higher in areas with thick faults like Soultz, Cooper Basin, Basel and Fjallbacka.

The discussion above indicates that for deep natural fractures, the slip condition cannot be satisfied mainly because the tensile stress at large confining stress cannot be larger than the local tensile strength. The slip criterion developed in this thesis is therefore more applicable to the case where the slip can produce a new fracture prior to the hydraulic fracture reaching the interface. In other words, it would be more useful for cases with less compressive stress environments. The offset fractures in shallow crust could be an example.
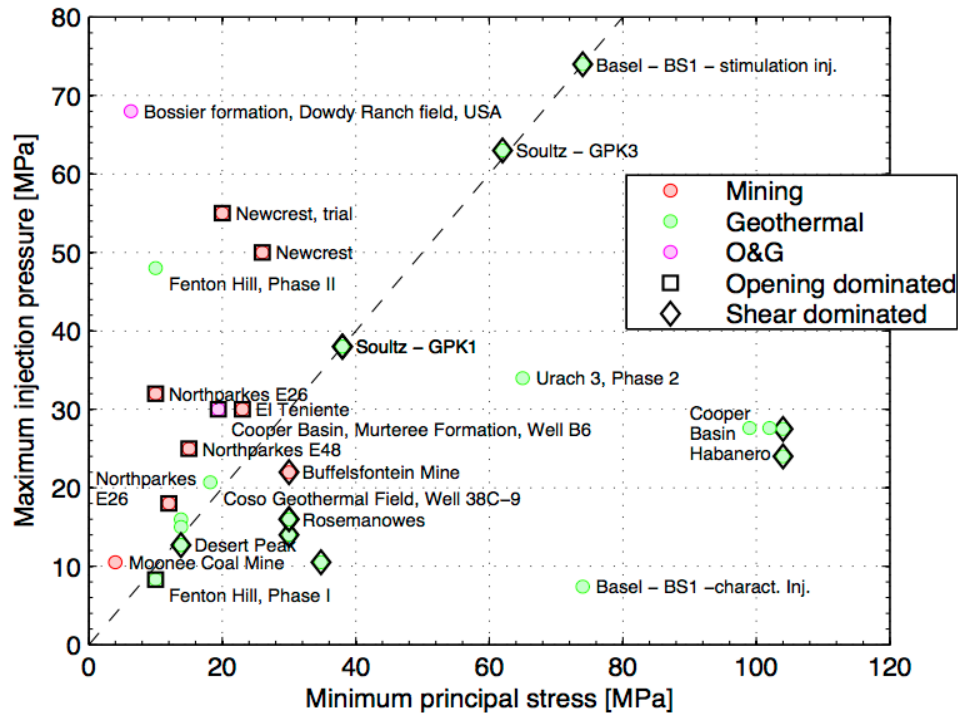
Figure 53. Cross plot of minimum principal stress and maximum injection pressure (from Kaiser et al., 2013).

6.3.   Summary

This thesis shows the complex intrinsic relationship between the viscosity used to propagate a hydraulic fracture and its possibility of inducing slip along an orthogonal frictional discontinuity subjected to loading conditions. In the last five years Chuprakov et al. (2010) and Chuprakov et al. (2013a, 2013b) have provided significant contributions to the understanding of the fracture interaction problem by means of a parametric and analytical model. To evaluate how this thesis fits into this rather comprehensive model, a comparison between approaches and outcomes has been made. This chapter presented an evaluation of some of the parameters involved prior to a hydraulic fracture approaching a discontinuity as well as at its contact and infiltration into the discontinuity.

Besides the well-documented effect of the angle between fractures and loading stress contrast, the comparison presented in this chapter reinforces the importance of the injected fluid viscosity. It is also understood that the injection rate is a parameter that requires further exploration.

Putting into perspective the discussion carried out in this chapter, the slip criterion developed in this thesis is more useful for cases subject to lower compressive stress environments.

Chapter 7

CONCLUSIONS AND RECOMMENDATIONS

Hydraulic fracturing has been used in the hydrocarbon industry for more than six decades. Nevertheless, the lessons learnt and the identified gaps of knowledge from the hydrocarbon industry together with the rising need of alternative sources of energy, such as geothermal, continuously open room for improvement of the science behind hydraulic fracturing. Research can result in improvements to all stages of the process, namely design, application, monitoring and analysis.

Pre-existing geological discontinuities have been well documented to affect hydraulic stimulation treatments. Failed or poorly performing stimulations result in significant financial losses and unrealised revenue. Therefore, understanding the parameters controlling the hydraulic fracture growth through pre-existing discontinuities is a key are of research. This thesis is a scientific contribution to this fundamental problem. As explained before, this study has been achieved through a combination of laboratory experiments and numerical and analytical modelling.

This chapter summarizes in bullet points the conclusions that can be drawn from results obtained in this thesis study. Finally, identified opportunities for improvement and considerations for future studies are also discussed.

CONCLUSIONS:

- To obtain valid experimental comparisons when considering the effects of the parameters controlling crossing, the experimental sample frictional surfaces used to represent natural fractures must be carefully prepared to ensure they are smooth and flat. This is required so the contact stresses on these surfaces can be controlled and known.

- The effect of discontinuities on hydraulic fracture propagation was observed as a retarded but stress-dependent growth associated with the propagation through the discontinuities.

- Consistency between crossing and non-crossing cases was not observed when comparing the uniaxial and the biaxial tests.

- The biaxial tests showed that crossing occurred for all stress conditions so the non-crossing comparison cannot be made.

- The biaxial experiments proved most useful in studying fracture growth and shape as affected by the crossing interactions.

- The hydraulic fractures may grow more quickly in the direction of the maximum stress or fewer discontinuities. An elliptical fracture shape, with the long axis along the direction of higher stress or fewer discontinuities, may develop as a result.

- The R & P (1995) and Gu and Weng (2010) criteria provide a lower limit on discontinuity strength that result in hydraulic fractures crossing geological discontinuities. Experimentally, a higher normal stress was found to be needed to generate a crossing condition than what was predicted by the either of these criteria.

- As normal stress acting on the discontinuities was increased, the ultimate fracture length in that direction becomes larger.

- As the experiments did not include a vertical load, fluid lag and the free-surface effects were observed when using high viscosity fracturing fluid.

- Crossing of the discontinuities was enhanced by the use of higher viscosity fluids, in part because the high viscosity fluids were not lost into the frictional discontinuity as easily as lower viscosity fluids.

- A hydraulic fracture propagating in a toughness-dominated regime is more likely to enter and pressurize a natural fracture during the interaction. This reduces the shear strength of the discontinuity and its ability to transmit shear stress into the rock on the other side.

- The results from this thesis together with the work by Bunger et al. (2015) suggest that the numerical work of Chuprakov et al. (2013) on the effect of natural fracture permeability on the crossing interaction should be acknowledged as being of higher importance than the friction itself.

- The modelling work undertaken in this thesis allowed finding universal curves and an analytical expression to determine the incipient point of frictional slip.

- A hydraulic fracture propagating in a toughness-dominated regime does not need to grow much in length before it induces irreversible slip on a discontinuity with low coefficient of friction and under low stress loading conditions.

- As the normal stress increases a longer hydraulic fracture is required for slip to occur.

- Plasticity (slip) is limited for discontinuities with friction values higher than 0.5.

- In contrast to these modelling results, the experimental data provide a new perspective in the hydraulic fracture growth through orthogonal discontinuities, suggesting it does not depend primarily on the friction coefficient of the interface.

- Both the fracturing fluid viscosity and the permeability of the discontinuity are parameters that need to be considered in developing criteria for predicting crossing interaction behaviour.

The strengths of the experimental setup used in this thesis start with the removal of asperities that could promote or retard crossing. Any stress disturbance from the hole affecting the stress on the first interface was removed by using a thicker central slab. However, in order to contribute more to the understanding of the problem of fracture height containment, future laboratory experiments should include layers with Young's modulus contrast.

The fluid lag observed in some experiments together with the free surface effect should be avoided by applying a vertical stress. Nevertheless, these results could still be useful for hydraulic stimulations in shallow environments or mining applications. The use of a rock with lower permeability should be considered so that fluid loss and lag do not limit the range of parameters that can be considered in obtaining experimental results. Although Bunger et al. (2015) proved these considerations to work; both studies could be improved by applying different horizontal stresses.

The strength of the numerical and analytical component of this thesis is that it differs from the work by Renshaw and Pollard (1995) in considering the non-singular stresses existing around a pressurised fracture. This work should be extended to non-orthogonal cases. Additionally, the numerical model presented in this thesis may be more useful in low normal stress environments, where slip may be associated with fracture arrest. Otherwise, if the normal stresses were more compressive, the OpenT model, by Chuprakov et al. (2013), would be better.

Therefore, based on the observations and results obtained in this thesis and considering its strengths and limitations, the items below are suggested as areas where additional research should be pursued.

RECOMMENDATIONS:

1) This study should be progress by means of using different rock materials. Natural fractures may be reproduced if pressing together rocks of different properties.

2) The work presented in this thesis that determined the onset for slip can be used to find the onset for opening of the natural fracture.

3) Similar experiments including experiments in a heated polyaxial test cell should be beneficial for the geothermal industry.

4) This study should be repeated for rocks of different values of tensile strength to evaluate whether the singular stress field at the tip might dominate the initial slip.

The subject matter studied in this thesis is one of the most important areas of research in hydraulic fracturing. The uniaxial and biaxial laboratory experiments carried out for this thesis provide some of the first experimental evidence for the impact of viscous fluid flow on the orthogonal interaction problem. Additionally, the fracture elliptical footprint reflects the importance of both the applied loading stress and the viscosity in the fracture propagation and interactions. The numerical experiments demonstrate some important concepts and lead to a set of universal curves for predicting interface slip. This thesis leads the path to further areas of research: consideration to oblique intersection cases as well as to exploring these topics under triaxial conditions; further exploration of the impact of intermediate and vertical loading stresses on the fracture propagation; connection between sliding of the interface and the propensity for crossing. Thus, this thesis helps in understating some important concepts in the complex problem of the hydraulic/natural fracture interaction as well as gives rise to opportunities for further research.

APPENDIX A: ROCK PROPERTIES

- **STRENGTH AND POROSITY**

The strength of a rock is the stress at which the rock fails and as obtained with a uniaxial test is called the uniaxial compressive strength (UCS). UCS is calculated by dividing the peak load at failure of a rock sample loaded axially without confinement by the sample cross-sectional area. Four UCS values were measured at CSIRO Hydraulic Fracturing Laboratories on cylinders of rock cores following the ISRM standard method, which requires compressing the samples between two platens and measuring the maximum load at which failure occurred. Several tests were done to achieve statistical significance of the results and a mean value for the Donybrook sandstone was 54.65 MPa with a standard deviation of 1.5 MPa (Table 9).

	A (mm^2)	Peak Load (N)	UCS (MPa)
Sample # 1	503.9196	27970	55.5
Sample # 2	503.9196	27450	54.5
Sample # 3	503.5200	28340	56.3
Sample # 4	503.5200	26330	52.3

Table 9. UCS measurements

Porosity is a quantification of the amount of void space in a rock mass. Empirical expressions such as equation 25 allow estimating the value of porosity ϕ if the UCS is known (Vernik et al., 1993). For the sandstone UCS value given above the estimated porosity would be 19.86%.

$$UCS = 254(1 - 2.7\phi)^2$$
<div align="right">Eq. 25</div>

However, this is an indirect method based on correlations. Therefore, for more accuracy, Core Laboratories Australia PTY Ltd (Core Lab) measured the porosity by using an ultrapore porosimeter. Direct pore volume measurements were made utilizing Boyle's Law methods with helium as the gaseous medium. Four measurements were carried out, as presented in Table 10, resulting in a mean value for the porosity of 15.4 with a standard deviation of 0.3.

	ϕ (%)
Sample # 1	15.6
Sample # 2	15.8
Sample # 3	15.3
Sample # 4	15.0

Table 10. Porosity measurements

- **PERMEABILITY**

The permeability to air and pore volume measurements of sandstone samples were made in Core Lab CMS™300 automated core measurement system. The instrument uses an integrated form of the combined Darcy, Klinkenberg and Forchheimer equations to accurately determine permeability. Table 11 summarizes the permeability measurements obtained. Permeability varied considerably for the samples tested. The mean permeability was 27.10 md with a standard deviation of 21.06 md.

	Kair (md)
Sample # 1	47.2
Sample # 2	49.1
Sample # 3	5.71
Sample # 4	6.40

Table 11. Permeability measurements.

- **DISCONTINUITY FRICTION COEFFICIENT**

Triaxial tests were undertaken for determining the frictional strength of discontinuities. The onset of slip as a function of the applied stress for the samples with a pre-cut surface is used to calculate the coefficient of friction of the surface. This method was used to obtain data for higher normal stress conditions than can be obtained in a direct shear test machine. These tests were conducted for several normal loads in order to obtain a failure envelope of the discontinuities.

The equipment used by CSIRO in Perth, the autonomous triaxial cell, acts independently of a loading frame. The axial stress is supplied by the actuator beneath the sample and upper platen reaction loads are carried through the cell walls. This avoids the need for bulky loading frames. The samples can be subjected to the stress applied by both the cell pressure and pore pressures applied through the top and bottom platens. External heating is provided by a removable oven and the cell can be used to perform both compressional and extensional tests. The data surpass the 1700 lines hence in Table 12 selected measurements are presented. Nevertheless, Figure 54 depicts all the results obtained which also allow estimating the discontinuity friction coefficient by finding the absolute value of the shear stress to normal stress ratio (τ / σ_n) as per Byerlee, 1978.

Axial strain (mstr)	Stress_1 (MPa)	Stress_3 (MPa)	Angle (rad)	Normal stress (MPa)	Shear stress (MPa)	Friction coefficient
0.00	0.00	3.03	2.62	2.27	1.31	0.58
2.35	6.24	3.04	2.62	3.84	-1.39	0.36
4.47	8.74	3.04	2.62	4.46	-2.47	0.55
6.47	10.13	3.04	2.62	4.81	-3.07	0.64
6.51	2.89	5.08	2.62	4.53	0.95	0.21
9.38	15.89	5.08	2.62	7.79	-4.68	0.60
10.24	2.68	5.09	2.62	4.49	1.04	0.23
11.76	19.86	7.18	2.62	10.35	-5.49	0.53
13.98	23.03	7.18	2.62	11.14	-6.86	0.62
12.67	1.79	5.16	2.62	4.32	1.46	0.34
13.71	1.76	5.16	2.62	4.31	1.47	0.34
14.59	12.94	3.12	2.62	5.57	-4.25	0.76
14.05	1.86	1.59	2.62	1.66	-0.12	0.07
13.88	-0.15	0.45	2.62	0.30	0.26	0.88

Table 12. Discontinuity friction coefficient measurements.
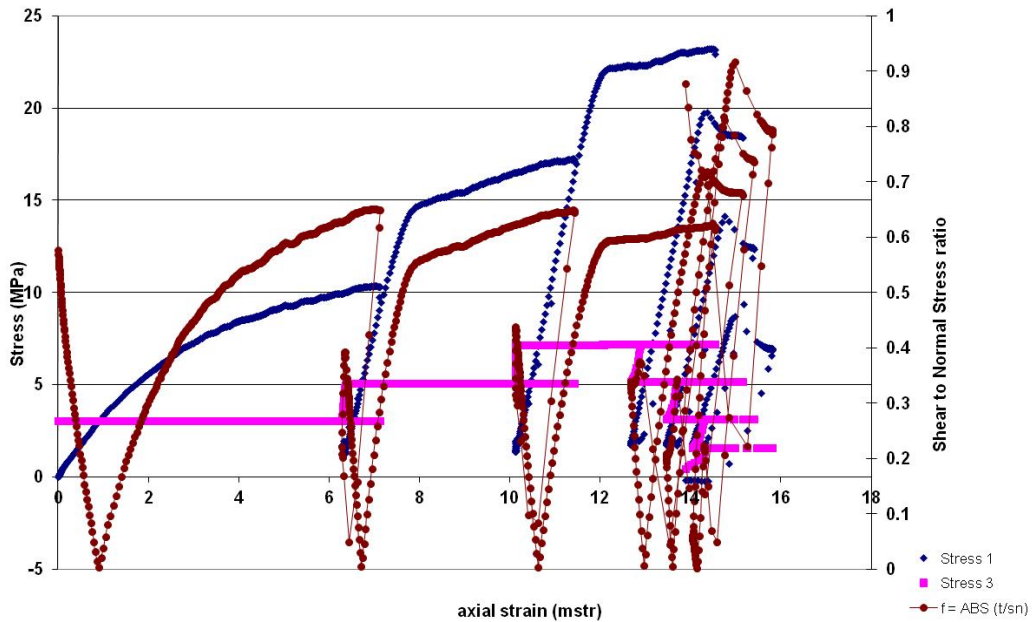
Figure 54. Autonomous triaxial cell results – shear vs normal stress

- **POISSON'S RATIO**

CSIRO's autonomous triaxial cell allowed obtaining values of axial and circumferential strain. Selected data are shown in Table 13. When these strains are plotted against each other, the slope of the straight line observed corresponds Poisson's ratio (Figure 55).

Load (KN)	Radial Long (mm)	Radial Short (mm))	Axial strain (mstr)	Circumferential strain (mstr)
0.00	-0.12	-0.13	0.00	0.00
2.76	-0.07	-0.11	2.12	0.66
0.96	-0.01	-0.10	4.37	1.20
4.84	0.01	-0.09	5.18	1.41
5.40	0.07	-0.07	7.47	2.12
7.23	0.08	-0.08	7.74	2.07
8.02	0.14	-0.06	10.45	2.86
2.54	0.15	-0.05	10.73	2.98
1.00	0.18	-0.04	11.90	3.46
0.99	0.21	-0.03	13.11	4.01
2.12	0.25	-0.01	14.71	4.59
2.14	0.25	-0.01	14.73	4.59
1.20	0.25	-0.01	14.70	4.58
0.04	0.25	-0.01	14.64	4.56
0.07	0.25	-0.01	14.75	4.76

Table 13. Poisson's ratio measurements.
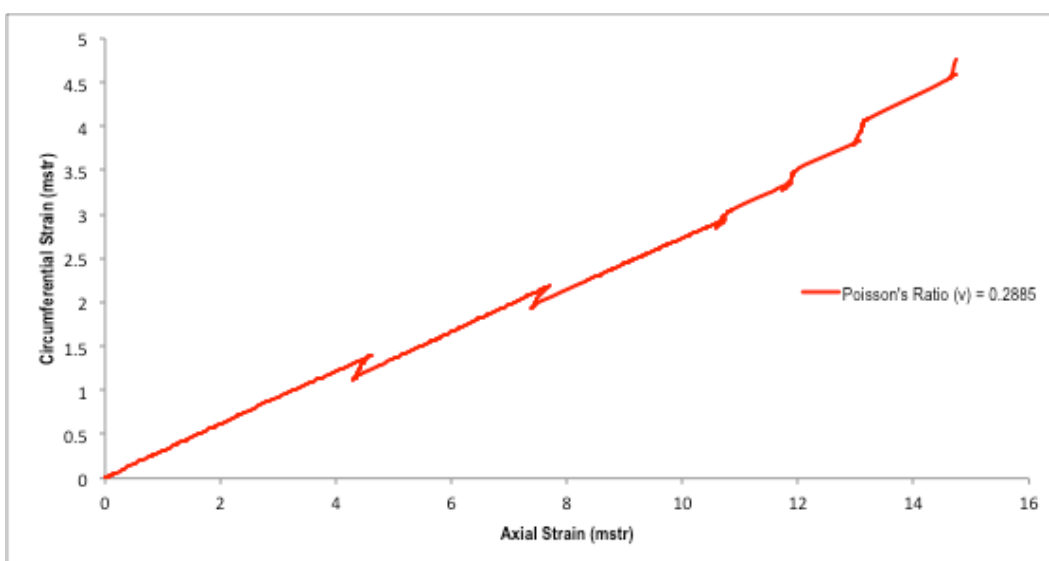
Figure 55. Triaxial testing results – Poisson's ratio

- **YOUNG'S MODULUS**

Triaxial tests were conducted by Strata Testing Services. The sample is wrapped in a rubber jacket. Axial stress is applied by a hydraulic ram in the testing machine and lateral pressure was applied by oil confining pressure. Three samples were tested to obtain the stress-strain response of the rock and selected values are presented in Table 14. The Young's modulus was determined from the slope of the curves displayed in an axial stress vs. axial strain plot (Figure 56).

Axial strain (mstr)	Stress_1 (MPa)	Stress_3 (MPa)	Angle (rad)	Normal stress (MPa)	Shear stress (MPa)	Friction coefficient
0.00	0.00	3.03	2.62	2.27	1.31	0.58
2.35	6.24	3.04	2.62	3.84	-1.39	0.36
4.47	8.74	3.04	2.62	4.46	-2.47	0.55
6.47	10.13	3.04	2.62	4.81	-3.07	0.64
6.51	2.89	5.08	2.62	4.53	0.95	0.21
9.38	15.89	5.08	2.62	7.79	-4.68	0.60
10.24	2.68	5.09	2.62	4.49	1.04	0.23
11.76	19.86	7.18	2.62	10.35	-5.49	0.53
13.98	23.03	7.18	2.62	11.14	-6.86	0.62
12.67	1.79	5.16	2.62	4.32	1.46	0.34
13.71	1.76	5.16	2.62	4.31	1.47	0.34
14.59	12.94	3.12	2.62	5.57	-4.25	0.76
14.05	1.86	1.59	2.62	1.66	-0.12	0.07
13.88	-0.15	0.45	2.62	0.30	0.26	0.88

Table 14. Young's modulus measurements.

Figure 56. Triaxial testing results – Young's modulus

- **TENSILE STRENGTH**

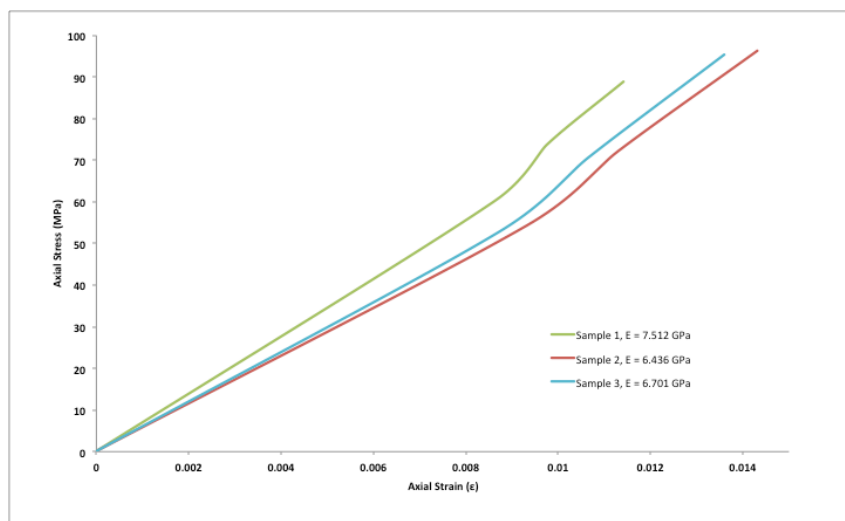The tensile strength of the Acrogem Sandstone used for this thesis was determined through a series of Brazilian tension tests on intact samples (Mellor and Hawkes, 1971 and ASTM D 3967-86). The Brazilian test measures the tensile strength of the rock, which is the maximum amount of tensile stress that a rock can be subjected to before failure. The method consists of compressing a disk shaped rock sample so that the load is applied along the diameter of the disk. The load on the specimen must be applied continuously and at a constant rate until failure occurs.

The solution for a disk loaded in this way shows that a region along the diameter of the disk is subject to tensile stress (Jaeger et al., 2007). The tensile strength T_O was calculated by means of an expression that involves the load at failure P, the diameter and thickness of the test specimen, D and t respectively (equation 26).

$$To = \frac{2P}{\pi Dt}$$

Eq. 26

The Brazilian tests series carried out for this thesis consisted of three rock specimens each machined to an average diameter of 53.25 mm and a thickness of 26.25 mm. The calculated mean tensile strength was estimated to be 4.4 MPa. To acknowledge any difference between the load at primary failure and the ultimate load bearing capacity the reported value for the tensile strength has a 10% error correction (Table 15). The standard deviation was estimated as 0.099 MPa.

	D (mm)	t (mm)	P (N)	To (MPa)	To (10%)
Sample # 1	53.15	27.92	8920	3.83	4.21
Sample # 2	53.39	24.43	8650	4.22	4.64
Sample # 3	53.23	26.40	8670	3.93	4.32
Mean	53.25	26.25	8746	3.99	4.39

Table 15. Brazilian tests parameters.

- **FRACTURE TOUGHNESS**

For this thesis, a semi-circular bending test was used to determine the fracture toughness K_{IC} (Lim et al., 1993). Determining the value of fracture toughness in the laboratory requires using a semi-circular rock sample containing a notch of known length. The tests measure the critical load and, therefore, the critical stress intensity factor K_{IC} at which the preexisting fracture is reinitiated (Table 16). The laboratory samples are measured to obtain their radius r and thickness t, as well as the notch length L. The mode I normalised stress intensity factor Y_I was obtained from numerical results by Lim et al. (1993). The test conditions such as maximum load applied P were also input data for the fracture toughness calculation (equation 27).

$$K_{IC} = \frac{Y_I P}{2rt} \sqrt{\pi L}$$

Eq. 27

	r (mm)	t (mm)	L (mm)	P (N)	Y_I	K_{IC} (MPa√m)
Sample # 1	30.245	25.4	14.015	765.62	4.911413	0.51354
Sample # 2	29.915	26.166	12.77	992.8	4.578842	0.581609

Table 16. Semi-circular beam tests parameters.

APPENDIX B: FLUID PROPERTIES

The experiments were designed to use a viscous fluid with Newtonian rheology. Honey combined with blue food dye was, therefore, used as the fracturing fluid. The lower viscosity fluids were prepared by adding water to the mixture whereas a heating process allowed slow removal of water from the fluid to obtain more viscous fluids.

When preparing the fluids the density was estimated by dividing the fluid mass by its total volume. The viscosity was calculated by measuring the time for a fluid to flow through a capillary tube of a glass tube viscometer. Glass tube viscometers have a reproducibility of 0.1% under ideal conditions, which requires immersed in a fluid bath to control temperature change, but are not ideally suited for measuring fluids with high viscosity.

The Newtonian viscosity of the honey solution was verified by measuring rheological properties such as viscosity and fluid behaviour using a cup and bob rheometer with testing carried out at the Rheological Consulting Services (RCS) (Report 4 - Job Reference: CSI012-04, 2004. The rest of the parameters were measured at CSIRO Hydraulic Fracturing Laboratories. RCS used a cup and bob rotational rheometer to obtain the viscosity, a measure of a fluid's resistance to flow. The operating principle of the rotational viscometer is based on the fact that the torque necessary to overcome the viscous resistance to the induced movement by rotation of a spindle is directly proportional to the viscosity of the fluid. The entire sample was subjected to a nearly uniform shear rate, and direct determination of viscosity by measurement of the corresponding shear stress was made at three different temperatures 15 °C, 20 °C and 25 °C.

Figure 57 presents the obtained results for the 100 and 10 Pa·s fluids (Sample A and B respectively). The trend lines were of the form $\tau = \mu \, \dot{\gamma}$ where τ is the shear stress, $\dot{\gamma}$ the shear rate and μ the viscosity. In Figure 57 the obtained viscosity values are displayed between brackets and referred to as 'm'. The fluid behaved is Newtonian with the viscosity constant over the range of applied shear rates
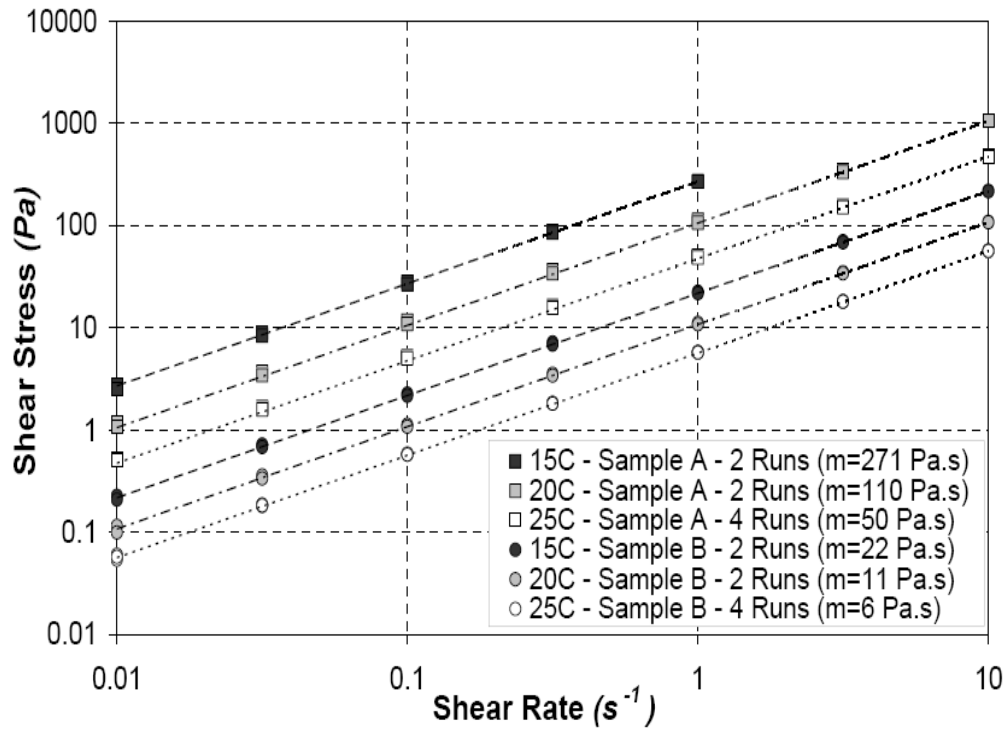
Figure 57. Shear rate vs. shear stress results for honey and blue food dye, at 15 ˚C, 20 ˚C and 25 ˚C (Report 4 - Job Ref.: CSI012-04, 2004)

APPENDIX C: SCRIPT FOR MATHEMATICA SOFTWARE

This example corresponds to a value of S = 1 and m = 0.9. It must be noted that all the lengths are normalised by L in the script. After obtaining the solutions for the choices of material parameters, the results were normalised based on the scalings presented in Chapter 4 to find the solution for the evolving parameter in a compact form.

```
a[H_] := (1 - H) / 2
x[H_] := (1 + H) / 2
rC[H_, y_] := √(x[H] * x[H] + y * y)
rL[H_, y_] := √((x[H] + a[H]) * (x[H] + a[H]) + y * y)
rR[H_, y_] := √((x[H] - a[H]) * (x[H] - a[H]) + y * y)
rstar[H_, y_] := √(rR[H, y] * rL[H, y])
θC[H_, y_] := ArcTan[y / x[H]]
θL[H_, y_] := ArcTan[y / (x[H] + a[H])]
θR[H_, y_] := ArcTan[y / (x[H] - a[H])]
θstar[H_, y_] := (θL[H, y] + θR[H, y]) / 2
fx[S_, H_, y_] :=
 1 -
    √(2 H / (π (1 - H))) / S *
      (-1 + rC[H, y] / 2 / rstar[H, y] *
          (2 Cos[θstar[H, y] - θC[H, y]] + 2 Sin[θC[H, y]] Sin[θstar[H, y]] -
            Sin[θR[H, y]] * Sin[θstar[H, y] + θR[H, y] - θC[H, y]] -
            Sin[θL[H, y]] * Sin[θstar[H, y] + θL[H, y] - θC[H, y]]))
fy[S_, H_, y_] := √(2 H / (π (1 - H))) / S * rC[H, y] / 2 / rstar[H, y] *
   (Sin[θR[H, y]] * Cos[θstar[H, y] + θR[H, y] - θC[H, y]] + Sin[θL[H, y]] * Cos[θstar[H, y] + θL[H, y] - θC[H, y]] -
     2 Sin[θC[H, y]] * Cos[θstar[H, y]])

g[m_, S_, H_, y_] = Simplify[fy[S, H, y] - m * fx[S, H, y]]
h[m_, S_, H_, y_] = Simplify[∂_y g[m, S, H, y]]

FindRoot[{g[0.9, 1, H, y] == 0, h[0.9, 1, H, y] == 0}, {{H, 0.1}, {y, 0.01}}]
```

APPENDIX D: DISPLACEMENT DISCONTINUITY ELEMENT SIZE

The element size is important in controlling accuracy of the numerical results. Therefore a sensitivity study checking for suitable element size has been done. The elements must be small enough to capture intricacies of deformation near the fracture tip, where slip and debonding occurs (Cooke and Underwood, 2001). Furthermore this length is more critical when the fracture tip is closest to the interface. A good match was observed when reducing the mesh size with up to 200 elements used, the maximum this version of MineHF2D can handle, as seen in Figure 58. For this purpose, the problem geometry was kept the same for each case, i.e. the same hydraulic and natural fractures lengths with more or fewer elements along these distances.
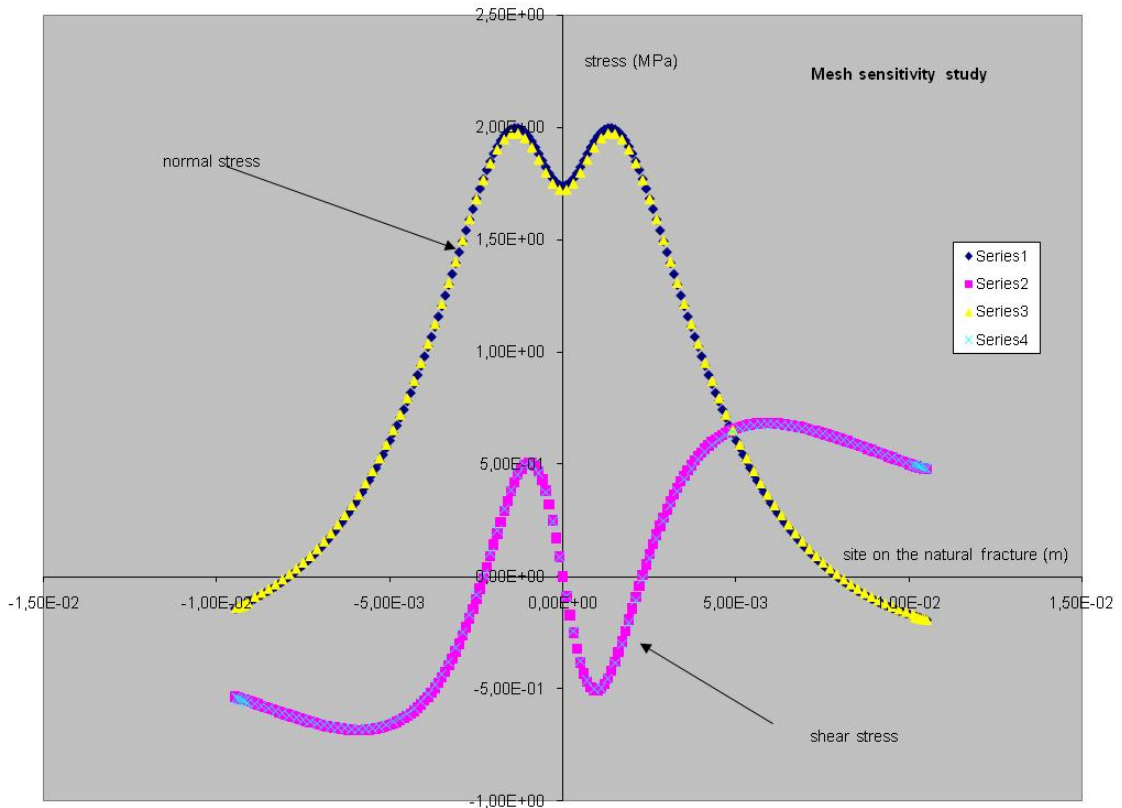
Figure 58. Element size sensitivity analysis – normal and shear stresses profile

APPENDIX E: UNIVERSAL CURVES

For simplicity selected plots are displayed here since there is little difference in the curves for the coefficients of friction between 0.5 and 1.0.
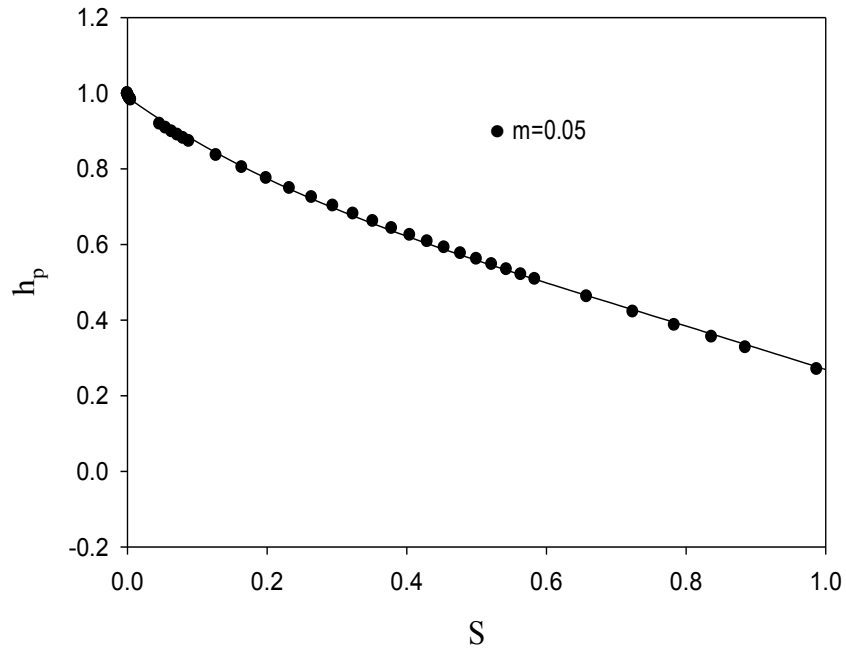
Figure 59. Universal curve, h_p as a function of S for m = 0.05
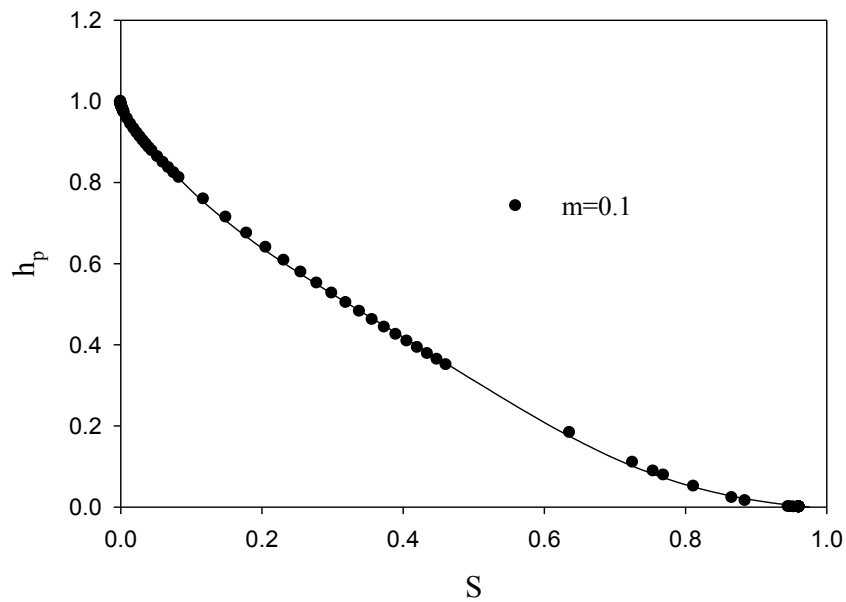
Figure 60. Universal curve, h_p as a function of S for m = 0.1
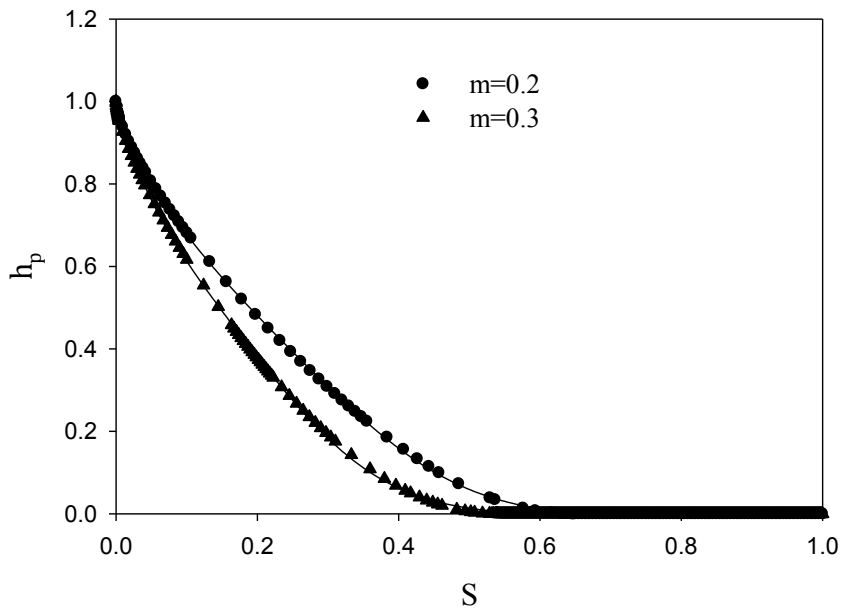
Figure 61. Universal curves, h_p as a function of S for m = 0.2 and m = 0.3
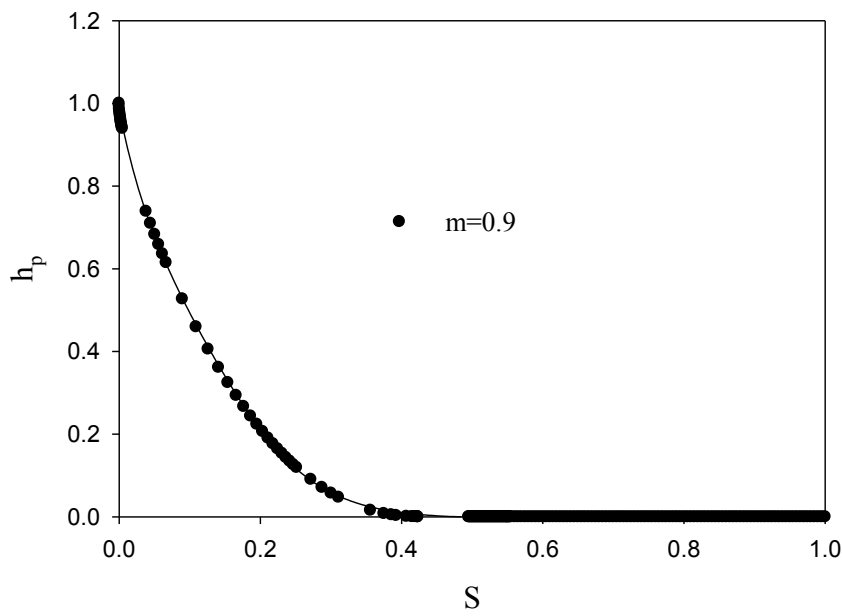
Figure 62. Universal curve, h_p as a function of S for m = 0.9

REFERENCES

Bahorich, B., J. E. Olson, and J. Holder, 2012, Examining the effect of cemented natural fractures on hydraulic fracture propagation in hydrostone block experiments: Society of Petroleum Engineers Annual Technical Conference and Exhibition, San Antonio, October 8 - 10 SPE Paper 160197, p. 21.

Bale, A., K. Owren, and M. B. Smith, 1993, Propped fracturing as a tool for sand control and reservoir management: Society of Petroleum Engineers /Production and Facilities, SPE Paper 26562.

Barenblatt, G. I., 2003, Scaling, Cambridge Texts in Applied Mathematics, Cambridge University Press, Cambridge.

Bennett, L., J. Le Calvez, D. R. Sarver, K. Tanner, W. S. Birk, G. Waters, J. Drew, G. Michaud, P. Primiero, L. Eisner, R. Jones, D. Leslie, M. J. Williams, J. Govenlock, R. C. Klem, and K. Tezuka, 2006, The source for hydraulic fracture characterization: Oilfield Review, p. 42 - 57.

Beugelsdijk, L. J., C. de Pater, and K. Sato, 2000, Experimental hydraulic fracture propagation in a multi-fractured medium: Society of Petroleum Engineers Asia Pacific Conference on Integrated Modelling for Asset Management, Yokohama, April 25 - 26, SPE Paper 59419, p. 8.

Blanton, T. L., 1982, An experimental study of interaction between hydraulically induced and pre-existing fractures: Society of Petroleum Engineers Unconventional Gas Technology Symposium, Pittsburgh, May 16 - 18, SPE Paper 10847, p. 613 - 627.

Blanton, T. L., and A. B. Yost, 1986, Induced/Natural fracture interactions in Devonian Shales of the Appalachian Basin: Society of Petroleum Engineers Forum Series, Naturally Fracture Reservoirs, v. 3, Number 2.

Bobet, A., and H. H. Einstein, 1996, Fracture coalescence in rock material under uniaxial and biaxial loading: Proceedings of the 2nd North American Rock Mechanics Symposium, Montréal, p. 1603 - 1609.

Bobet, A., and H. H. Einstein, 1998a, Fracture coalescence in rock-type materials under uniaxial and biaxial compression: International Journal of Rock Mechanics and Mining Sciences and Geomechanics, p. 863 - 889.

Bobet, A., and H. H. Einstein, 1998b, Numerical modeling of fracture coalescence in a model rock material: International Journal of Fracture, v. 92, p. 221 - 252.

Boyer, C. M., S. Glenn, B. Claypoool, S. D. Weida, and C. D. Crain, 2005, Application of viscoelastic fracturing fluids in Appalachian Basin reservoirs: Society of Petroleum

Engineers / Eastern Regional Meeting, Morgantown, September 14 - 16, SPE Paper 98068.

Brady, B., J. Elbel, M. Mack, H. Morales, K. Nolte, and B. Poe, 1992, Cracking rock: Progress in fracture treatment design: Oilfield Review, p. 4-17.

Britt, L. K., C. J. Hager, and J. W. Thompson, 1994, Hydraulic fracturing in naturally fractured reservoir: Society of Petroleum Engineers / International Petroleum Conference and Exhibition, Veracruz, October 10 - 13, SPE Paper 28717.

Bruner, K. R., and R. Smosna, 2011, A comparative study of the Mississippian Barnett Shale, Fort Worth Basin, and Devonian Marcellus Shale, Appalachian Basin: United States Department of Energy, National Energy Technology Laboratory, Report 1478.

Bunger, A. P., 2005, Near-surface hydraulic fracture: PhD thesis, University of Minnesota, Minneapolis.

Bunger, A. P., R. G. Jeffrey, and E. Detournay, 2005, Application of scaling laws to laboratory-scale hydraulic fractures: U.S. Symposium on Rock Mechanics, Anchorage, Alaska, June 25 - 29, ARMA/USRMS Paper 05-818, p. 9.

Bunger, A. P., and E. Detournay, 2007, Early-time solution for a radial hydraulic fracture: Journal of Engineering Science, v 133, p. 534 - 540.

Bunger, A. P., J. Kear, R. G. Jeffrey, R. Prioul and D. Chuprakov, 2015, Laboratory investigation of hydraulic fracture growth through weak discontinuities with active ultrasound monitoring: Proceedings of the 13th International Congress on Rock Mechanics, Montréal, May 10 - 13, ISRM.

Byerlee, J. D., 1978, Friction of rocks: Pure and Applied Geophysics, v. 116, p. 616 - 626 .

Casas, L. A., J. L. Miskimins, A. D. Black, and S.J. Green, 2006, Laboratory hydraulic fracturing test on a rock with artificial discontinuities: Society of Petroleum Engineers Annual Technical Conference and Exhibition, San Antonio, September 24 - 27 SPE Paper 103617, p. 9.

Chan, H. C., V. Li, and H. H. Einstein, 1990, A hybridized displacement discontinuity and indirect boundary element method to model fracture propagation: International Journal of Fracture, v. 45, p. 263 - 282.

Chase, B., W. Chmilowski, Y. Dang, K. Krauss, T. Lantz, C. Parham, and J. Plummer, 1997, Clear fracturing fluids for increased well productivity: Oilfield Review, p. 20-33.

Chuprakov, D., A. V. Akulich, E. Siebrits and M. Thiercelin, 2010, Hydraulic fracture propagation in a naturally fractured reservoir: Society of Petroleum Engineers Oil and Gas India Conference and Exhibition, Mumbai, Jan 20 - 22, SPE Paper 128715-PP, p. 13.

Chuprakov, D., O. Melchaeva, and R. Prioul, 2013a, Hydraulic fracture propagation across a weak discontinuity controlled by fluid injection: In Bunger, A.P., J. McLennan, and R. G. Jeffrey, editors, Effective and Sustainable Hydraulic Fracturing, chapter 8. Intech, Rijeka, Croatia.

Chuprakov, D., O. Melchaeva, and R. Prioul, 2013b, Injection-sensitive mechanics of hydraulic fracture interaction with discontinuities: 47th U.S. Rock Mechanics/Geomechanics Symposium, San Francisco, California, June 23 - 26, ARMA Paper 13-252, p. 18.

Chuprakov, D., and R. Prioul, 2015, Hydraulic fracture height containment by weak horizontal interfaces: Society of Petroleum Engineers Hydraulic Fracturing Technology Conference, The Woodlands, February 3-5, SPE Paper 173337.

Clark, J. B., 1949, A hydraulic process for increasing the productivity of wells: Petroleum Trans. American Institute of Mining and Energy, v. 186, p. 1 - 8.

Cleary, M. P., 1994, Critical issues in hydraulic fracturing of high-permeability: Society of Petroleum Engineers /European Production Operations Conference and Exhibition, Aberdeen, March 15-17, SPE Paper 27618.

Cook, P., V. Beck, D. Brereton, R. Clark, B. Fisher, S. Kentish, J. Toomey, and J. Williams, 2013, Engineering Energy: Unconventional Gas Production: Report for the Australian Council of Learned Academies.

Cooke, K. L., and C. A. Underwood, 2001, Fracture termination and step-over at bedding interfaces due to frictional slip and interface opening: Journal of Structural Geology, v. 23, p. 223 - 238.

Dahi Taleghani, A., and J. E. Olson, 2014, How natural fractures could affect hydraulic-fracture geometry: Society of Petroleum Engineers Journal, SPE Paper 167608, p. 11.

Daneshy, A. A., 1971, True and apparent direction of hydraulic fractures: Society of Petroleum Engineers Drilling and Rock Mechanics Conference, Austin, Jan 5 - 6, SPE Paper 3226, p. 15.

Daneshy, A. A., 1974, Hydraulic fracture propagation in the presence of planes of weakness: Society of Petroleum Engineers European Spring Meeting, Amsterdam, May 29 - 30, SPE Paper 4852, p. 8.

Daneshy, A. A., 1976, Rock properties controlling hydraulic fracture propagation: Society of Petroleum Engineers European Petroleum Conference, Amsterdam, April 7 - 9, SPE Paper 5752, p. 10.

Daniels, J., K. Delay, G. Waters, J. LeCalvez, J. Lassek, and D. Bentley, 2007, Contacting more of the Barnett Shale through and integration of real - time microseismic monitoring,

petrophysics, and hydraulic fracture design: Society of Petroleum Engineers / Annual Technical Conference and Exhibition, Anaheim, November 11 - 14, SPE Paper 110562.

de Pater, C. J., M. P. Cleary, T. S. Quinn, D. T. Barr, D. E. Johnson and L. Weijers, 1994, Experimental verification of dimensional analysis for hydraulic fracturing: Society of Petroleum Engineers Production and Facilities, November, p. 230 - 238.

Detournay, E., 2004, Propagation regimes of fluid-driven rractures in impermeable rocks: International Journal of Geomechanics, v. 4, p. 35– 45.

Diamond, W. P., and D. C. Oyler, 1987, Effects of stimulation treatments on coalbeds and surrounding strata - Evidence from underground observations: United States Department of the Interior, Bureau of Mines, Report of investigations 9083.

Dollar, A., and P. S. Steif, 1988, A tension crack impinging upon frictional interfaces: Journal of Applied Mechanics, v. 56, p. 291– 298.

Duchane, D., and D. Brown, 2002, Hot Dry Rock (HDR) geothermal energy research and development at Fenton Hill, New Mexico: GHC Bulletin, December, p. 13 - 19.

EIA, 2012, Annual energy outlook 2012, with projections to 2035, June.

EIA/ARI, 2013, World shale gas and shale oil resource assessment, May.

EIA, 2014, United States Energy Information Administration, Drilling Productivity Report: For key tight oil and shale gas regions, October.

Engelder, T., 1993, Stress regimes in the lithosphere: Princeton, N.J.: Princeton University Press, p. 457.

Entingh, D. J., 2000, Geothermal well stimulation experiments in the United States: Proceedings World Geothermal Congress, Japan, 28 May - 10 June, p. 3689 - 3694.

Erdogan, F., and V. Biricikoglu, 1973, Two bonded half planes with a crack going through the interface: International Journal of Engineering Science, v 11, p. 745 - 766.

Fisher, K., and N. Warpinski, 2011, Hydraulic Fracture-Height Growth: Real Data: Society of Petroleum Annual Technical Conference and Exhibition, Denver, October 30 - November 2, SPE Paper 145949, p. 18.

Garagash, D., and E. Detournay, 2000, The tip region of a fluid-driven fracture in an elastic medium: American Society of Mechanical Engineers Journal of Applied Mechanics, v. 67, p. 183– 192.

Grand View Research, Market Research and Consulting, 2014, Hydraulic Fracturing Market Analysis by Technology (Plug & Perf, Sliding Sleeve), Material (Proppant), Application (Shale Gas, Tight Gas, Tight Oil, CBM) and Segment Forecasts to 2020: Real Data: ISBN Code: 978-1-68038-249-5, October.

Gu, H., and E. Siebrits, 2008, Effect of formation modulus contrast on hydraulic fracture height containment: Society of Petroleum Engineers International Oil and Gas conference, Beijing, December 5 - 7.

Gu, H., and X. Weng, 2010, Criterion for fractures crossing frictional interfaces at non-orthogonal angles: 44th US Rock Mechanics Symposium and 5th U.S. - Canada Rock Mechanics Symposium, Salt Lake City, UT, June 27 - 30, ARMA Paper 10-198, p. 6.

Gu, H., X. Weng, J. Lund, M. Mack, U. Ganguly, and R. Suárez-Rivera, 2011, Hydraulic fracture crossing natural fracture at non-orthogonal angles, a criterion, its validation and applications: Society of Petroleum Engineers /Hydraulic Fracturing Technology Conference and Exhibition, The Woodlands, January 24-26, SPE Paper 139984.

Gudmundsson, A., and S. L. Brenner, 2001, How hydraulic fractures become arrested: Terra Nova, v. 13, p. 456-462.

Haimson, B., and C. Fairhurst, 1969, Hydraulic fractures in porous-permeable materials: Journal of Petroleum Technology, v. 21, p. 811-817.

Hasting, M., J. Albaric, V. Oye, P. Reid, M. Messeiller, E. Llanos, P. Malin, E. Shalev, M. Hogg, M. Alvarez, A. Miller, C. Walter, C. Boese, and N. Voss, 2011, Real-time induced seismicity monitoring during wellbore stimulation at Paralana-2 South Australia: Proceedings, Australian Geothermal Energy Conference, p. 85-101.

He, M., and J. Hutchinson, 1989, Crack deflection at an interface between dissimilar elastic materials: International Journal of Solids Structures, v. 25, p. 1053-1067.

Helgeson, D. E., and A. Aydin, 1991, Characteristics of joint propagation across layer interfaces in sedimentary rocks: Journal of Structural Geology, v. 13, p. 897-911.

Holl, H., and C. Barton, 2015, Habanero field - structure and state of stress: World Geothermal Congress, Melbourne, April 19-25.

Hopkins, C. W., R. L. Rosen, and D. G. Hill, 1998, Characterization of an induced hydraulic fracture completion in a naturally fractured Antrim Shale reservoir: Society of Petroleum Engineers /Eastern Regional Meeting, Pittsburgh, November 9-11, SPE Paper 51068.

Hubbert, M. K., and D. G. Willis, 1957, Mechanics of hydraulic fracturing: Trans. AIME, v. 210, p. 153 - 166.

Jaeger, J., N. G. Cook, and R. Zimmerman, 2007, Fundamentals of rock mechanics: 4th Edition, Blackwell Publishing.

Jeffrey, R. G., L. Vandamme, and J. C. Roegiers, 1987, Mechanical interactions in branched or subparallel hydraulic fractures: Society of Petroleum Engineers/DOE Low Permeability Reservoirs Symposium, Denver, May 18-19, SPE Paper 16422, p. 333 - 341.

Jeffrey, R. G., R. P. Brynes, P. J. Lynch, and D. J. Ling, 1992, An analysis of hydraulic fracture and mineback data for a treatment in the German Creek Coal Seam: Society of Petroleum Engineers Rocky Mountain Regional Meeting, Casper, May 18-21, SPE Paper 24362, p. 445 - 457.

Jeffrey, R., G., J. R. Enever, T. Ferguson, and J. Bride, 1993, Small-scale hydraulic fracturing and mineback experiments in coal seams: Proceedings of the International Coalbed Methane Symposium, The University of Alabama/Tuscaloosa, May 17-21, p. 79-88.

Jeffrey, R. G., 1996, Asymmetrically propped hydraulic fractures: Society of Petroleum Engineers/ISRM Rock Mechanics in Petroleum Engineering Conference, Delft, August 29-31, SPE Paper 28079, p. 244 - 249.

Jeffrey, R. G., A. Bunger, B. Lecampion, X. Zhang, Z. R. Chen, A. van As, D.P. Allison, W. de Beer, J. W. Dudley, E. Siebrits, M. Thiercelin, and M. Mainguy, 2009, Measuring hydraulic fracture growth in naturally fractured rock: Society of Petroleum Engineers Annual Technical Conference and Exhibition, New Orleans, October 4-7, SPE Paper 124919.

Jeffrey, R., Z. Chen, K. Mills, and S. Pegg, 2013, Monitoring and Measuring Hydraulic Fracturing Growth During Preconditioning of a Roof Rock over a Coal Longwall Panel: In International Conference for Effective and Sustainable Hydraulic Fracturing, 1–22. Brisbane.

Jeffrey, R. G., J. Kear, D. Kasperczyk, X. Zhang, D. Chuprakov, R. Prioul, and J. Schouten, 2015, A 2D experimental method with results for hydraulic fractures crossing discontinuities: In 49th US Rock Mechanics / Geomechanics Symposium, ARMA. San Francisco, June 28 - July 1, p. 12.

Kaiser, P. K., B. Valley, M.B. Dusseault and D. Duff, 2013, Hydraulic fracturing mine back trials – Designe rationale and project status: In Bunger, A.P., J. McLennan, and R. G. Jeffrey, editors, Effective and Sustainable Hydraulic Fracturing, chapter 44. Intech, Rijeka, Croatia.

Keer, L. M., and S. H. Chen, 1981, The intersection of a pressurized crack with a joint: Journal of Geophysical Research, v. 86, p. 1032 - 1038.

King, G. E, 2012, Hydraulic fracturing 101: What every representative, environmentalist, regulator, reporter, investor, university researcher, neighbor and engineer should know about estimating frac risk and improving frac performance in unconventional gas and oil wells: Society of Petroleum Engineers Hydraulic Fracturing Technology Conference, The Woodlands, February 6-8, SPE Paper 152596.

Kresse, O., W. Xiaowei, D. Chuprakov, R. Prioul and C. Cohen, 2013, Effect of flow rate and viscosity on complex fracture development in UFM model: In Bunger, A.P., J. McLennan, and R. G. Jeffrey, editors, Effective and Sustainable Hydraulic Fracturing, chapter 9. Intech, Rijeka, Croatia.

Lam, K. Y., and M. P. Cleary, 1982, General branching and frictional slippage at crack tips with applications to hydraulic fracturing: reports of research in mechanics and materials, Department of Mechanical Engineering Massachusetts Institute of Technology. REL-82-1.

Lam, K. Y., and M. P. Cleary, 1984, Slippage and re-initiation of hydraulic fractures at frictional interfaces: International Journal of Numerical and Analytical Methods Geomechanics, v. 8, p. 589 - 604.

Lamont, N., and F. W. Jessen, 1963, The effects of existing fractures in rocks on the extension of hydraulic fractures: Society of Petroleum Engineers Annual Technical Conference and Exhibition, Los Angeles, October 7-10, SPE Paper 419, p. 203 - 209.

Lecampion, B., and X. Zhang, 2005, Onset of the interaction between a hydraulic fracture and a natural joint: scaling considerations: North America Rock Mechanics Symposium, Alaska, June 25 - 29, ARMA/NARMS Paper 05-768, p. 8.

Lecampion, B., R. G. Jeffrey, and E. Detournay, 2005, Resolving the geometry of hydraulic fractures from tilt measurements: Pure and applied geophysics, v. 162, p. 2433-2452.

Lee, J. C., and L. M. Keer, 1984, Propagation of a crack through and interfacial boundary: Proceedings 25th Rock Mechanics Symposium, p. 135-144.

Lhomme, T., 2005, Initiation of hydraulic fractures in natural sandstones: PhD thesis, Technische Universiteit, Delft.

Lim, I. L., I. W. Johnston and S. K. Choi, 1993, Stress intensity factors for semi-circular specimens under three-point bending: Engineering Fracture Mechanics, v. 44, p. 363-382.

Llanos, E. M., R. G. Jeffrey, R. R. Hillis, and X. Zhang, 2006, Study of the interaction between hydraulic fractures and geological discontinuities: Rock Mechanics in Underground Construction / 4th Asian Rock Mechanics Symposium, Singapore, November 8 - 10.

Llanos, E. M., S. J. Zarrouk, and R. Hogarth, 2015, Numerical model of the Habanero geothermal reservoir, Australia: Geothermics, v. 53, p. 308-319.

Long, C.S., A. Aydin, S. R. Brown, H. H. Einstein, K. Hestir, P. A. Hsieh, L. R. Myer, K. G. Nolte, D. L. Norton, O. L. Olsson, F. L. Paillet, J. L. Smith, and L. Thomsen, 1996, Rock

fractures and fluid flow - contemporary understanding and applications, National Academy Press, Washington D.C.

Mahrer, K. D., and W. W. Aud, 1996, Far-field hydraulic fracture geometry: A changing paradigm: Society of Petroleum Engineers /Annual Technical Conference and Exhibition, Denver, October 6-9, SPE Paper 36441.

Maxwell, S. C., T. I. Urbancic, N. Steinsberger, and R. Zinno, 2003, Fracs tracked using microseismic images: Hart's E&P, August, p. 58 - 59.

McClure, M. W., and R. N. Horne, 2013, Is pure shear stimulation always the mechanism of stimulation in EGS?: Proceedings of the 38th Workshop on Geothermal Reservoir Engineering, Stanford, California, February 11 – 13, p. 11.

McClure, M. W., and R. N. Horne, 2014, An investigation of stimulation mechanisms in enhanced geothermal systems: International Journal of Rock Mechanics and Mining Sciences and Geomechanics, p. 242 - 260.

McCoy, T. F., M. J. Fekovitch, R. B. Needham, and D. E. Reese, 1990, Analysis of Kansas Hugoton infill drilling: part I, total field results: Society of Petroleum Engineers Annual Technical Conference and Exhibition, New Orleans, September 23 - 26, SPE Paper 20756, p. 403-415.

McMahon, A., and S. Baisch, 2013, Case study of the seismicity associated with the stimulation of the enhanced geothermal system at Habanero, Australia. In: Proceedings, 35th New Zealand Geothermal Workshop, Rotorua.

Mellor, M., and I. Hawkes, 1971: Measurement of tensile strength by diametral compression of discs and annuli. Engineering Geology, v. 5, p. 173 - 225.

Montgomery, C. T., and M. B. Smith, 2010: "Hydraulic Fracturing: History of an Enduring Technology." Society of Petroleum Engineers, Journal of Petroleum Technology (62 (12): 26-32.

Moore J. R., and S. D. Glaser, 2005: "Self-Potential Observations during Hydraulic Fracturing in the laboratory". ARMAR/USRMS 05-696.

Moschovidis, Z. A., D. C. Gardner, and R. W. Veatch, 1994, Disposal of oily cuttings by downhole periodic fracturing injections, Valhall, North Sea: case study and modeling concepts: Society of Petroleum Engineers Drilling and Completions, December, SPE Paper 25757, p. 256 - 262.

Nelson, E. J., S. T. Chipperfield, R. R. Hillis, J. Gilbert, and J. McGowen, 2007, Using geological information to optimize fracture stimulation practices in the Cooper Basin, Australia: Petroleum Geoscience, v. 13, p. 3 -16.

Osborn, S. G., A. Vengosh, N. R. Warner, and R. Jackson, 2011, Methane contamination of drinking water accompanying gas-well drilling and hydraulic fracturing: Proceedings of the National Academy of Science, v. 108, p. 8172 - 8176.

OTA-Report, 1985, US Natural Gas Availability: Gas supply through the year 2000 (Washington, DC: U.S. Congress, Office of Technology Assessment, OTA-E-245, February), p. 233 - 234.

Pine, R. J., and A. S. Batchelor, 1984, Downward migration of shearing in jointed rock ruding hydraulic injections: International Journal of Rock Mechanics and Mining Sciences, v. 21, p. 249 - 263.

Pollard, D. D., and A. Aydin, 1988, Progress in understanding of jointing over the past century: Geological Society of America Bulletin, v. 100, p. 1181 - 1204.

Potluri, N., D. Zhu, and A. D. Hill, 2005, Effect of natural fractures on hydraulic fracture propagation: Society of Petroleum Engineers /European Formation Damage Conference, Scheveningen, May 25-27, SPE Paper 94568.

Reed, A. C., J. L. Mathews, and M. S. Bruno, 2001, Safe disposal of one million barrels of NORM in Louisiana through slurry fracture injection: Society of Petroleum Engineers / Annual Technical Conference, New Orleans, September 30 - October 3, SPE Paper 71434.

Reid, P., M. Messeiller, E. M. Llanos, and M. Hasting, 2011, Paralana 2 - Well Testing and Stimulation: Proceedings, Australian Geothermal Energy Conference, p. 193-195.

Reid, P., M. Messeiller, and M. Hasting, 2012, The Paralana engineered geothermal project - case history and results of the hydraulic fracture stimulation: Proceedings, Australian Geothermal Energy Conference, p. 161-164.

Renshaw, C. E., and D. D. Pollard, 1995, An experimentally verified criterion for propagation across unbounded frictional interfaces in brittle, linear elastic materials: International Journal of Rock Mechanics and Mining Sciences and Geomechanics, p. 237 - 249.

Sarmadivaleh, M., and V. Rasouli, 2013, Modified Renshaw and Pollard criteria for a non-orthogonal cohesive natural interface intersected by an induced fracture: Rock Mechanics and Rock Engineering, 47(6): 2107-2115, DOI 10.1007/s00603-013-0509-1.

Sarmadivaleh, M., and V. Rasouli, 2015, Test design and sample preparation procedure for experimental investigation of hydraulic fracturing interaction modes: Rock Mechanics and Rock Engineering, 48:93-105, DOI 10.1007/s00603-013-0543-z.

Savitski, A. A., and E. Detournay, 2002, Propagation of a penny-shaped fluid-driven fracture in an impermeable rock: asympotic solutions: International Journal of Solids and Structures, v. 39, p. 6311 - 6337.

Shaffer, R. J., R. K. Thorpe, A. R. Ingraffea, and F. E. Heuze, 1984, Numerical and physical studies of fluid-driven fracture propagation in jointed rock: Society of Petroleum Engineers /DPOE/GRI Unconventional Gas Recovery Symposium, Pittsburgh, May 13-15, SPE Paper 12881, p. 471 - 482.

Shaffer, R. J., R. N. Nilson, F. E. Heuze, and R. P. Swift, 1987, Unconventional gas and coal gasification / Quasi-Static and dynamic arbitrary fracture propagation in jointed rock: report prepared by LLNL Unconventional Gas Program, under contract W-7405-ENG-48 with the US_DOE.

Siegel, D. I., N. A. Azzolina, B. J. Smith, A. E. Perry, and R. L. Bothun, 2015, Methane concentrations in water wells unrelated to proximity to existing oil and gas wells in northeastern Pennsylvania: Environmental Science and Technology, v.49, p. 4106 - 4112.

Simonson, E. R., A. S. Abou-Sayed, and R. J. Clifton, 1976, Containment of massive hydraulic fractures: Society of Petroleum Engineers Annual Technical Conference and Exhibition, New Orleans, October 3-6, SPE Paper 6089, p. 27 - 32.

Smith, M. B., W. K. Miller, and J. Haga, 1987, Tip Screenout Fracturing: A technique for soft, unstable formations: Society of Petroleum Engineers, SPE Paper 13273.

Sneddon, I. N., 1995, Fourier Transforms: Published by Courier Dover Publications, ISBN 0486685225, 9780486685229, 542 pages.

Spence, D. A., and D. L. Turcotte, 1985, Magma-driven propagation crack: Journal of Geophysical Research, v. 90, p. 575 - 580.

Tester, J. W., B. J. Anderson, A. S. Batchelor, D. D. Blackwell, R. DiPippo, E. M. Drake, J. Garnish, B. Livesay, M. C. Moore, K. Nichols, S. Petty, M. N. Toksöz and R. W. Veatch, 2007, The future of geothermal energy: impact of enhanced geothermal systems (EGS) on the United States in the 21st century, Cambridge, MA, p. 358.

Teufel, L. W., and J. A. Clark, 1981, Hydraulic fracture propagation in layered rock: Experimental studies of fracture containment: Society of Petroleum Engineers Journal, v. 24, p. 19 - 32.

Thiercelin, M., J. C. Roegiers, T. J. Boone, and A. R. Ingraffea, 1987, An investigation of the material parameters that govern the behaviour of fractures approaching rock interfaces: Proceedings of the 6th International Congress on Rock Mechanics, Montréal, p. 263-269.

Tiemann, M., and A. Vann, 2013, Hydraulic frcturing and safe drinking water act regulatory issues: Congressional Research Service.

Tyler, L. D., and W. C. Vollendorf, 1975, Physical observations and mapping of cracks resulting from hydraulic fracturing: in-situ stress measurements: Society of Petroleum Engineers 50th Annual Technical Conference and Exhibition, Dallas, September 28, SPE Paper 5542.

van As, A., and R. G. Jeffrey, 2002, Hydraulic fracture growth in naturally fractured rock: mine through mapping and analysis: Proceedings of the 5th North American Rock Mechanics Symposium, Toronto, p. 1461 - 1469.

Vernik, L., M. Bruno, and C. Bovberg, 1993, Empirical relations between compresive strength and porosity of siliciclastic rocks: International Journal of Rock Mechanics and Mining Sciences and Geomechanics, Abstr. 30, p. 677 - 680.

Warpinski, N. R., 1990, Dual leakoff behavior in hydraulic fracturing of tight, lenticular gas sands: Society of Petroleum Engineers, SPE Paper 18259.

Warpinski, N. R., R. A. Schmidt, and D. A. Northrop, 1982, In-Situ Stresses: the predominant influence on hydraulic fracture containment: Society of Petroleum Engineers, March, SPE Paper 8932.

Warpinski, N. R., and L. W. Teufel, 1987, Influence of geologic discontinuities on hydraulic fracture propagation: Journal of Petroleum Technology, February, p. 209 - 220.

Weertman, J., 1980, The stopping of a rising, liquid-filled crack in the earth's crust by a freely slipping horizontal joint: Journal of Geophysical Research, v. 85, p. 967 - 976.

Weertman, J., 1996, Dislocation based fracture mechanics, World Scientific Publishing Co.

Young, C., 1999, Controlled-foam injection for hard rock excavation: U. S. Rock Mechanics Symposium - Vail, Colorado, 6 - 9 June, p. 8.

Zhang, X., R. Jeffrey, and E. Llanos, 2004, A study of shear hydraulic fracture propagation: American Rock Mechanics Association, Houston, June 5 - 9, ARMA/NARMS Paper 491, p. 10.

Zhang, X., R. G. Jeffrey, and E. M. Llanos, 2005a, On plane-strain fluid-driven shear fracture propagation in elastic solids: Geophysics Journal International, v. 163, p. 419 - 430.

Zhang, X., R. Jeffrey, E. Llanos, and B. Lecampion, 2005b, Plane-strain analysis of post-coalescence interaction between fluid-driven cracks and natural fractures: North America Rock Mechanics Symposium, Alaska, June 25 - 29, ARMA/NARMS Paper 05 - 719, p. 12.

Zhang, X., and R. G. Jeffrey, 2006, The role of friction and secondary flaws on deflection and re-initiation of hydraulic fractures at orthogonal pre-existing fractures: Geophysics Journal International, v. 166, p. 1454 - 1465.

Zhang, X., R. G. Jeffrey, and M. Thiercelin, 2006, Deflection and propagation of fluid-driven fractures at frictional bedding interfaces: A numerical investigation: Journal of Structural Geology, v. 29, p. 396 - 410.

Zhang, X., and R. G. Jeffrey, 2007, Hydraulic fracture propagation across frictional interfaces: North America Rock Mechanics Symposium, Vancouver, May 27 - 31, ARMA/NARMS Paper 07 - 204.

Zhang, X., R. G. Jeffrey, and M. Thiercelin, 2007, Effects of frictional geological discontinuities on hydraulic fracture propagation: Society of Petroleum Engineers / Hydraulic Fracturing Technology Conference, College Station, January 29 - 31, SPE Paper 106111.

Zhang, X., and R. G. Jeffrey, 2008, Reinitiation or termination of fluid-driven fractures at frictional bedding interfaces: Journal of Geophysical Research, v. 113, p. 16.

Zhang, X., and R. G. Jeffrey, 2011, Can reservoir conductivity be enhanced by shear fracture alone?: Australian Geothermal Energy Conference, Melbourne.

Zhou, J., M. Chen, Y. Jin, and G. Zhang, 2008, Analysis of fracture propagation behaviour and fracture geometry using a tri-axial fracturing system in naturally fractured reservoirs: International Journal of Rock Mechanics and Mining Sciences, v. 45, p. 1143 – 1152.